Review

Emergence of Impurity-Doped Nanocrystal Light-Emitting Diodes

Dongxiang Luo [1], Lin Wang [2], Ying Qiu [3],*, Runda Huang [4] and Baiquan Liu [5],*

[1] Institute of Semiconductors, South China Normal University, Guangzhou 510631, China; luodx@gdut.edu.cn
[2] Division of Physics and Applied Physics, School of Physical and Mathematical Sciences, Nanyang Technological University, Singapore 637371, Singapore; lin_wang@ntu.edu.sg
[3] Guangdong R&D Center for Technological Economy, Guangzhou 510000, China
[4] School of Materials and Energy, Guangdong University of Technology, Guangzhou 510006, China; hrd76287211@163.com
[5] State Key Laboratory of Optoelectronic Materials and Technologies and the Guangdong Province Key Laboratory of Display Material and Technology, School of Electronics and Information Technology, Sun Yat-sen University, Guangzhou 510275, China
* Correspondence: srawoyjs@sina.com (Y.Q.); l.baiquan@mail.scut.edu.cn (B.L.)

Abstract: In recent years, impurity-doped nanocrystal light-emitting diodes (LEDs) have aroused both academic and industrial interest since they are highly promising to satisfy the increasing demand of display, lighting, and signaling technologies. Compared with undoped counterparts, impurity-doped nanocrystal LEDs have been demonstrated to possess many extraordinary characteristics including enhanced efficiency, increased luminance, reduced voltage, and prolonged stability. In this review, recent state-of-the-art concepts to achieve high-performance impurity-doped nanocrystal LEDs are summarized. Firstly, the fundamental concepts of impurity-doped nanocrystal LEDs are presented. Then, the strategies to enhance the performance of impurity-doped nanocrystal LEDs via both material design and device engineering are introduced. In particular, the emergence of three types of impurity-doped nanocrystal LEDs is comprehensively highlighted, namely impurity-doped colloidal quantum dot LEDs, impurity-doped perovskite LEDs, and impurity-doped colloidal quantum well LEDs. At last, the challenges and the opportunities to further improve the performance of impurity-doped nanocrystal LEDs are described.

Keywords: light-emitting diode; impurity doping; quantum dot; perovskite; quantum well

1. Introduction

Nanocrystal light-emitting diodes (LEDs) have huge potential in display, lighting, and signaling applications because of their exceptional advantages including high efficiency, excellent luminance, low voltage, impressive power consumption, and long lifetime [1–5]. In 1994, Alivisatos et al. reported the first nanocrystal LED by using CdSe colloidal quantum dots (CQDs), achieving a maximum external quantum efficiency (EQE) of 0.01% [6]. Since then, plenty of endeavors have been taken to enhance the performance (e.g., EQE, current efficiency (CE), power efficiency (PE), voltage, luminance, and stability) of CQD-LEDs [7–11]. Nowadays, the performance of CQD-LEDs can be comparable to or even better than that of state-of-the-art organic LEDs (OLEDs) [12–16]. For example, the maximum EQE of CQD-LEDs exceeds 20% [1], while the maximum luminance of CQD-LEDs overtakes 614,000 cd m^{-2} [17]. As a comparison, the maximum EQE of OLEDs is above 36% [13], but the maximum luminance of OLEDs is usually below 200,000 cd m^{-2} [15]. Benefiting from the understanding of CQD-LEDs, researchers have also explored other types of nanocrystal LEDs. As a representative class of optoelectronic materials, both organic-inorganic hybrid and all-inorganic

perovskites have been intensively studied for LEDs in the recent years [18–23]. In 2014, Friend et al. realized the first successful organic-inorganic $MAPbBr_3$ (MA= CH_3NH_3) perovskite LED (PeLED), yielding an EQE of 0.1% [18]. With the combined efforts from scientists worldwide, the performance of PeLEDs has been significantly enhanced [24]. So far, the maximum EQE of PeLEDs surpasses 20% [25–27], while the maximum luminance of PeLEDs surmounts 591,197 cd m^{-2} [28]. In addition, colloidal quantum wells (CQWs), also commonly nicknamed as semiconductor nanoplatelets, are considered to be another highly promising family of emitters for nanocrystal LEDs [29–33]. In 2014, Dubertret et al. developed the first CQW-LED by using CdSe/CdS core/shell heterostructures, obtaining a maximum EQE of 0.63% [34]. Over the past few years, the performance of CQW-LEDs has been improved step-by-step. Currently, the maximum EQE of CQW-LEDs is close to the theoretical limit of 20% [35]. These exciting facts demonstrate that the rapid development of nanocrystal LEDs will become real commercialization in the near future.

Impurity doping is a broadly exploited strategy to endow nanocrystals exhibiting a multitude of novel electronic, optical, catalytic, transporting and magnetic properties [36–40]. By intentionally inserting atoms or ions of appropriate elements (e.g., transition metal, alkali metal, rare earth, and lanthanide impurities) into host lattices or nonstoichiometry-induced self-doping, various impurity-doped nanocrystals with desirable properties and functions can be achieved [41–45]. Since the self-quenching and reabsorption from enlarged Stokes shift can be eliminated, impurity-doped nanocrystals are much less sensitive than undoped ones to the chemical, thermal, and photochemical disturbances [46–50]. In particular, extra holes (p-type doping) or electrons (n-type doping) are provided with the utilization of impurities, enriching the electronic applications [51]. Doping levels and dopant positions are varied according to the synthesis schemes (e.g., reaction parameters, working temperatures, and doping agents), leading to the changed dopant luminescence and electronic impurities [52–55]. For instance, Norris et al. obtained p-type and n-type Ag doping through different doping levels by using the cation-exchange reaction between PbSe/CdSe and ethanolic Ag$^+$ [56]. Klimov et al. incorporated Mn ions into $CsPbX_3$ (X= Cl, Br, or I) perovskites through elucidating the function of bond strengths within the precursor and perovskite lattice, showing that the energy transfer between perovskites and Mn^{2+} played a key role in the intensity of band-edge and Mn emissions [57]. Eychmüller et al. observed that high-temperature synthesis methods (e.g., 240 °C) lead to a firm binding of Hg atoms within CQWs responsible for the single peak emission, while low-temperature means (e.g., 200 °C) caused both loosely (probably via interstitial incorporation) and firmly (substitutional) bound Hg atoms for double radiative recombination channels of lower and higher energies (i.e., two red PL signals) [58]. As a matter of fact, it has been demonstrated that impurities can afford CQDs, perovskites, and CQWs with new functionalities.

Generally, impurity-doped nanocrystals can exhibit not only the intrinsic merits of nanocrystals but also additional advantages including enhanced thermal and chemical stability, improved photoluminescence quantum efficiency (PLQY), reduced Auger recombination, impurity-related emission, and tailored charge mobility [59–63]. Owing to these superiorities, impurity-doped nanocrystals have sparked efforts to satisfy the requirement of many optoelectronic applications. For example, Manoj et al. realized high-performance luminescent solar concentrators by using Cu-doped CQWs, whose quantum efficiency is near-unity (up to ≈97%) [64]. Huang et al. improved hole extraction through Ag doping (1% concentration) in PbS CQD solar cells, boosting the power conversion efficiency from 9.1% to 10.6% [65]. In the case of LEDs, impurity-doped nanocrystals have been extensively explored as versatile emitters. In general, impurity-doped nanocrystal LEDs can emit not only band-edge emissions but also impurity-related emissions [66–68]. As a consequence, three emission phenomena exist in impurity-doped nanocrystal LEDs (i.e., LEDs exhibit only host emissions, LEDs show only impurity emissions, and LEDs possess both host and dopant emissions). This is different from undoped nanocrystal LEDs, where only band-edge emissions can be observed [69–71]. Additionally, both the efficiency and luminance of impurity-doped nanocrystal LEDs can be enhanced compared with those of undoped counterparts. For example, nine times the EQE in CQW-LEDs [72]

and ~10 times the luminance in PeLEDs [73] were accomplished via impurity doping. Furthermore, the stability of impurity-doped nanocrystal LEDs could be improved related to that of undoped ones [74]. Owing to the unique characteristics and impressive advantages (e.g., enhanced efficiency, improved luminance, lowered voltage, and increased stability), impurity-doped nanocrystal LEDs, especially for CQD-LEDs, PeLEDs and CQW-LEDs, are hugely promising for the new-generation display, lighting, and signaling technologies.

Herein, the recent state-of-the-art concepts to achieve high-performance impurity-doped nanocrystal LEDs will be concluded. First, the fundamental concepts of impurity-doped nanocrystal LEDs will be presented. Second, the efforts to enhance the performance of impurity-doped nanocrystal LEDs via both material design and device engineering will be introduced. In particular, the emergence of various types of impurity-doped nanocrystal LEDs (e.g., CQD-LEDs, PeLEDs, and CQW-LEDs) will be comprehensively highlighted. Finally, the issues and ways to further improve the device performance will be clarified.

2. Fundamental Concepts of Impurity-Doped Nanocrystal LEDs

2.1. Impurity-Doped Nanocrystal Emitters

Nowadays, CQDs, perovskites, and CQWs are the three most extensively studied nanocrystals for LEDs. In this work, CQDs, perovskites, and CQWs do not belong to the same category. Here, the materials of zero-dimensional (0D) CQDs and 2D CQWs are formed by IV elemental nanocrystal semiconductors (e.g., Si, Ge), the common groups being II-VI (e.g., CdSe, CdTe), III-V (e.g., InP, InAs), and IV-VI (e.g., PbSe, PbS), binary nanocrystal semiconductors, and nanocrystal semiconducting materials of ternary chalcogenide compounds AB_mC_n (A= Cu, Ag, Zn, Cd, etc.; B= Al, Ga, In; C= S, Se, Te) [7–11]. Perovskites here refer to the materials possessing the formula ABX_3, in which A-site is MA^+, $[CH(NH_2)_2]^+$ (FA^+) or Cs^+, B-site is mostly Pb^{2+}, and X-site is Cl, Br, I or mixed halide systems (Cl/Br, Br/I) [24–28]. Although perovskite materials can have different morphologies (e.g., nanowires, quantum dots, and nanoplatelets), perovskites in this work are indicated to be different from CQDs and CQWs from the perspective of material composition instead of the morphology, which is used to avoid confusion since the same material can have different morphologies and different materials can have identical morphologies [29–33]. In the following parts, we will focus on these three impurity-doped nanocrystals (i.e., CQDs, perovskites, and CQWs).

With the successful synthesis of colloidal nanocrystals, size-dependent quantum confinement effects and controlled tunability of physical characteristics are allowed [75–77]. Since the representative work in 1993 [78], CdSe CQDs have functioned as a representative system for wet-chemical syntheses. Continuous endeavors enable the manipulation of size, shape, composition, and crystal structure of nanocrystals, giving rise to a large number of nanocrystals including core-only CQDs (e.g., CdSe, ZnS, ZnSe, CdS, and InP), core/shell CQDs (e.g., CdSe/ZnS, CdSe/ZnSe, and CdSe/CdS), and core/shell/shell CQDs (e.g., CdSe/ZnSe/ZnS, CdSe/CdS/ZnS, and CdTe/CdS/ZnS) [79–83]. Currently, the CQD-LED technology is entering the display market. In addition, halide perovskites are found to be a new family of LED emitters because of the outstanding characteristics such as high PLQY, narrow spectrum, and tunable emission in the entire visible region through controlling over anion identity or perovskite size [84–88]. To date, both organic-inorganic hybrid perovskites (e.g., $MAPbX_3$, $FAPbX_3$) and all-inorganic perovskites (e.g., $CsPbX_3$) have attracted a great deal of attention from both academic and industrial scientists [89–91]. Usually, the halide exchange method is exploited to tune the composition post synthetically at mild conditions since anions exhibit good mobility in relatively open perovskite crystal structures, controlling the bandgap [92]. Aside from CQDs and perovskites, CQWs, which possess the tight quantum confinement only in the vertical direction, have emerged as another novel class of emitting materials for LEDs thanks to their ultranarrow emission linewidth, excellent PLQY, and short radiative fluorescence lifetime [93–97]. Since Joo et al. used a low-temperature solution-phase strategy to synthesize the first 2D CdSe nanoribbons/CQWs showing a wurtzite

structure 1D confinement in 2006 [98] and Dubertret et al. prepared 2D zinc blende CQWs in 2008 [99], various colloidal synthesis pathways have been reported to engineer the electronic structure and optical characteristic of CQWs. Nowadays, apart from the core-only structures, CQWs with heterostructures are available (e.g., core/shell CQWs, core/crown CQWs, and core/crown/shell CQWs), which greatly widen the application range of CQW emitters [100–102]. In particular, the recently developed hot-injection shell growth technique enables CQWs with near-unity PLQY, which renders CQWs able to yield desirable performance in both lasers and LEDs [103–105].

As undoped nanocrystals are well developed, researchers have also turned their attention to explore new functionalities in impurity-doped nanocrystals [106–108]. The investigation of impurity-doped nanocrystals began in 1994 when Bhargava et al. reported that Mn-doped ZnS nanocrystals simultaneously yielded good PLQY and shortening lifetime [109]. Since then, impurity-doped nanocrystals have emerged as a novel family of materials. A popular doping scheme is to use the precursor with an intentional impurity during syntheses, where the resulting nanocrystals are needed to be carefully characterized (e.g., the electron paramagnetic resonance technique, the magnetic circular dichroism technology) to determine whether impurities are incorporated or surface-bound [109–112]. In 2016, Klimov et al. introduced Mn^{2+} into $CsPbX_3$ to show that doped perovskites were indeed a new family of materials [57]. In terms of impurity-doped CQWs, Demir et al. took the first step to incorporate Mn ions into CdSe/CdS core/multishell CQWs to manifest the carrier-dopant exchange interaction effect in 2015, where the colloidal atomic layer deposition technology was used to grow a $Cd_{0.985}Mn_{0.015}S$ monolayer shell onto CdSe CQWs [113]. After these pioneering works, impurity-doped nanocrystals have been explored to be highly promising emitters for LEDs. It is worth noting that doping in CQWs has not been investigated to the same extent as CQDs or perovskites and most of the impurity-doped CQWs are based on core-only CdSe structures [114]. In addition, more attention about doping has been paid on all-inorganic perovskites due to their superior stability, compared with organic-inorganic hybrid ones [115].

2.2. Device Architectures

On top of emissive materials, the design of device architectures plays a vital role in the performance of impurity-doped nanocrystal LEDs [116–118]. In particular, the optimization of device engineering has been verified to be a feasible way to gain high performance, since charge injection, transporting, accumulation, leakage, balance and recombination are strongly associated with device engineering [119–123]. For example, three-fold luminance improvement was accomplished through sandwiching a perfluorinated ionomer (PFI) as a hole injection layer (HIL) between the hole transporting layer (HTL) and $CsPbBr_3$ emitting layer (EML) in PeLEDs [124], while seven-fold EQE enhancement was fulfilled by using a stepwise dual-HTL 4,4'-bis-(m-tolyphenylamino)biphenyl (TPD)/4,4',4''-Tri(N-carbazolyl)triphenylamine (TCTA) in type II $CdSe/CdSe_{0.8}Te_{0.2}$ core/crown EML-based CQW-LEDs [125]. So far, many well-developed concepts in OLEDs have been applied to accelerate the innovation of device engineering for nanocrystal LEDs [126–130].

In principle, both forward and inverted device architectures are effective to organize undoped or impurity-doped nanocrystal LEDs [131–135], as shown in Figure 1. According to the employed charge transporting/injecting materials, three types of device architectures can be classified, regardless of forward or inverted nanocrystal LEDs. First, nanocrystal LEDs with organic charge transporting layers (CTLs) (Type I, Figure 1b), formed by organic HTLs and organic electron transporting layers (ETLs), are broadly used to fabricate extremely efficient PeLEDs. For example, Kido et al. employed poly(4-butylphenyl-diphenyl-amine) (poly-TPD) HTL and tris-(1-phenyl-1H-benzimidazole) (TPBi) ETL in a forward architecture to demonstrate the first $CsPb(Br/I)_3$ PeLED with a maximum EQE of >20% [27], while Wei et al. reported a green PeLED with a maximum EQE of 20.3% by using poly(ethylenedioxy thiophene):polystyrene sulfonate (PEDOT:PSS) HTL and $C_{37}H_{26}N_6$ (B3PYMPM) ETL [25]. In general, polymer CTLs are prepared by the solution-processed technique, while small-molecule CTLs are established by either the solution-processed or vacuum-evaporated

technology [136–140]. In particular, the evaporated CTLs show no damage to the underlying layers, averting solvent penetrating problems. Since a huge number of polymer and small-molecule organic charge transporting materials can be synthesized and selected [141–145], this type of device architecture possesses a vast potential to attain high-performance nanocrystal LEDs.
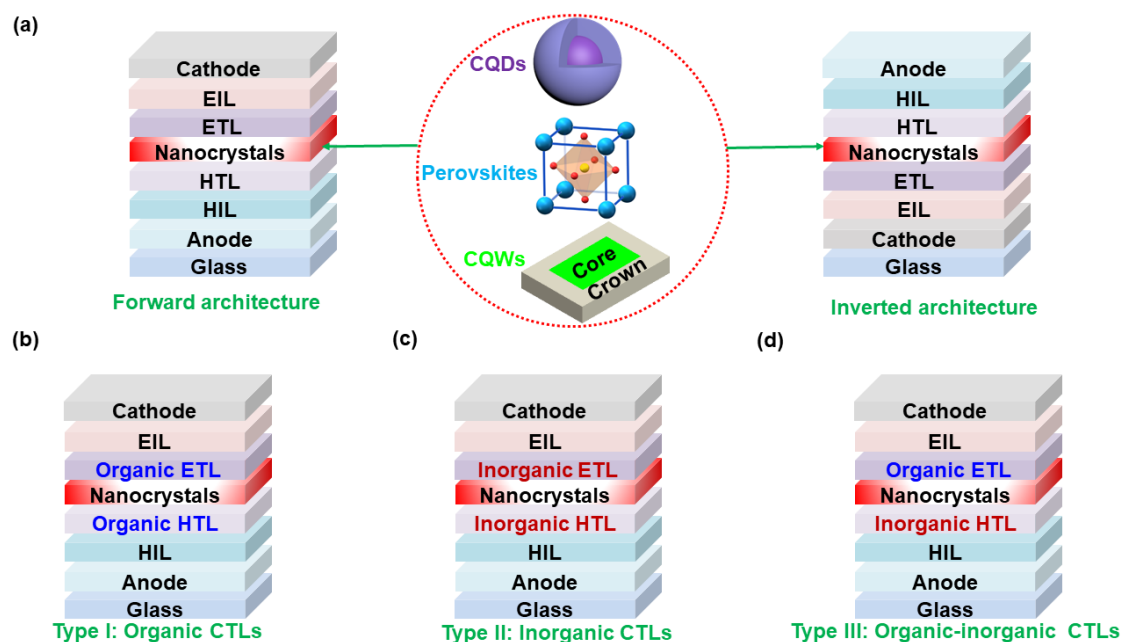

Figure 1. Diagram of device architectures for nanocrystal light-emitting diodes (LEDs). (**a**) Forward and inverted device architectures, where core/shell colloidal quantum dot (CQD), perovskite, and core/crown colloidal quantum well (CQW) material structures are used to clarify the corresponding nanocrystal emitters. EIL is the electron injection layer. (**b**) Nanocrystal LEDs with organic charge transporting layers (CTLs) (Type I). (**c**) Nanocrystal LEDs with inorganic CTLs (Type II). (**d**) Nanocrystal LEDs with organic-inorganic hybrid CTLs (Type III).

Second, nanocrystal LEDs with inorganic CTLs (Type II, Figure 1c), constructed by inorganic HTLs and inorganic ETLs, usually exhibit outstanding stability since inorganic materials are insensitive to the oxygen and water [146–150]. Recently, Ji et al. also demonstrated that CQD-LEDs with all-inorganic device architectures could possess a high efficiency (20.5 cd A^{-1}) and impressive luminance (20,000 cd m^{-2}) simultaneously, where nickel oxide (NiO) and zinc oxide (ZnO) were used as HTL and ETL, respectively [151]. However, relatively few effective inorganic charge transporting materials are available, which restricts the further development of this type of device architecture [152].

Third, nanocrystal LEDs with organic-inorganic hybrid CTLs (Type III, Figure 1d), built by the combination of organic HTLs and inorganic ETLs or the alliance of inorganic HTLs and organic ETLs, are the most extensively investigated type for high device performance [153–157]. Type III device architectures are considered to be able to collate the advantages from both Type I and Type II device architectures, leading to the simultaneous achievement of excellent efficiency, high luminance and long lifetime [158–160]. As a matter of fact, a lot of attention has been paid to the hybrid device architecture. For example, Peng et al. sandwiched CdSe/CdS EML between the inorganic ZnO ETL and organic poly(9-vinylcarbazole) (PVK) HTL, achieving a CQD-LED with a high EQE of 20.5% and a long lifetime of over 100,000 h at 100 cd m^{-2} [1]. In addition, the most efficient CQW-LED is also fulfilled via hybrid device architecture [35].

2.3. Emission Mechanisms

To boost the device performance, it is beneficial to unveil the emission mechanism of impurity-doped nanocrystal LEDs. The electroluminescence (EL) procedure can be summarized

as follows [161–166]. Upon connecting power sources, electrons and holes are injected through the cathode and anode, respectively. Then, electrons reach the EML by drawing on the electron injection layer (EIL) and ETL, while holes arrive at the EML through HIL and HTL. Excitons are generated for radiative recombination when electrons and holes meet each other in the EML, leading to the intentional emissions based on the used emitters. To guarantee excitons being radiatively decayed, the nonradiative channels (e.g., Auger recombination) should be avoided [167–169]. In particular, charge imbalance is harmful to the device performance [170–174]. For example, excess electrons or holes will easily cause nanocrystals charging, leading to poor performance [175–178]. Thus, the good understanding of the EL process is essential to guarantee the efficient emissions.

To date, Mn, Cu, and Ag are the three most well-studied impurities for nanocrystals. In the case of Mn-doped nanocrystals, the impurity emission peak is located in the yellow-orange range (e.g., 580–600 nm) because Mn-emission is attributed to the intrinsic $^4T_1$-$^6A_1$ transition of Mn ion [179–182]. For Cu-doped nanocrystals, the impurity can show a large emission window affected by the size, composition, and nature of matrix materials (e.g., Cu-doped ZnS showing blue-green emissions [183], Cu-doped ZnSe exhibiting green-yellow emissions [184], Cu-doped CdS possessing orange-red emissions [185], and Cu-doped InP displaying near-infrared emissions [186]). In terms of Ag-doped nanocrystals, the dopant emission can also cover a broad spectral range, which is somewhat similar to that of Cu-emission [187–189]. However, the recent study showed that Ag-doped nanocrystals and Cu-doped nanocrystals possessed different electronic structures, where photogenerated holes mainly localized in Cu($3d$) orbitals for Cu^+-doped CdSe (Cu^+ was oxidized to Cu^{2+}) while holes primarily localized in $4p$ orbitals of four neighboring Se^{2-} ligands for Ag^+-doped CdSe (Ag^+ was unoxidized) [190].

For undoped nanocrystals, photogenerated excitons will be formed upon excitation and then decay radiatively, furnishing the band-edge emissions [191–193], as shown in Figure 2a. Thanks to the extra impurity electronic energy levels, impurity-doped nanocrystal LEDs can show impurity-related emissions apart from the generation of band-edge emissions [194–202]. Thus, three emission mechanisms occur in impurity-doped nanocrystal LEDs, i.e., LEDs exhibit only host emissions, LEDs show only impurity emissions, and LEDs possess both host and dopant emissions. These phenomena are unlike undoped nanocrystal LEDs, where only band-edge emissions are generated. To insightfully understand such distinguished behavior, the emission mechanism of Mn ions doped nanocrystals is analyzed as an example below, considering that all the first doped CQDs [109], the first doped perovskites [57], and the first doped CQWs [113] are based on the Mn impurity.
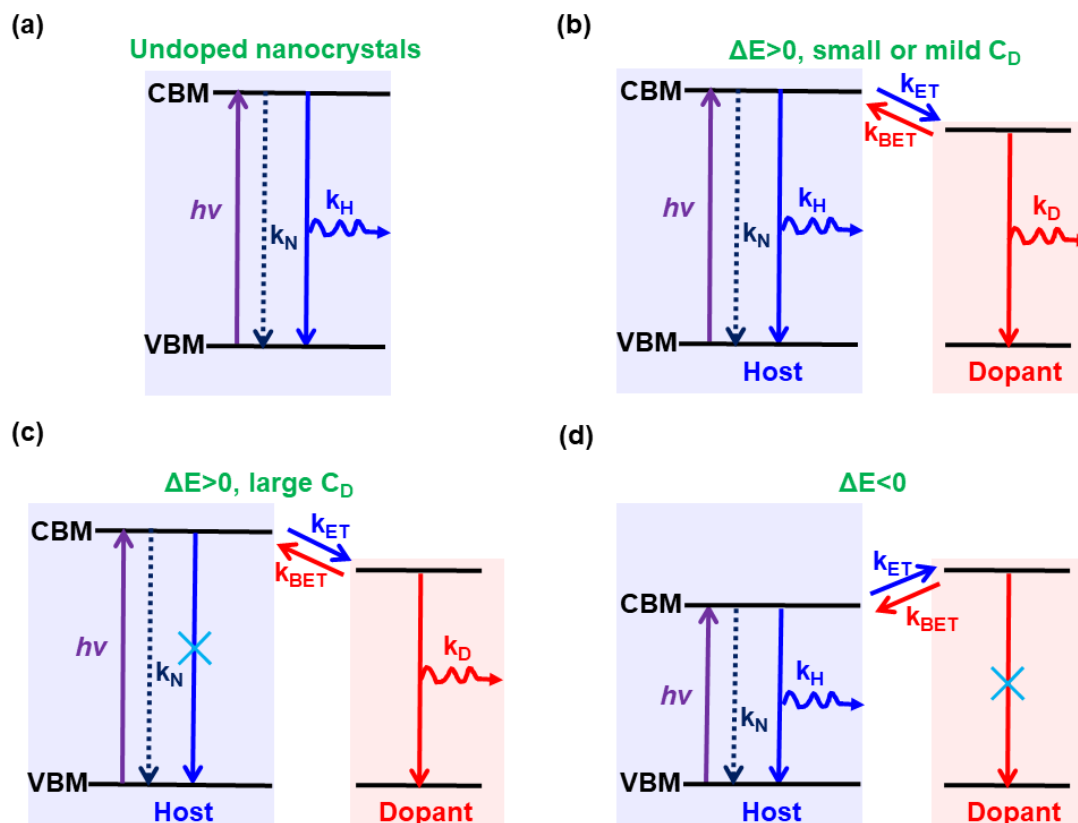
(a) Undoped nanocrystals

(b) $\Delta E > 0$, small or mild C_D

(c) $\Delta E > 0$, large C_D

(d) $\Delta E < 0$

Figure 2. Diagram of photoluminescence (PL) emission mechanisms for undoped and Mn-doped nanocrystals. (**a**) Emission mechanism for undoped nanocrystals. VBM and CBM denote the valance band maximum and conduction band minimum, respectively. Both host and dopant emissions (**b**), only the host emission (**c**), and only the dopant emission (**d**) exist in Mn-doped nanocrystals.

The host and dopant PL emissions in Mn-doped nanocrystals is dependent on the interplay of rates of several competing processes, including band-edge electron-hole recombination (k_H), nonradiative recombination (k_N), deactivation of the impurity dopant (k_D), forward (k_{ET}) and back (k_{BET}) energy transfer between the host and dopant. Additionally, the competition between k_{ET} and k_{BET} is strongly influenced by (i) the energy difference (ΔE) between the host and dopant transitions, and (ii) the dopant concentration (C_D). If ΔE is positive and C_D is small or mild, both host and dopant emissions will be generated, since k_{ET} is favored and the energy transfer between host and dopant is not complete (Figure 2b). If ΔE is positive but C_D is large enough, only dopant emission will be formed, because the favored k_{ET} enables the complete energy transfer between host and dopant, quenching the host emission (Figure 2c). If ΔE is negative, only host emission will be furnished, as k_{BET} is favored and the exciton energy of host cannot be transferred to the dopant, diminishing the dopant emission (Figure 2d).

Phonon participation in cooperative energy transfer processes plays a critical role in energy migration; however, this participation is usually not considered in impurity-doped nanocrystal LEDs. One of the critical reasons for this phenomenon may be the fact that the emission mechanism becomes complicated if phonon participation is considered [57]. Therefore, following the previous impurity-doped nanocrystal LEDs [66–74], we do not consider phonon participation. Additionally, it is still somewhat controversial for the mechanism of charge-phonon interactions. Hence, further understanding and control will depend on pinpointing the molecular motions, organic/inorganic interfaces and nanocrystals phonons "bottleneck problem" that can cause substantial change to the band structure. Hence, more and new systematic and comprehensive papers are needed to study them, which is beyond the scope of this review.

3. Strategies to Achieve High-Performance Impurity-Doped Nanocrystal LEDs

3.1. Basic Aspects of Impurity-Doped Nanocrystal LEDs

Based on the above-mentioned concepts, impurity-doped nanocrystal emitters, device architectures, and emission mechanisms are three major factors which are necessary to be considered when establishing high-performance devices. However, it is important to note that these three major factors are not equally important for a specific device/application, thus understanding which of these factors play more significant role for a given material/device is important. After the preparation of LEDs, EQE is the most widely adopted parameter to determine the device performance [203–205]. In thermal-evaporated OLEDs, the EQE is generally written as follows [206–208]:

$$EQE = \eta \cdot r \cdot q \cdot \gamma \tag{1}$$

where η, r, q, and γ are the factor of outcoupling, the fraction of excitons being decayed radiatively, the PLQY of emitters, and the factor of charge balance, respectively. For solution-processed LEDs, the EML film morphology plays a key role in the performance [1]. Hence, the EQE of solution-processed LEDs (EQE') can be defined below [35]:

$$EQE' = \alpha \cdot \eta \cdot r \cdot q \cdot \gamma \tag{2}$$

where α is the factor of film morphology extracted out from γ to emphasize the effect of film roughness on the leakage current ($\gamma = \alpha \cdot \gamma'$). α is nearly not considered thanks to the extremely smooth films formed through vacuum-evaporated processes in OLEDs [209–211], while α is considered to be ≤1 in solution-processed LEDs. For $\alpha = 1$, a superior film morphology that has a negligible influence on the performance will be formed. In such cases, EQE' is equal to EQE, or else EQE' is lower than EQE. Because η is not influenced by the internal operation while r is ≈1 owing to the low energetic separation between 'bright' and 'dark' band-edge excitonic states (<25 meV) [8], the EQE' of impurity-doped nanocrystal LEDs is decided by α, q, and γ'. In other words, the film morphology is a crucial element to determine the efficiency of impurity-doped nanocrystal LEDs, aside from the consideration of emitters and the innovation of device engineering.

To evaluate whether impurity-doped nanocrystal LEDs can satisfy the demand of real commercialization, other parameters are also required to be considered, such as CE, PE, efficiency droop, operational voltage, luminance, lifetime, and color purity [212–216]. In general, CE is directly proportional to EQE. Despite CE not being an important parameter for lighting technology, it is significant to displays. Low voltages are not only essential to fulfill the high PE, since PE is inversely proportional to voltages, but also beneficial to the long lifetime, because Joule heating can be reduced [217]. Low efficiency droop is significant to practical applications, since high efficiency is required at high luminance or current density. For high luminance, enough electrons and holes are necessary to be provided for the generation of excitons, apart from the excellent charge balance [218]. Despite color purity being mainly dependent on the exploited emitters, the emissions from the neighboring CTLs should be avoided, indicating that materials with excellent charge confining ability are desirable [219]. According to these aspects, plenty of strategies to enhance the performance of impurity-doped nanocrystal LEDs have been reported, particularly for CQD-LEDs, PeLEDs, and CQW-LEDs, which will be described in the following sections.

3.2. Impurity-Doped CQD-LEDs

Impurity-doped CQD-LEDs emerged in the late 1990s [220,221]. Nevertheless, only EL spectra were usually reported at the initial stage, while negligible attention was paid to other important EL performances (e.g., EQE). One of the critical reasons is that the performance of impurity-doped CQD-LEDs is very poor at that time due to the scarce understanding of this new type of LEDs [221–224]. For example, Yang et al. used Mn-doped ZnS (2.14 mol%) as the EML to fabricate an LED with the device architecture of indium tin oxide (ITO)/PEDOT:PSS/PVK/EML/Al, where very high working

voltages (20–28 V) were needed to measure the EL spectra [225]. By step-by-step discovering the excellent properties of impurity-doped nanocrystals along with unlocking the potential of device engineering, the performance of impurity-doped nanocrystal LEDs has been vastly enhanced [226]. In particular, more attention has been paid to the factor of impurity-doped materials as compared to the factor of device architecture or emission mechanism in impurity-doped CQD-LEDs.

3.2.1. Improving the Charge Injection via Cu-Doped CQDs

A significant factor limiting the efficiency of impurity-doped CQD-LEDs is the ineffective charge injection into CQDs. In 2008, Janssen et al. demonstrated a strategy to overcome this limitation, where the charge recombination readily occurred on Cu-doped CdS CQDs when blended into the mixed matrix PVK: 2-(4-biphenylyl)-5-(4-tert-butylphenyl)-1,3,4-oxadiazole (PBD) [227]. The improved performance of doped LEDs as compared to undoped counterparts was attributed to efficient hole injection into the Cu-doped CdS CQDs via the Cu energy levels. The charge imbalance might be reduced owing to the enhanced hole injection directly into the energy levels of Cu ions located near the QD surface, leading to the high EQE. Without inorganic passivating shells, the doped LED exhibited a maximum EQE of 5.1% and a CE of 9 cd A^{-1}, which were the highest values among CQD-LEDs at that time [227]. To achieve such a high performance, it was first found that the PL spectra of Cu-doped CdS CQDs could be tuned via two ways, i.e., enhancing the amount of Cu during the synthesis, and adjusting the size of CQDs through reaction temperatures. Thus, emissions were influenced by electronic levels of Cu as well as CdS. Then, LEDs with the device architecture of ITO/PEDOT:PSS/PVK: PBD: CQDs/TPBi/Ba: Al were developed, in which 1% Cu-doped CdS CQDs were synthesized at 200 °C. The working mechanism of the LED could be summarized as follows. If the concentration of Cu-doped CdS CQDs was not high (e.g., 10%), the EL emissions of CQDs and PVK/PBD matrix could be simultaneously obtained, as shown in Figure 3a. To exclude the matrix emissions (i.e., 460 nm for PVK and 490 nm for PBD), an increased concentration of Cu-doped CdS CQDs was utilized (e.g., 30%), where only the CQD emission (620 nm) was achieved thanks to the efficient Förster energy transfer. In addition, holes were directly injected into the energy levels of Cu ions, which reduced the hole barrier since the highest occupied molecular orbital (HOMO) of PVK was better aligned with the Cu level (Figure 3b). Hence, the effective trapping of charges in LEDs resulted in the predominant CQD emissions for high efficiencies. Another key factor for the high device performance was the use of PVK/PBD matrix, since (i) PVK showed good hole-transporting ability while PBD improved the electron transporting, (ii) the UV/blue emissions emitted by PVK and PBD were well overlapped with absorption spectra of Cu-doped CdS CQDs, leading to a good Förster energy transfer upon excitons being generated at the matrix. In fact, this mixed bipolar matrix is very efficient and is also adopted by other types of LEDs. For example, Gao et al. employed PVK/PBD as the matrix to develop $MAPbBr_3$ PeLEDs with a high luminance of 10,590 cd m^{-2}, which was one of the brightest values for PeLEDs in 2006 [228].
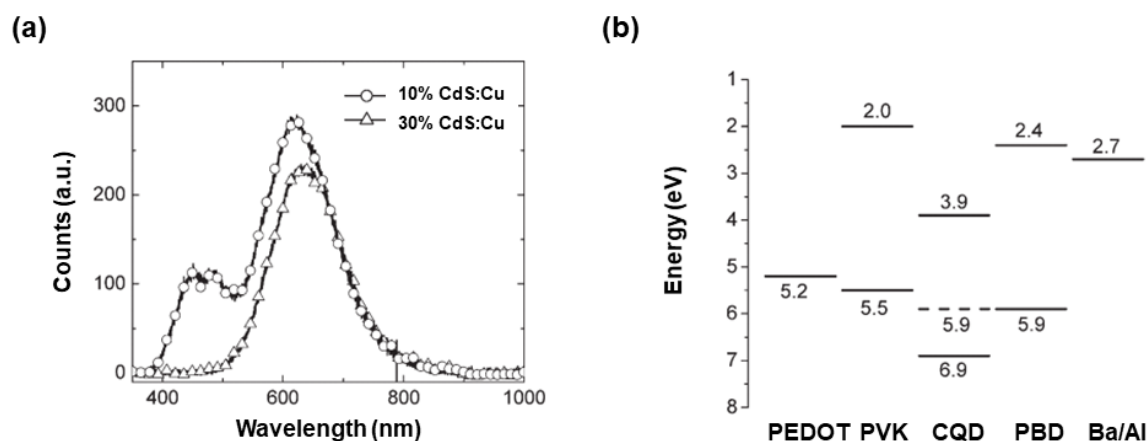
Figure 3. (**a**) Electroluminescence (EL) spectra of LEDs with 10% and 30% *w/w* Cu-doped CdS CQDs in the matrix of PVK/PBD. (**b**) Band diagram of LEDs. The dash line represented the Cu energy level. Reproduced from reference [227].

3.2.2. Increasing Solid-State Luminescence for High Device Performance

In general, solution-processed routes are used to fabricate the EMLs of nanocrystal LEDs, where solid-state EML films are formed within devices. Nanocrystals will easily suffer from luminescence quenching in solid states, despite they are highly luminescent in solutions [229–233]. Hence, an important factor to improve the performance of nanocrystal LEDs is the achievement of intense solid-state luminescence for EMLs. Toward this end, Acharya et al. reported that high concentration Cu-doped CdS with overcoated CdS shell could exhibit an excellent solid-state PLQY of ~55% [234]. To prepare the samples, copper oleate and cadmium oleate with dodecanethiol were first heated in air (for core), and then TOP-S complex solution (0.1 mmol) and cadmium oleate (0.1 mmol) were added dropwise to the nanocrystal solution at 170 °C (for shell). The samples were substantially stable in air for nearly a year, retaining bright solid-state luminescence. By using these core/shell samples as the emitters, LEDs with the device architecture of ITO/PEDOT:PSS/TPD/emitters/ZnO/Al were constructed, as shown in Figure 4. The LED responded with an outstanding low turn-on voltage below 2 V, which might be ascribed to the low oxidation potential of 0.85 V as confirmed by the cyclic voltammetry of the core/shell nanocrystals solution (inset of Figure 4c). Additionally, the resulting LED showed stable EL spectra in a broad range of working voltages. Nevertheless, the device engineering was required to be studied furhter, considering the undesirable luminance (~280 cd m^{-2}) and EQE (0.25%).

3.2.3. Exploiting Heavy-Metal-Free Impurity-Doped CQDs for LEDs

Nanocrystals show bright prospects for fabricating LEDs. However, the dependence on heavy-metal cations (e.g., Cd, Pb, and Hg) is usually required to attain high performance, which is a drawback that cannot be neglected in nanocrystal LEDs [235–239]. To solve this issue, a strategy is to develop heavy-metal-free nanoemitters. Ternary chalcogenide compounds AB_mC_n are promising as environmental-friendly and nontoxic alternatives thanks to the amazing composition-tunable optical and electronic characteristics [240]. So far, plenty of ternary chalcogenide compounds have served as hosts, such as Zn-In-Se, Zn-Cd-S, and ZnS/Zn-Cd-S [241–243]. However, impurity-doped heavy-metal-free CQDs usually exhibit narrow emission ranges and intermediate efficiencies. For example, Cu-doped Zn-In-Se CQDs only covered from 540 to 660 nm (120 nm) with a PLQY of 30% [244]. Thus, efficient impurity-doped heavy-metal-free CQDs with a large emission range are desirable.
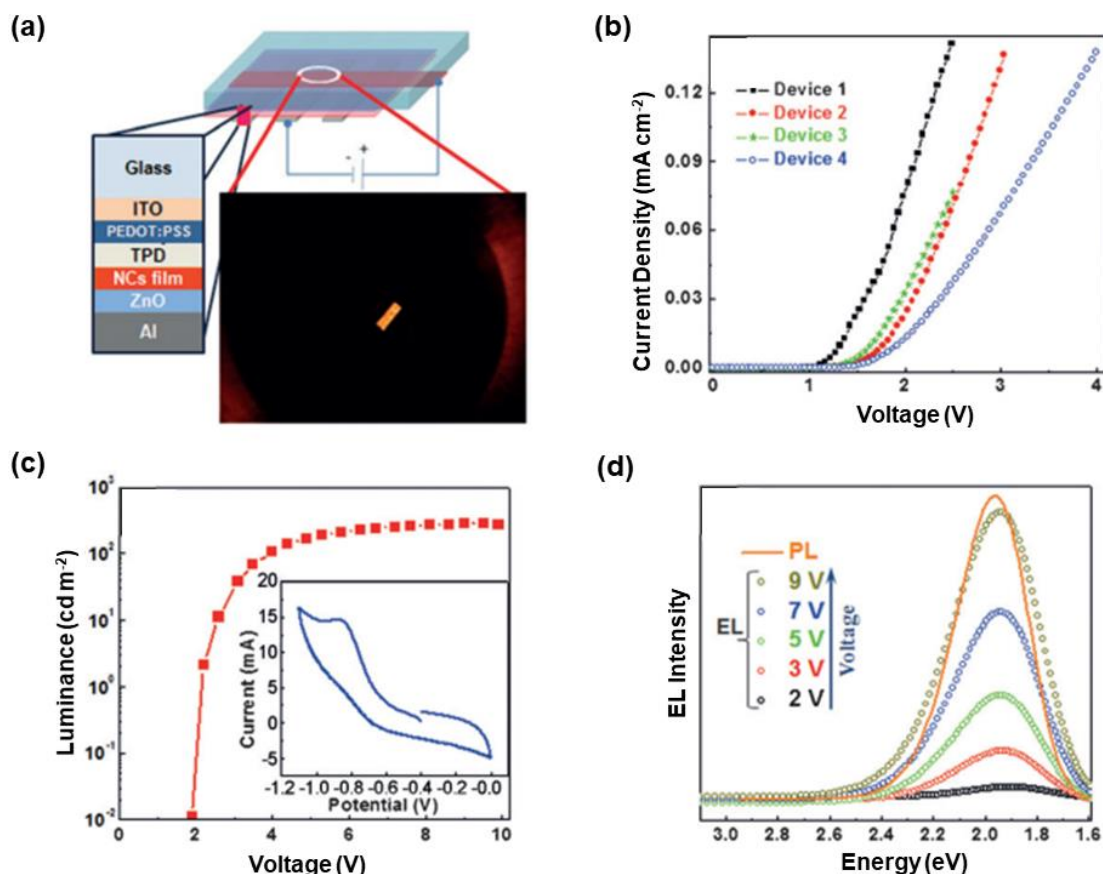
Figure 4. (**a**) Device architecture and photograph of a LED at 5 V. (**b**) Current density of LEDs. (**c**) Luminance of LEDs. Inset: Cyclic voltammetry of the core/shell samples in N_2-purged dichloromethane solution. (**d**) EL spectra with increasing voltages. Reproduced from reference [234].

To loosen the above bottleneck, Zhong et al. established LEDs by using color-tunable highly bright PL of Cu-doped Zn-In-S CQDs [245]. A critical reason for the improved performance of doped LEDs as compared to undoped counterparts might be the excellent PLQY of Cu-doped Zn-In-S CQDs. By virtue of a one-pot noninjection synthetic method, metal acetate salts, sulfur powder, and dodecanethiol in oleylamine media were heated for Cu-doped Zn-In-S cores. ZnS shell was directly overcoated in the crude reaction solution, leading to Cu-doped Zn-In-S/ZnS core/shell CQDs showing composition-tunable emissions over a large spectral window (450–810 nm). The PLQY could be up to 85%, which was not only the best one for transition-metal-doped nanocrystals but also among the highest luminescent semiconductor nanocrystals at that time. With the efficient yellow-emission (580 nm) Cu-doped Zn-In-S/ZnS core/shell emitters, LEDs with the device architecture of ITO/PEDOT:PSS (10 nm)/poly-TPD (40 nm)/emitters/TPBi (40 nm)/LiF (0.5 nm)/Al (100 nm) were fabricated, as shown in Figure 5. Compared with the PL spectrum, the full width at half-maximum (FWHM) of EL spectrum was only a little wider. Hence, EL emissions were mainly derived from CQDs. The turn-on voltage was 3.6 V, lower than that of the previous lowest $CuInS_2$-based CQD-LEDs (4.4 V) [246]. The peak luminance reached 220 cd m^{-2}. The CE of 2.45 cd A^{-1} and PE of 2.14 lm W^{-1} were also higher in comparison with $CuInS_2$-based CQD-LEDs [246,247]. Thus, Cu-doped Zn-In-S/ZnS core/shell CQDs may be potentially excellent heavy-metal-free candidate LED emitters. In fact, Cu-Zn-In-S nanocrystals have been extensively used in various technologies (e.g., photocatalyst for H_2 generation) [248–251]. In addition, ternary chalcogenide Zn-In-S has been found to be a near-ideal host for various impurities because of the excellent chemical stability, well-developed synthetic method, and composition-tunable bandgap [252]. For instance, Chen et al. doped Ag into Zn-In-S hosts, realizing Ag-Zn-In-S quaternary CQDs with outstanding optical characteristics [253].
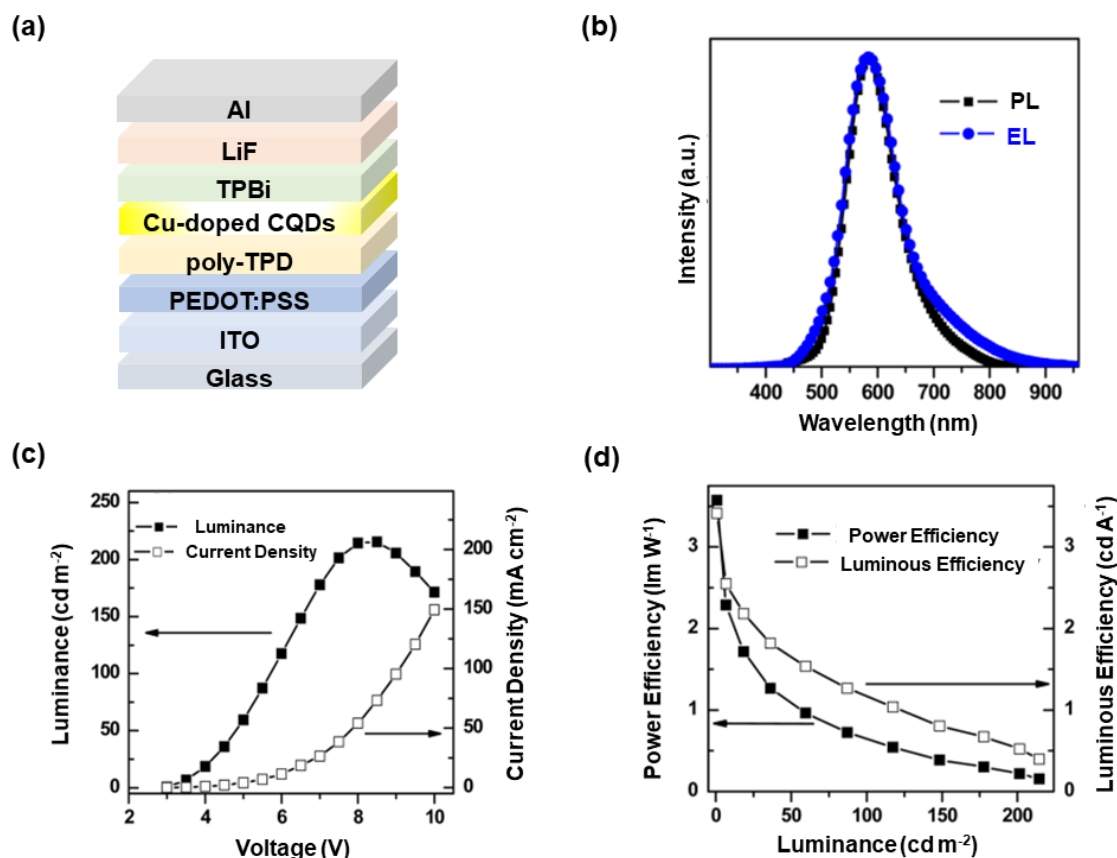
Figure 5. (**a**) Device architecture of LEDs. (**b**) PL spectra and corresponding EL of Cu-doped Zn-In-S/ZnS with yellow emissions. (**c**) Current density and luminance of LEDs. (**d**) CE and PE of LEDs. Reproduced from reference [245].

3.3. Impurity-Doped PeLEDs

In 2014, the first successful organic-inorganic hybrid $MAPbBr_3$ PeLED was reported [18]. In 2015, the first all-inorganic PeLED was developed [19]. In 2016, the first bright $FAPbBr_3$ PeLED was demonstrated [254]. Since then, the development of PeLEDs has flourished. Currently, the EQE of both hybrid and all-inorganic PeLEDs can exceed 20%, indicating the huge potential for optoelectronic applications [255]. However, the stability of PeLEDs may need to be further improved, given that the longest lifetime was only ~250 h at 100 cd m^{-2} for all-inorganic PeLEDs in 2019 [174]. In addition, the luminance of red and blue PeLEDs is still not satisfactory enough. For example, Kido et al. realized all-inorganic PeLEDs with an EQE of 21.3%; nevertheless, the lifetime was only 3 h at 100 cd m^{-2} and the maximum luminance was only 794 cd m^{-2} [27]. Furthermore, it is still a challenge for blue PeLEDs to achieve high efficiency, although both green and red PeLEDs can exhibit EQEs ≥20%. Moreover, the high toxicity of lead may hinder the commercial applications.

One of the effective approaches to overcome the above restrictions is the exploitation of impurity-doped ABX_3 perovskites to develop PeLEDs. Generally, the poor thermal stability issue exists in organic-inorganic hybrid perovskites because of volatile organic A-site cations (e.g., MA$^+$, FA$^+$), which is probably resolved by replacing organic cations with inorganic Cs$^+$ [256–260]. In the case of B-site cations, although the whole substitution of Pb^{2+} with other metal ions usually causes poor optoelectronic characteristics (e.g., Ge^{2+}, Sn^{2+} will be readily oxidized to +4 states), the partial substitution (from doping to alloying) is possible to enhance the thermal and phase stability [261–264]. In particular, both isovalent/divalent and heterovalent cations can be used to partially replace the Pb^{2+} ions in the lattice structure of perovskites. Meanwhile, the toxicity is reduced [265]. For X-site anions, mixed halide systems (Cl/Br, Br/I) are commonly used to tune the emissions (e.g., yellow

and orange emissions are generated by AB(Cl/Br)$_3$ [19]. In fact, X-site doping or halogen-doping is the predominant and most well-known strategy to develop various-color PeLEDs. Therefore, A-, B-, and X-site doping can amazingly broaden the applications of perovskites. In brief, A- or B-site doping is commonly exploited to reduce the trap state, diminish the nonradiative recombination, and enhance the stability, while X-site doping is mainly employed to tune the emission colors [266–269]. Hence, it is easy to note that the current research focus is the factor of impurity-doped materials in impurity-doped PeLEDs. Based on these facts, strategies to boost the device performance of red, green, and blue PeLEDs are generally focused on A- and B-site doping, which will be introduced in the below sections.

3.3.1. Approaches to Achieve Impurity-Doped Red PeLEDs

The A-site doping strategy for red PeLEDs was first noticed by Rogach et al., where doping and surface passivation of CsPbI$_3$ films with silver simultaneously occurred [270]. A key factor to realize this approach was the design of a special device architecture, which was formed by Ag (cathode)/ZnO/polyethylenimine (PEI)/CsPbI$_3$/TCTA/MoO$_3$/Au/MoO$_3$ (anode), as shown in Figure 6. In such devices, Ag cathode not only lowered the electron injection barrier, but also provided Ag$^+$ ions which diffused into the lattice structure of CsPbI$_3$ for Ag-doped perovskites. Hence, Ag$^+$ partially substituted Cs$^+$ in CsPbI$_3$ for the stabilization, while passivation of CsPbI$_3$ surface with Ag$^+$ converted nonradiative trap states into radiative states for enhancing the PLQY and stability. Hence, the factor of device architecture enabled the efficient impurity doping. Compared with PeLEDs with ITO cathode, the maximum EQE of Ag-based PeLEDs was enhanced from 7.3% to 11.2% and the stability of nonencapsulated devices was improved in both the nitrogen and the ambient atmosphere. For the MoO$_3$-1/Au/MoO$_3$-2 (MAM) trilayer, 20 nm MoO$_3$-1 was the HIL, 10 nm Au ensured high transparency and good conductivity, and 25 nm MoO$_3$-2 reduced the light reflection at the Au/air interface. The transmittance of MAM at 690 nm was increased from 57% to 67% due to the similar EL emission of CsPbI$_3$. Additionally, the resistance of MAM was as low as 15 Ω sq^{-1}. As a consequence, the best-performing devices showed the maximum EQE of 12.1%, which was the highest among CsPbI$_3$ PeLEDs at that time [270]. In fact, metal oxide/metal/metal oxide electrodes have been broadly studied in OLEDs owing to the high transparency and low resistance [271–273].

The B-site doping strategy for red PeLEDs was also reported by Rogach et al., where SrCl$_2$ was selected to be a co-precursor to improve the efficiency and stability of CsPbI$_3$ [274]. A key factor to achieve this approach was the design of material syntheses, in which the introduction of co-precursor SrCl$_2$ played a crucial role in the synthesis of CsPbI$_3$. For example, the PLQY of CsPbI$_3$ was improved from 65% to 84% when the synthetic ratio of SrCl$_2$: PbI$_2$ was equal to 0.1 (CsPbI$_3$-0.1). In such synthesis, the Sr^{2+} doping owing to the smaller ion radius of 1.18 Å for Sr^{2+} (1.19 Å for Pb^{2+}) and surface defect states of Cl$^-$ passivation (converting nonradiative trap states to radiative states) simultaneously occurred. With Sr^{2+} cations, the stability of perovskites was enhanced due to the increased formation energy and thus the slightly improved environment tolerance. Importantly, the hole transporting characteristic of CsPbI$_3$-0.1 was better than that of pristine CsPbI$_3$, which resulted in enhanced charge balance, as confirmed by electron-only and hole-only devices. PeLEDs were developed with the device architecture of ITO/ZnO/PEI/perovskites/TCTA/MoO$_3$/Au, where CsPbI$_3$-0.1 and pristine CsPbI$_3$ were emitters, as shown in Figure 7. Although the turn-on voltage of CsPbI$_3$-0.1 and pristine CsPbI$_3$-based PeLEDs was similar (~2.0 V), the maximum luminance and EQE of CsPbI$_3$-0.1-based PeLEDs (1152 cd m^{-2} and 13.5%) were much higher than those of pristine CsPbI$_3$-based PeLEDs (510 cd m^{-2} and <8%). Additionally, the operational stability of CsPbI$_3$-0.1-based PeLEDs was enhanced thanks to the addition of SrCl$_2$ [274]. Recently, Yao et al. also demonstrated that the Sr^{2+} substitution was very effective, which could be used to enhance the efficiency and stability of red α-CsPbI$_3$ PeLEDs [275]. For example, the maximum EQE of 5.92% was obtained for Sr^{2+}-substituted-based PeLEDs, which was three-fold higher than that of unsubstituted PeLEDs [275].
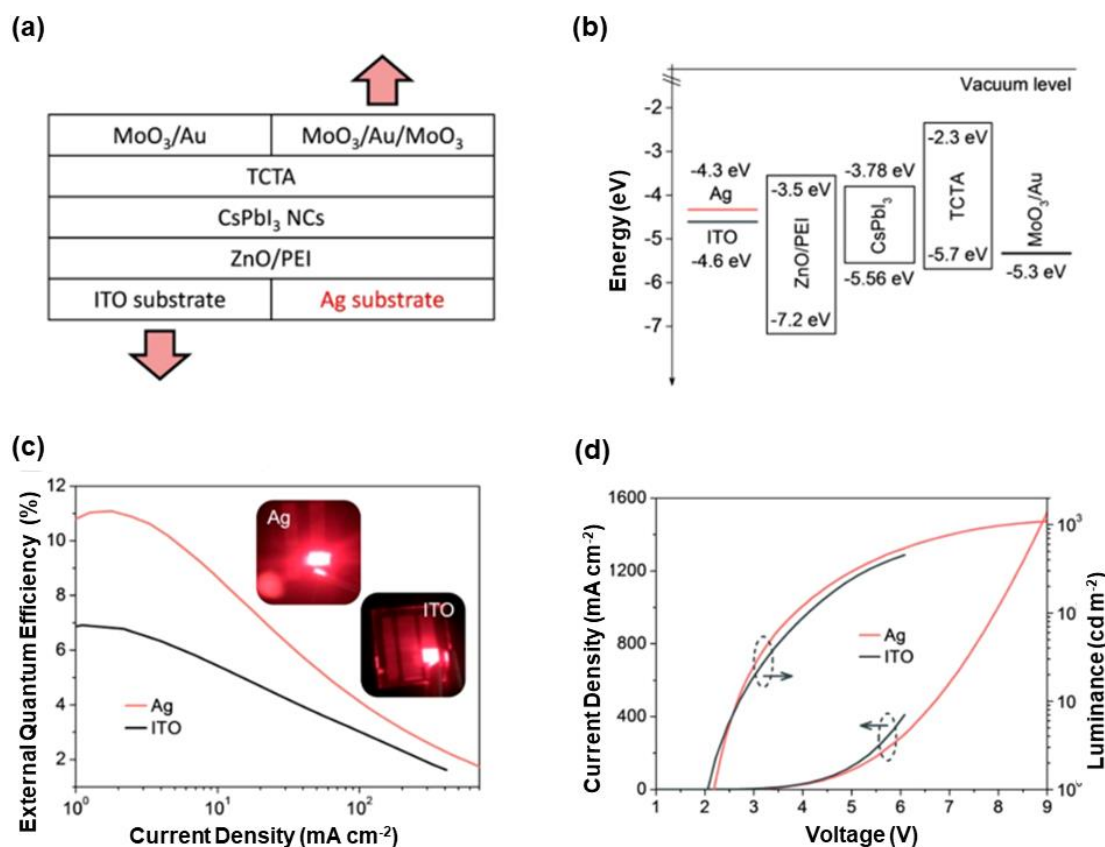
Figure 6. (**a**) Device architectures of PeLEDs with ITO and Ag. Red arrows suggested the transparent side. (**b**) Energy level diagram. (**c**) External quantum efficiency (EQE) of LEDs with Ag and ITO. Inset: photographs of working devices. (**d**) Current density and luminance. Reproduced from reference [270].

Besides the Sr^{2+} B-site doping, other isovalent cations are also reported to partly replace the Pb^{2+} ions in the lattice structure of red perovskites for high-performance PeLEDs, such as Zn^{2+}, Mn^{2+}, and Cu^{2+} [276–278]. For instance, Song et al. used a zinc non-halide dopant approach to study the effect of Zn^{2+} on $CsPbI_3$, where Zn-doped $CsPbI_3$ showed 120% higher PLQY than pristine $CsPbI_3$ [279]. As a result, PeLEDs using Zn-doped $CsPbI_3$ exhibited approximately two times higher EQE (14.6%) versus control PeLEDs. On the other hand, heterovalent elements B-site doping (e.g., Bi^{3+}, Eu^{3+}, and Gd^{3+}) is another significant scheme to prepare red perovskites for PeLEDs possessing enhanced optoelectronic performance [280]. For example, Demir et al. discovered that Gd^{3+} doping could result in enhanced PLQY, increased PL lifetime, and improved α-phase stability of $CsPbI_3$ because of the distorted cubic symmetry, reduced defect density, and increased Goldschmidt's tolerance factor [281]. In addition, both the isovalent and the heterovalent B-site doping strategies have been extensively applied to green and blue perovskites.
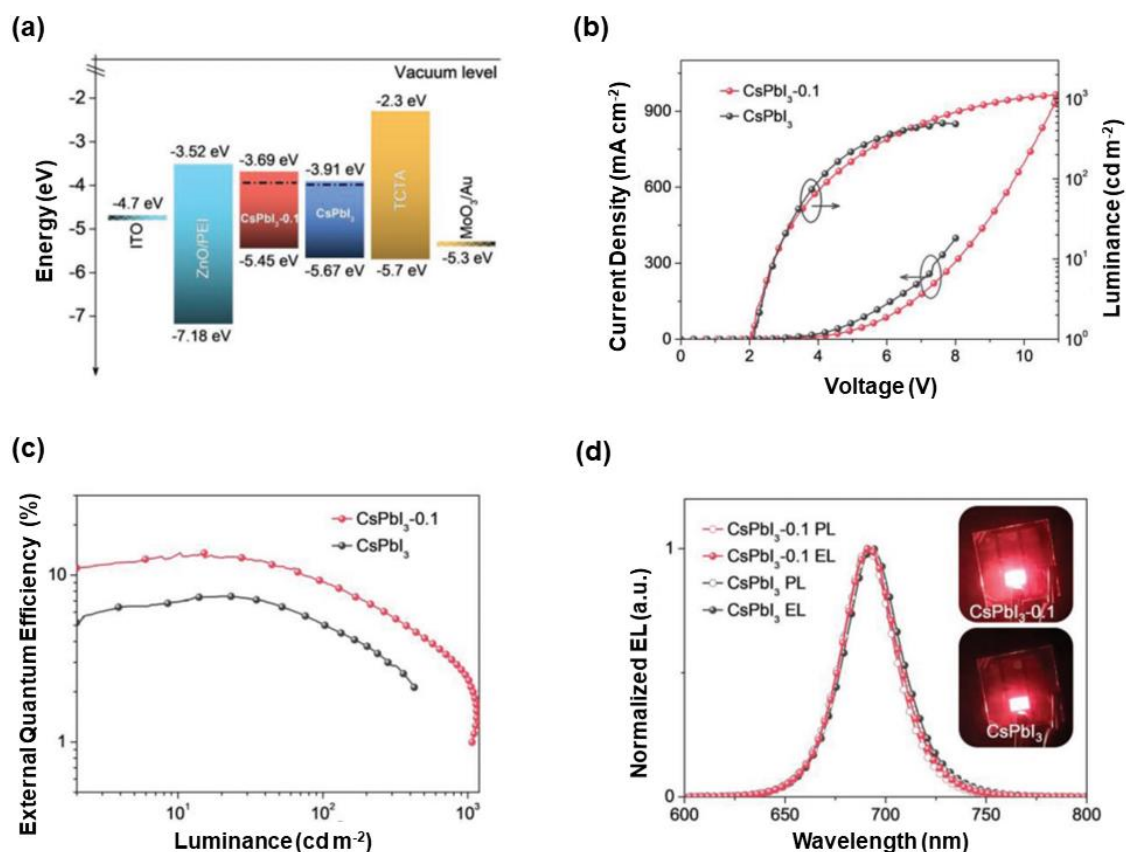
Figure 7. (**a**) Energy level diagram of PeLEDs. (**b**) Current density and luminance the $CsPbI_3$ and $CsPbI_3$-0.1 PeLEDs. (**c**) EQE of PeLEDs. (**d**) PL and EL spectra of PeLEDs. Inset: photographs of working devices. Reproduced from reference [274].

3.3.2. Methods to Obtain Impurity-Doped Green PeLEDs

Currently, the efficiency of organic cation (e.g., FA^+, MA^+)-based PeLEDs is comparable to that of state-of-the-art OLEDs. Nevertheless, organic cation-based perovskites are usually criticized due to the inherent instability, including easy sensitivity to oxygen, moisture, and temperature. Such instability originates from the chemical noninertness of organic cations coupled with the underlying weak interaction between cations and surrounding halides because of the eight equivalent orientations of the cation along the body diagonals in the unit cell, which hinders the future applications [282–286]. To overcome this issue, a popular A-site doping method in green PeLEDs was the mixture of organic cations and alkali metal cations (e.g., Cs^+, Rb^+, K^+, Na^+). For example, the relatively small ionic radius of 1.81 Å for Cs (e.g., 2.79 Å for FA, 2.70 Å for MA) is conductive to assist the crystallization of the black phase of FA perovskites because of the entropic stabilization [287]. With alkali metal doping, a superior stability, higher PLQY, longer exciton lifetime, less exciton binding energy, lower trap density, better crystallinity, and more tuned tolerance factor can be accomplished [288–290]. Furthermore, alkali metal halides can passivate the grain boundaries and interface states and fill the dangling bond, averting the fluorescence quenching [291]. Moreover, alkali metals are oxidation-stable A-site cations that avoid perovskite electronic property distortion because of oxidation-prone Pb/Sn mixtures [292]. Therefore, by taking the advantages of alkali-metal-doped perovskites, high-performance green PeLEDs can be expected.

Sun et al. took the first step to develop green PeLEDs by utilizing mixed-cation perovskite emitters, where cations in $FA_{(1−x)}Cs_xPbBr_3$ were formed by partially substituting FA^+ with Cs^+ during the synthesis process (i.e., FABr and $PbBr_2$ were precursors, while CsBr provided Cs^+ doping) [293]. Two major aspects, chemical composition engineering of $FA_{(1−x)}Cs_xPbBr_3$ and PeLED application, were highlighted in their work. First, the chemical composition of $FA_{(1−x)}Cs_xPbBr_3$ with various ratios

of FA/Cs was studied to ensure outstanding optical characteristics, including high PLQY, narrow emission, and tunable bandgap. Then, PeLEDs were fabricated with the device architecture of ITO/PEDOT:PSS, poly[(9,9-dioctylfluorenyl-2,7-diyl)-co-(4,4′-(N-(4secbutylphenyl)diphenylamine)] (TFB)/perovskites/TPBi/LiF/Al, as shown in Figure 8. A key factor to achieve the high device performance was the matching of energy levels. This was because electrons were injected from the lowest unoccupied molecular orbital (LUMO) of TPBi into the CBM of perovskites, while holes were transferred from the HOMO of TFB into the VBM of perovskites. The VBM of $FA_{(1-x)}Cs_xPbBr_3$ could be gradually lowered with the Cs^+ increasing, facilitating the hole injection thanks to the reduced barrier at the TFB/perovskite interface. As a result, the optimized $FA_{(1-x)}Cs_xPbBr_3$ PeLED exhibited the maximum luminance and CE of 55,005 cd m^{-2} and 10.09 cd A^{-1}, respectively, suggesting 6.4- and 3.7-fold higher than $FAPbBr_3$ PeLEDs. In particular, the luminance of 55,005 cd m^{-2} was the highest for nanocrystal PeLEDs at that time, which resulted from the proper energy level, homogeneous film morphology, and the improved stability of perovskites.
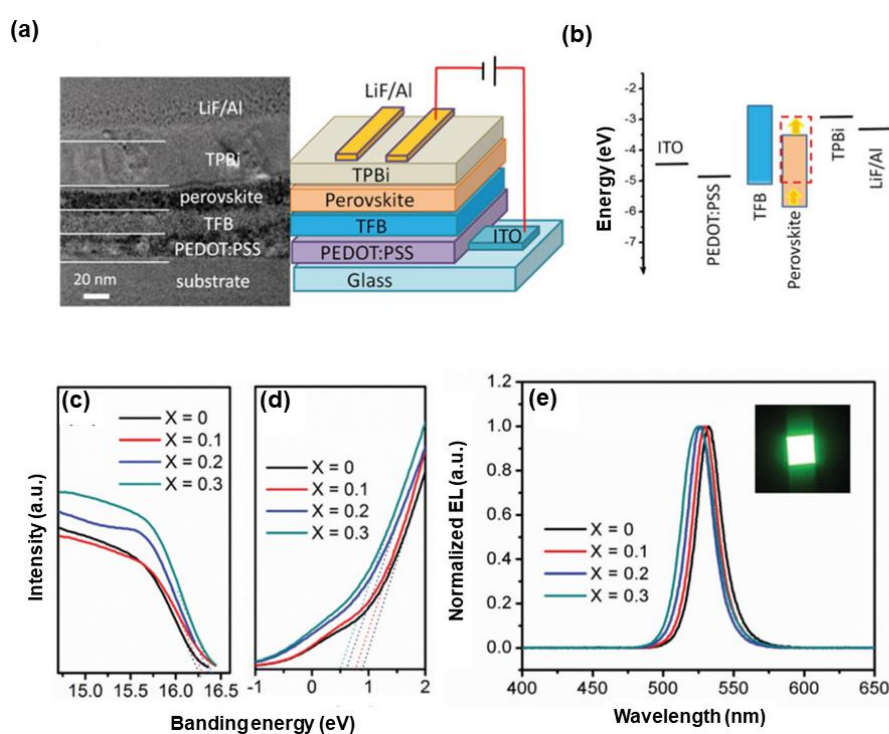

Figure 8. (**a**) Schematic illustration and cross-section of PeLEDs. (**b**) Energy band diagram. (**c**) High-binding energy secondary-electron cutoff regions of perovskite nanocrystals. (**d**) Valance band (VB)-edge region of perovskites. (**e**) EL spectra and photograph, driven at 4 V, for PeLEDs. Reproduced from reference [293].

Later, Wu et al. found that Rb^+ doping has a great influence on the crystal growth, structure, photoelectric, and optical characteristics of $FAPbBr_3$, which importantly improved the PLQY of $FAPbBr_3$ film (~10-fold) on account of the substantially suppressed trap density [73]. Hence, the maximum luminance and CE of PeLEDs with Rb-doped $FAPbBr_3$ were improved by ~10-fold and ~5-fold to 66,353 cd m^{-2} and 24.22 cd A^{-1} compared to the controlled devices, respectively, which were the highest for $FAPbBr_3$-based PeLEDs at that time. On the other hand, the realization of Cs^+ doping in MA-based perovskites [294], MA^+ doping in FA-based perovskites [295], and FA^+ doping in Cs-based perovskites [296] have also been demonstrated to be effective methods to considerably enhance the performance of green PeLEDs.

In the case of B-site doping for green PeLEDs, the partial replacement of Pb^{2+} with isovalent or heterovalent cations via well-designed synthetic methods is also effective in enhancing the device performance, which is similar to the situation in impurity-doped red PeLEDs. For example,

the maximum EQE was increased from 0.81% for pure $CsPbBr_3$ PeLEDs to 1.49% for Mn^{2+}-doped $CsPbBr_3$ PeLEDs [297], while the EQE was improved from 1.6% for pure $CsPbBr_3$ PeLEDs to 4.4% for Ce^{3+}-doped devices [298]. Additionally, the maximum luminance was enhanced from 4727 cd m^{-2} for pure $CsPbBr_3$ PeLEDs to 12,500 cd m^{-2} for Sn^{4+}-doped PeLEDs [299]. Remarkably, the maximum CE of Mg^{2+}-doped $CsPbBr_3$ PeLEDs was up to 13.13 cd A^{-1}, which was a ~100-fold improvement compared to undoped counterparts [300]. In particular, Sn^{2+} doping in $CsPbBr_3$ is easier relative to many other divalent ions (e.g., Cd^{2+}, Co^{2+}, Zn^{2+}, Sr^{2+}) since $CsSnBr_3$ and $CsPbBr_3$ possess similar ABX_3-type perovskite crystalline structures [301–303]. Nevertheless, Sn^{2+}-based $CsSnX_3$ is unstable since Sn^{2+} easily oxidizes to Sn^{4+}, resulting in low PLQY [304]. Hence, the highly conductive and stable Sn^{4+} doping in $CsPbBr_3$ is more approximate than Sn^{2+} doping for PeLEDs [299].

3.3.3. Ways to Fulfill Impurity-Doped Blue PeLEDs

Compared with impurity-doped red and green PeLEDs, relatively little attention has been paid to impurity-doped blue PeLEDs. This may be because it is more difficult to synthesize high-performance blue perovskites together with the fact that it becomes harder to manipulate the device engineering due to the wide bandgap of blue emitters [305–308]. Encouragingly, B-site doping has been found to be a crucial way to fulfill high-performance blue PeLEDs [309]. In particular, Mn^{2+} doping is widely adopted to enhance the performance of blue all-inorganic perovskites [310,311]. The key reasons may be (i) identical octahedral coordination environment of host cations surrounded by six halide atoms for $CsPbX_3$ and $CsMnX_3$, (ii) higher formation energies of $CsMnX_3$ than those of $CsPbX_3$ to avoid the thermal instability issue that is associated with the intrinsically low formation energies of perovskite lattices, iii) smaller ion radius of Mn^{2+} (~0.97 Å) [312–314].

The first successful Mn-doped blue PeLEDs was reported by Congreve et al., where a small amount of Mn^{2+} increased the PLQY over three-fold for $CsPbCl_3$ films (28%) without an Mn-emission peak [315]. A significant point to achieve this method was the realization of the high blue color purity, since the band-edge emission not only competed with nonradiative recombination but also transferred energy to Mn^{2+} for Mn emissions. By employing a two-step synthetic scheme to adjust Mn^{2+} doping, the PLQY and lifetime were increased while trap states were reduced. In addition, perovskites became more monodisperse, narrowing the emission bandwidth. PeLEDs were constructed with the device architecture of ITO/PEDOT:PSS/TFB/PFI/perovskites/TPBi/LiF/Al, where Mn-doped $CsPbCl_3$ was blue perovskite emitters, as shown in Figure 9. Mn emissions disappeared in such devices, since the very long emissive lifetime of Mn^{2+} saturated the emission in the thin EML layer and TFB may further lower Mn emission, enabling the mild doping for enhanced performance without sacrificing color purity. Compared with undoped PeLEDs, the maximum of EQE of PeLEDs with the 0.19% Mn doping showed a four-fold improvement, reaching 2.12%, which was the highest for blue PeLEDs at that time [315]. Later, Congreve group also demonstrated that Mn^{2+} doping could enhance the luminance, efficiency, and stability of bulk sky-blue $CsPbBr_{1.9}Cl_{1.1}$ PeLEDs [316]. In this work, a maximum luminance of 11,800 cd m^{-2} was yielded, which was among the highest for blue PeLEDs. More recently, Song et al. reported that the maximum EQE of Ni^{2+}-doped blue $CsPbBr_{0.99}Cl_{2.01}$ PeLEDs was up to 2.4%, which was the best for blue $CsPbX_3$ PeLEDs [317].
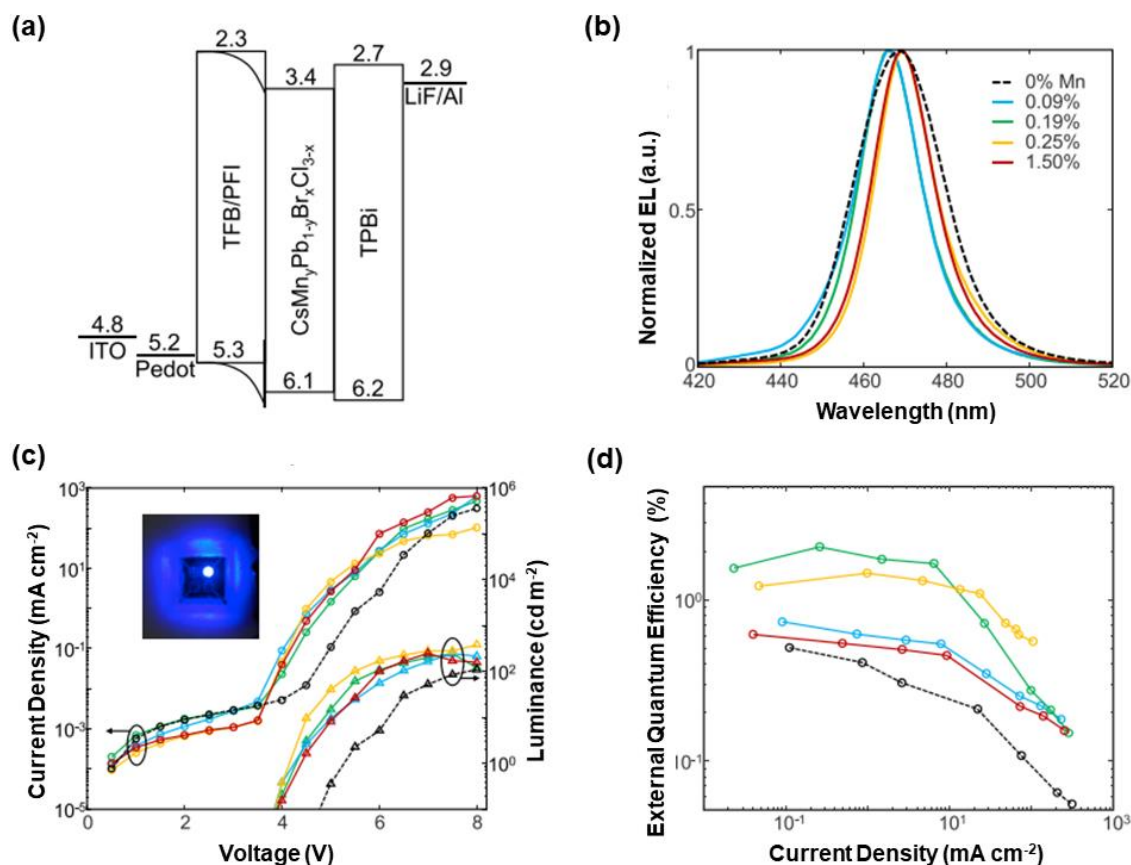
Figure 9. (**a**) Device architecture and energy levels of PeLEDs. (**b**) EL spectra of PeLEDs with varying Mn content. (**c**) Current density–voltage–luminance characteristics. Inset: an image of the 0.19% Mn device. (**d**) EQE of PeLEDs. Reproduced from reference [315].

3.4. Impurity-Doped CQW-LEDs

Since the first demonstration of CQW-LEDs in 2014 [34], the investigation of this new type of LEDs has been thriving. Various kinds of CQWs have been attempted as the emitters for LEDs, such as core-only, core/crown, and core/shell CQWs [35,72,125,318–322]. Nevertheless, it is important to point out that the development of CQW-LEDs is still in its infant stage. On one hand, neither blue nor yellow CQW-LEDs have been reported up to now. In particular, efficient blue CQWs are difficult to synthesize, which restricts the realization of blue CQW-LEDs. On the other hand, some significant parameters (e.g., CE, PE, luminance, and lifetime) to judge the performance of CQW-LEDs lag far behind other types of advanced LEDs, including OLEDs, CQD-LEDs, and PeLEDs. For example, the maximum PE of CQW-LEDs is 9.44 lm W^{-1} [125], which is much lower than that of OLEDs surpassing 100 lm W^{-1} [323–325]. Fortunately, CQW-LEDs can exhibit superior color purity on account of the strong quantum confinement solely in the vertical direction for CQWs [326–328]. In addition, the maximum EQE of CQW-LEDs can be close to 20% via the understanding of the shape-, composition- and device-engineering [35]. Furthermore, the easy solution-processed fabrication procedures and good compatibility with flexible electronics enable CQW-LEDs to satisfy the low-cost commercial requirements. All these encouraging characteristics render CQW-LEDs able to offer great potential for the optoelectronic applications.

In terms of impurity-doped CQW-LEDs, only one work has been reported to date [72]. Specifically, Liu et al. revealed the Cu-doping effect in LEDs through controlling the Cu concentration in CdSe CQWs. The improved performance of doped LEDs as compared to undoped counterparts was ascribed to: (i) the better PLQY of Cu-doped CQWs, (ii) an advanced emission mechanism since two decay channels for exciton recombination simultaneously occurred in Cu-doped CQW-LEDs. CQW-LEDs

were established with the device architecture of ITO/ZnO/emitters/4,4-N,N-dicarbazolebiphenyl (CBP) or 1-bis[4 -[N,N-di(4-tolyl)amino]phenyl]-cyclohexane (TAPC)/MoO$_3$/Al, where CQWs with different doping concentrations served as the emitters, CBP and TAPC HTLs were used to understand the device engineering. Firstly, CQW-LEDs with 0% Cu-doped concentration exhibited the narrow EL FWHM of 12 nm and the Commission Internationale de L'Eclairage (CIE) 1931 coordinates of (0.103, 0.797), rendering than the color gamut covered 104% of the International Telecommunication Union Recommendation BT 2020 (Rec. 2020) standard in the CIE 1931 color space. Secondly, CQW-LEDs with 0.5% Cu-doped concentration possessed dual emission with an EQE of 0.146% (Figure 10), demonstrating that impurity doping was an effective strategy to vastly enhance the performance (i.e., realizing nine-fold higher EQE than a 0% concentration-based device). Importantly, the dual emission could be tuned by manipulating the device engineering, since two decay channels for exciton recombination existed (i.e., excitons were recombined from electrons at CdSe CBM with holes at Cu level to produce Cu$^+$ emission or holes at CdSe VBM for CdSe emission). In the case of CBP-based CQW-LEDs, the Cu$^+$ emission was lowered with increasing voltage. In greater detail, the charge trapping issue existed in the doped LEDs, since holes transported from CBP were more easily trapped by Cu under a low electrical field while saturated at high voltages due to the high Cu level (5.05 eV) compared with CdSe VBM (5.69 eV), resulting in relatively more holes transported from CBP being injected into the VBM of CdSe after saturation at the dopant site. Hence, a lower current density in doped LEDs was obtained as compared to undoped counterparts. Furthermore, the ideality factor for the doped LEDs was nearly twice that of undoped counterparts, suggesting that Cu-doping was an impurity defect site.
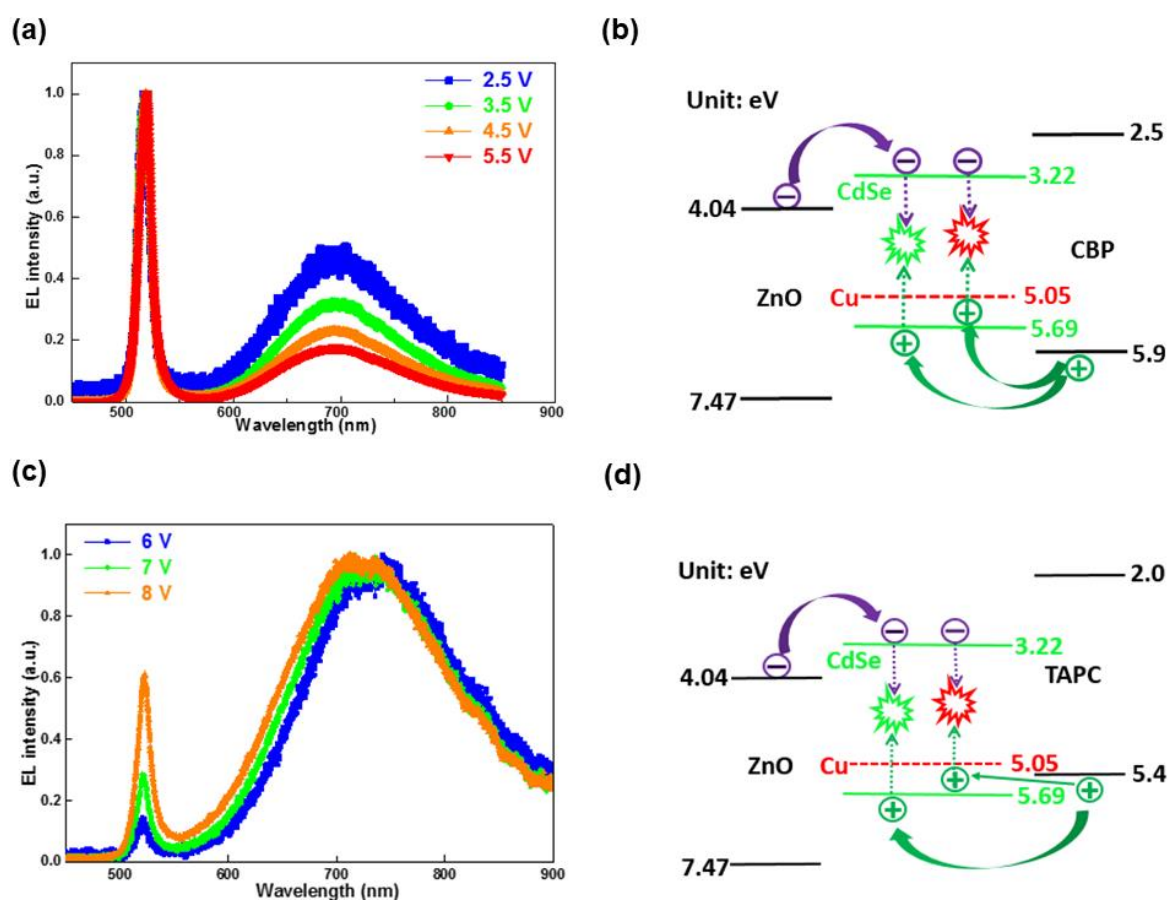

Figure 10. (**a**) EL spectra at various voltages, and (**b**) emission mechanism for CQW-LEDs with 0.5% Cu-doped concentration (CBP HTL). (**c**) EL spectra at various voltages, and (**d**) emission mechanism for CQW-LEDs with 0.5% Cu-doped concentration (TAPC HTL). Reproduced from reference [72].

For TAPC-based CQW-LEDs, the EL emission peak of CdSe was lower than that of Cu^+, since holes were readily injected into Cu due to the barrier-free characteristic between the HOMO of TAPC (5.4 eV) and Cu level while the existing hole barrier between TAPC and CdSe. Finally, a white LED based on CQWs was explored, in which a high Cu-doped concentration of 2.4% was used. Such findings could be further extended to other impurity (e.g., Mn, Ag)-doped CQWs to realize LEDs, considering the well-developed impurity-doped CQD-LEDs and PeLEDs. Therefore, the factor of impurity-doped materials played a significant role in improving the efficiency and stability, while the factor of device architecture affected the emission mechanism in impurity-doped CQW-LEDs.

4. Summary and Outlook

By virtue of impurity doping, the electronic, optical, catalytic, transporting and magnetic properties of nanocrystals can be controlled to satisfy the requirement of optoelectronic and microelectronic applications. With the gradual comprehending of the effect of impurity doping (e.g., enhancing synthesis control over impurity incorporations, studying the concentrations, and exploring emerging phenomena), the development of impurity-doped nanocrystal LEDs is flourishing [329–331]. Nowadays, impurity-doped nanocrystal LEDs can possess many exceptional merits (e.g., enhanced efficiency, improved luminance, reduced driving voltage, and prolonged lifetime), making them highly promising for the future-generation displays, lighting, and signaling. Remarkably, the efficiency of state-of-the-art impurity-doped nanocrystal LEDs is comparable to that of the best undoped counterparts. In this review, we have mainly focused on the recent progress in the realization of impurity-doped CQD-LEDs, impurity-doped PeLEDs, and impurity-doped CQW-LEDs. In particular, we have emphasized various representative strategies to boost the device performance, including (i) improving the charge injection, increasing solid-state luminescence, and exploiting heavy-metal-free dopant for impurity-doped CQD-LEDs; (ii) A- and B-site doping for red, green and blue PeLEDs; (iii) the establishment of impurity-doped CQW-LEDs. More specific performances of impurity-doped nanocrystal LEDs are given in Table 1.

Table 1. Performances for representative impurity-doped nanocrystal LEDs.

Emitters [a]	V_{on} [b] (V)	EQE_{max} [c] (%)	PE_{max} [d] (lm W^{-1})	CE_{max} [e] (cd A^{-1})	L_{max} [f] (cd m^{-2})	Reference
CQDs	4.2	5.1	-	9.0	300	[227]
CQDs	2.0	0.25	-	-	280	[234]
CQDs	3.6	-	2.14	2.45	220	[245]
Perovskites	~2.2	12.1	-	-	1106	[270]
Perovskites	2.0	13.5	-	-	1152	[274]
Perovskites	3.5	2.8	-	10.09	55,005	[293]
Perovskites	-	2.12	-	-	245	[315]
CQWs	2.4	0.146	0.179	0.282	1153	[72]

[a] Impurity-doped nanocrystal emitters in LEDs. [b] Turn-on voltage. [c] Maximum EQE. [d] Maximum PE. [e] Maximum CE. [f] Maximum luminance.

After extensive efforts made by researchers worldwide, the performance of impurity-doped nanocrystal LEDs has been gradually improved. Given the facile solution-processed fabrication procedures, it is believed that impurity-doped nanocrystal LEDs can be well applied to low-cost flexible electronics and transparent products [332–334]. Additionally, the performance of impurity-doped nanocrystal LEDs is projected to be further enhanced if outcoupling technologies can be used, since only approximate 20% light is extracted from the substrate according to the classical ray optical model [335]. Furthermore, impurity-doped white nanocrystal LEDs may be anticipated by designing emitters with polychromatic emissions or utilizing effective device architectures (e.g., the mixture of blue, green and red impurity-doped nanocrystals in single EML unit, and the combination of various-color nanocrystals in tandem devices [336–338]), which will further broaden their real applications. Moreover, the development of impurity-doped nanocrystal LEDs is expected to shed

light on the other EL applications, such as alternating current thin-film electroluminescent device [339], and light-emitting field-effect transistors [340].

Currently, some effects of impurity-doped nanocrystal LEDs are still unknown. For example, (i) only a few impurity-doped blue nanocrystal LEDs have been studied, limiting the general full-color applications; (ii) in spite of the remarkable evolution of impurity-doped nanocrystal emitters, the deep insight of device engineering is urgently required to be explored; (iii) although impurity-doped visible-color nanocrystal LEDs have been widely investigated, scarce attention is paid to infrared and ultraviolet devices; (iv) despite rare earth impurity-doped nanocrystals having been intensively probed, almost no LEDs based on this type of emitter have been reported; (v) pursuing the real commercialization of impurity-doped nanocrystal LEDs still faces a number of challenging tasks, including efficiency, efficiency droop, toxicity and lifetime.

For the traditional III-Nitride-based LEDs, the maximum EQE exceeds 84% [341], while high power LEDs offer a luminance level of 60 Mnit and blue-laser-based phosphor-converted white sources enable a luminance above 800 Mnit [342]. To resolve the efficiency issue of impurity-doped nanocrystal LEDs, the introduction of current state-of-the-art concepts from III-Nitride-based LEDs (e.g., solving critical challenges related to material quality, light extraction, and internal quantum efficiency) may be helpful in the anticipated future [343–346]. In brief, the PE of impurity-doped nanocrystal LEDs is far behind that of the best undoped ones or OLEDs, despite the EQE being greatly improved. In addition, the EQE, CE, and PE of impurity-doped blue nanocrystal LEDs are not comparable to those of red and green devices, considering the best EQE is only 2.4% [315]. Since the highest EQE of undoped blue PeLEDs can reach 11% [4], advanced design concepts in undoped blue PeLEDs (e.g., an antisolvent dripping process can control the crystallization of perovskites) may be also effective to enhance the efficiency of impurity-doped blue PeLEDs [347]. To further enhance the efficiency, the optimization of material design, the innovation of device architecture, and the management of emission mechanism are required, which is also useful in the efficiency droop, driving voltage, color stability and lifetime [348–352].

To overcome the toxicity problem, more endeavors should be taken in the development of heavy-metal-free impurity-doped nanocrystal LEDs [353–355], otherwise it will be difficult to enter the mainstream display, lighting, and signaling markets. For the lifetime issue, no impurity-doped nanocrystal LEDs with satisfactory operational stability have been reported. Hence, there is still a long way for the commercial utilization (e.g., the lifetime of $\geq$100,000 h at $\geq$100 cd m^{-2} for displays and $\geq$10,000 h at $\geq$1000 cd m^{-2} for the solid-state lighting are necessary) [356–359]. In addition to synthesize stable impurity-doped nanocrystals, more attention needs to be paid to the careful manipulation of device engineering (e.g., using inorganic HTL and ETL, lowering charge injection barrier, improving charge balance, and reducing charge leakage) [360–363] and the introduction of advanced encapsulation technologies to avoid the moisture and oxygen (e.g., multilayer Al_2O_3 and SiO_2 atomic layer deposition [364] and organic-inorganic multilayer structures [365] to reduce the water vapor transmission rate toward the ideal encapsulating barriers (10^{-6} g^{-1} m^{-2} day^{-1}) [366]). Upon loosening these bottlenecks, the prospect for mass production of impurity-doped nanocrystal LEDs will be undoubtedly bright and the proposed solutions are also conducive to the related optoelectronic fields (e.g., solar cells, lasers, photodetectors, sensors, X-ray imaging, and light communication) [367–372].

References

1. Dai, X.; Zhang, Z.; Jin, Y.; Niu, Y.; Cao, H.; Liang, X.; Chen, L.; Wang, J.; Peng, X. Solution-processed, high-performance light-emitting diodes based on quantum dots. *Nature* **2014**, *515*, 96–100. [CrossRef] [PubMed]

2. Shen, Y.; Cheng, L.; Li, Y.; Li, W.; Chen, J.; Lee, S.; Tang, J.-X. High-Efficiency Perovskite Light-Emitting Diodes with Synergetic Outcoupling Enhancement. *Adv. Mater.* **2019**, *31*, 1901517. [CrossRef]

3. Liu, Y.; Cui, J.; Du, K.; Tian, H.; He, Z.; Zhou, Q.; Yang, Z.; Deng, Y.; Chen, N.; Zuo, X.; et al. Efficient blue light-emitting diodes based on quantum-confined bromide perovskite nanostructures. *Nat. Photonics* **2019**, *13*, 760. [CrossRef]

4. Wang, Q.; Wang, X.; Yang, Z.; Zhou, N.; Deng, Y.; Zhao, J.; Xiao, X.; Rudd, P.; Moran, A.; Yan, Y.; et al. Efficient sky-blue perovskite light-emitting diodes via photoluminescence enhancement. *Nat. Commun.* **2019**, *10*, 5633. [CrossRef]

5. Zhang, F.; Cai, B.; Song, J.; Han, B.; Zhang, B.; Zeng, H. Efficient Blue Perovskite Light-Emitting Diodes Boosted by 2D/3D Energy Cascade Channels. *Adv. Funct. Mater.* **2020**. [CrossRef]

6. Colvin, V.L.; Schlamp, M.C.; Alivisatos, A.P. Light-emitting diodes made from cadmium selenide nanocrystals and a semiconducting polymer. *Nature* **1994**, *370*, 354. [CrossRef]

7. Mashford, B.S.; Stevenson, M.; Popovic, Z.; Hamilton, C.; Zhou, Z.; Breen, C.; Steckel, J.; Bulović, V.; Bawendi, M.; Coe-Sullivan, S.; et al. High-efficiency quantum-dot light-emitting devices with enhanced charge injection. *Nat. Photonics* **2013**, *7*, 407–412. [CrossRef]

8. Shirasaki, Y.; Supran, G.J.; Bawendi, M.G.; Bulović, V. Emergence of colloidal quantum-dot light-emitting technologies. *Nat. Photonics* **2012**, *7*, 13–23. [CrossRef]

9. Yang, Y.; Zheng, Y.; Cao, W.; Titov, A.; Hyvonen, J.; Manders, J.R.; Xue, J.; Holloway, P.H.; Qian, L. High-efficiency light-emitting devices based on quantum dots with tailored nanostructures. *Nat. Photonics* **2015**, *9*, 259–266. [CrossRef]

10. Shen, P.; Li, X.; Cao, F.; Ding, X.; Yang, X. Highly efficient, all-solution-processed, flexible white quantum dot light-emitting diodes. *J. Mater. Chem. C* **2018**, *6*, 9642–9648. [CrossRef]

11. Chen, J.; Zhao, D.; Li, C.; Xu, F.; Lei, W.; Sun, L.; Nathan, A.; Sun, X.W. All Solution-processed Stable White Quantum Dot Light-emitting Diodes with Hybrid ZnO@TiO$_2$ as Blue Emitters. *Sci. Rep.* **2014**, *4*, 4085. [CrossRef] [PubMed]

12. Fan, C.; Yang, C. Yellow/orange emissive heavy-metal complexes as phosphors in monochromatic and white organic light-emitting devices. *Chem. Soc. Rev.* **2014**, *43*, 6439–6469. [CrossRef] [PubMed]

13. Lin, T.-A.; Chatterjee, T.; Tsai, W.; Lee, W.-K.; Wu, M.-J.; Jiao, M.; Pan, K.-C.; Yi, C.-L.; Chung, C.-L.; Wong, K.-T.; et al. Sky-Blue Organic Light Emitting Diode with 37% External Quantum Efficiency Using Thermally Activated Delayed Fluorescence from Spiroacridine-Triazine Hybrid. *Adv. Mater.* **2016**, *28*, 6976–6983. [CrossRef] [PubMed]

14. Zhang, D.; Duan, L.; Zhang, Y.; Cai, M.; Zhang, D.; Qiu, Y. Highly efficient hybrid warm white organic light-emitting diodes using a blue thermally activated delayed fluorescence emitter: Exploiting the external heavy-atom effect. *Light. Sci. Appl.* **2015**, *4*, e232. [CrossRef]

15. Liu, B.; Li, X.-L.; Tao, H.; Zou, J.; Xu, M.; Wang, L.; Peng, J.; Cao, Y. Manipulation of exciton distribution for high-performance fluorescent/phosphorescent hybrid white organic light-emitting diodes. *J. Mater. Chem. C* **2017**, *5*, 7668–7683. [CrossRef]

16. Luo, D.; Xiao, P.; Liu, B. Doping-Free White Organic Light-Emitting Diodes. *Chem. Rec.* **2018**, *18*, 1–16. [CrossRef]

17. Shen, H.; Gao, Q.; Zhang, Y.; Lin, Y.; Lin, Q.; Li, Z.; Chen, L.; Zeng, Z.; Li, X.; Jia, Y.; et al. Visible quantum dot light-emitting diodes with simultaneous high brightness and efficiency. *Nat. Photonics* **2019**, *13*, 192–197. [CrossRef]

18. Tan, Z.-K.; Moghaddam, R.S.; Lai, M.L.; Docampo, P.; Higler, R.; Deschler, F.; Price, M.B.; Sadhanala, A.; Pazos-Outón, L.M.; Credgington, D.; et al. Bright light-emitting diodes based on organometal halide perovskite. *Nat. Nanotechnol.* **2014**, *9*, 687–692. [CrossRef]

19. Song, J.; Li, J.; Li, X.; Xu, L.; Dong, Y.; Zeng, H. Quantum Dot Light-Emitting Diodes Based on Inorganic Perovskite Cesium Lead Halides (CsPbX$_3$). *Adv. Mater.* **2015**, *27*, 7162–7167. [CrossRef]

20. Yantara, N.; Bhaumik, S.; Yan, F.; Sabba, D.; Dewi, H.A.; Mathews, N.; Boix, P.P.; Demir, H.V.; Mhaisalkar, S.G. Inorganic Halide Perovskites for Efficient Light-Emitting Diodes. *J. Phys. Chem. Lett.* **2015**, *6*, 4360–4364. [CrossRef]

21. Kim, Y.-H.; Cho, H.; Heo, J.H.; Kim, T.-S.; Myoung, N.; Lee, C.-L.; Im, S.H.; Lee, T.-W. Light-Emitting Diodes: Multicolored Organic/Inorganic Hybrid Perovskite Light-Emitting Diodes. *Adv. Mater.* **2015**, *27*, 1248–1254. [CrossRef]

22. Kim, Y.-H.; Cho, H.; Lee, T.-W. Metal halide perovskite light emitters. *Proc. Natl. Acad. Sci. USA* **2016**, *113*, 11694–11702. [CrossRef] [PubMed]

23. Yang, X.; Zhang, X.; Deng, J.; Chu, Z.; Jiang, Q.; Meng, J.; Wang, P.; Zhang, L.; Yin, Z.; You, J. Efficient green light-emitting diodes based on quasi-two-dimensional composition and phase engineered perovskite with surface passivation. *Nat. Commun.* **2018**, *9*, 570. [CrossRef] [PubMed]

24. Zhan, H.W.; Jun, X. The rise of perovskite light-emitting diodes. *J. Phys. Chem. Lett.* **2019**, *10*, 3035–3042.

25. Lin, K.; Xing, J.; Quan, L.N.; Arquer, F.P.G.; Gong, X.; Lu, J.; Xie, L.; Zhao, W.; Zhang, D.; Yan, C.; et al. Perovskite light-emitting diodes with external quantum efficiency exceeding 20 percent. *Nature* **2018**, *562*, 245–248. [CrossRef]

26. Cao, Y.; Wang, N.; Tian, H.; Guo, J.; Wei, Y.; Chen, H.; Miao, Y.; Zou, W.; Pan, K.; He, Y.; et al. Perovskite light-emitting diodes based on spontaneously formed submicrometre-scale structures. *Nature* **2018**, *562*, 249–253. [CrossRef]

27. Chiba, T.; Hayashi, Y.; Ebe, H.; Hoshi, K.; Sato, J.; Sato, S.; Pu, Y.-J.; Ohisa, S.; Kido, J. Anion-exchange red perovskite quantum dots with ammonium iodine salts for highly efficient light-emitting devices. *Nat. Photonics* **2018**, *12*, 681–687. [CrossRef]

28. Li, J.; Shan, X.; Bade, S.G.R.; Geske, T.; Jiang, Q.; Yang, X.; Yu, Z. Single-Layer Halide Perovskite Light-Emitting Diodes with Sub-Band Gap Turn-On Voltage and High Brightness. *J. Phys. Chem. Lett.* **2016**, *7*, 4059–4066. [CrossRef]

29. Ithurria, S.; Tessier, M.D.; Mahler, B.; Lobo, R.; Dubertret, B.; Efros, A.L. Colloidal nanoplatelets with two-dimensional electronic structure. *Nat. Mater.* **2011**, *10*, 936–941. [CrossRef]

30. Grim, J.Q.; Christodoulou, S.; Di Stasio, F.; Krahne, R.; Cingolani, R.; Manna, L.; Moreels, I. Continuous-wave biexciton lasing at room temperature using solution-processed quantum wells. *Nat. Nanotechnol.* **2014**, *9*, 891–895. [CrossRef]

31. Rowland, C.E.; Fedin, I.; Zhang, H.; Gray, S.K.; Govorov, A.O.; Talapin, D.V.; Schaller, R. Picosecond energy transfer and multiexciton transfer outpaces Auger recombination in binary CdSe nanoplatelet solids. *Nat. Mater.* **2015**, *14*, 484–489. [CrossRef] [PubMed]

32. Riedinger, A.; Ott, F.D.; Mule, A.S.; Mazzotti, S.; Knüsel, P.N.; Kress, S.J.P.; Prins, F.; Erwin, S.C.; Norris, D.J. An intrinsic growth instability in isotropic materials leads to quasi-two-dimensional nanoplatelets. *Nat. Mater.* **2017**, *16*, 743–748. [CrossRef] [PubMed]

33. Mahler, B.; Nadal, B.; Bouet, C.; Patriarche, G.; Dubertret, B. Core/Shell Colloidal Semiconductor Nanoplatelets. *J. Am. Chem. Soc.* **2012**, *134*, 18591–18598. [CrossRef] [PubMed]

34. Chen, Z.; Nadal, B.; Mahler, B.; Aubin, H.; Dubertret, B. LEDs: Quasi-2D Colloidal Semiconductor Nanoplatelets for Narrow Electroluminescence. *Adv. Funct. Mater.* **2014**, *24*, 295–302. [CrossRef]

35. Liu, B.; Altintas, Y.; Wang, L.; Shendre, S.; Sharma, M.; Sun, H.; Mutlugun, E.; Demir, H.V. Record High External Quantum Efficiency of 19.2% Achieved in Light-Emitting Diodes of Colloidal Quantum Wells Enabled by Hot-Injection Shell Growth. *Adv. Mater.* **2019**, *32*, 1905824. [CrossRef]

36. Erwin, S.C.; Zu, L.; Haftel, M.I.; Efros, A.L.; Kennedy, T.A.; Norris, D.J. Doping semiconductor nanocrystals. *Nature* **2005**, *436*, 91–94. [CrossRef]

37. Norris, D.J.; Efros, A.L.; Erwin, S.C. ChemInform Abstract: Doped Nanocrystals. *Science* **2008**, *319*, 1776–1779. [CrossRef]

38. Huang, H.; Polavarapu, L.; Sichert, J.A.; Susha, A.S.; Urban, A.S.; Rogach, A.L. Colloidal lead halide perovskite nanocrystals: Synthesis, optical properties and applications. *NPG Asia Mater.* **2016**, *8*, e328. [CrossRef]

39. Viswanatha, R.; Brovelli, S.; Pandey, A.; Crooker, S.A.; Klimov, V.I. Copper-Doped Inverted Core/Shell Nanocrystals with "Permanent" Optically Active Holes. *Nano Lett.* **2011**, *11*, 4753–4758. [CrossRef]

40. Tang, J.; Liu, H.; Zhitomirsky, D.; Hoogland, S.; Wang, X.; Furukawa, M.; Levina, L.; Sargent, E.H. Quantum Junction Solar Cells. *Nano Lett.* **2012**, *12*, 4889–4894. [CrossRef]

41. Singh, A.; Singh, S.; Levcenko, S.; Unold, T.; Laffir, F.; Ryan, K.M. Compositionally Tunable Photoluminescence Emission in Cu$_2$ZnSn(S$_{1-x}$Se$_x$)4 Nanocrystals. *Angew. Chem. Int. Ed.* **2013**, *52*, 9120–9124. [CrossRef] [PubMed]

42. Kriegel, I.; Rodríguez-Fernández, J.; Wisnet, A.; Zhang, H.; Waurisch, C.; Eychmüller, A.; Dubavik, A.; Govorov, A.O.; Feldmann, J. Shedding Light on Vacancy-Doped Copper Chalcogenides: Shape-Controlled Synthesis, Optical Properties, and Modeling of Copper Telluride Nanocrystals with Near-Infrared Plasmon Resonances. *ACS Nano* **2013**, *7*, 4367–4377. [CrossRef] [PubMed]

43. Luo, J.; Im, J.H.; Mayer, M.T.; Schreier, M.; Nazeeruddin, M.K.; Park, N.G.; Tilley, S.D.; Fan, H.J.; Grätzel, M. Water photolysis at 12.3% efficiency via perovskite photovoltaics and Earth-abundant catalysts. *Science* **2014**, *345*, 1593–1596. [CrossRef] [PubMed]

44. Pradhan, N.; Sarma, D.D. Advances in Light-Emitting Doped Semiconductor Nanocrystals. *J. Phys. Chem. Lett.* **2011**, *2*, 2818–2826. [CrossRef]

45. Xie, Y.; Carbone, L.; Nobile, C.; Grillo, V.; D'Agostino, S.; Della Sala, F.; Giannini, C.; Altamura, D.; Oelsner, C.; Kryschi, C.; et al. Metallic-like Stoichiometric Copper Sulfide Nanocrystals: Phase- and Shape-Selective Synthesis, Near-Infrared Surface Plasmon Resonance Properties, and Their Modeling. *ACS Nano* **2013**, *7*, 7352–7369. [CrossRef]

46. Wu, P.; Yan, X.-P. Doped quantum dots for chemo/biosensing and bioimaging. *Chem. Soc. Rev.* **2013**, *42*, 5489. [CrossRef]

47. Wang, X.; Yan, X.; Li, W.; Sun, K. Doped Quantum Dots for White-Light-Emitting Diodes Without Reabsorption of Multiphase Phosphors. *Adv. Mater.* **2012**, *24*, 2742–2747. [CrossRef]

48. Qiu, H.; Chen, G.; Fan, R.; Cheng, C.; Hao, S.; Chen, D.; Yang, C. Tuning the size and shape of colloidal cerium oxide nanocrystals through lanthanide doping. *Chem. Commun.* **2011**, *47*, 9648–9650. [CrossRef] [PubMed]

49. Yin, Y.; Alivisatos, A.P. Colloidal nanocrystal synthesis and the organic–inorganic interface. *Nature* **2005**, *437*, 664–670. [CrossRef] [PubMed]

50. Wang, F.; Han, Y.; Lim, C.S.; Lu, Y.; Wang, J.; Xu, J.; Chen, H.; Zhang, C.; Hong, M.; Liu, X. Simultaneous phase and size control of upconversion nanocrystals through lanthanide doping. *Nature* **2010**, *463*, 1061–1065. [CrossRef] [PubMed]

51. Ahmed, G.H.; Yin, J.; Bakr, O.M.; Mohammed, O.F. Near-unity photoluminescence quantum yield in inorganic perovskite nanocrystals by metal-ion doping. *J. Chem. Phys.* **2020**, *152*, 020902. [CrossRef] [PubMed]

52. Liu, J.; Zhao, Q.; Liu, J.-L.; Wu, Y.-S.; Cheng, Y.; Ji, M.; Qian, H.-M.; Hao, W.; Zhang, L.-J.; Wei, X.-J.; et al. Heterovalent-Doping-Enabled Efficient Dopant Luminescence and Controllable Electronic Impurity Via a New Strategy of Preparing II−VI Nanocrystals. *Adv. Mater.* **2015**, *27*, 2753–2761. [CrossRef] [PubMed]

53. Beaulac, R.; Schneider, L.; Archer, P.I.; Bacher, G.; Gamelin, D.R. Light-Induced Spontaneous Magnetization in Doped Colloidal Quantum Dots. *Science* **2009**, *325*, 973–976. [CrossRef]

54. Liu, X.; Wang, X.; Zhou, B.; Law, W.-C.; Cartwright, A.N.; Swihart, M.T. Size-Controlled Synthesis of Cu2-xE (E = S, Se) Nanocrystals with Strong Tunable Near-Infrared Localized Surface Plasmon Resonance and High Conductivity in Thin Films. *Adv. Funct. Mater.* **2013**, *23*, 1256–1264. [CrossRef]

55. Kang, M.S.; Sahu, A.; Frisbie, C.D.; Norris, D.J. Influence of Silver Doping on Electron Transport in Thin Films of PbSe Nanocrystals. *Adv. Mater.* **2012**, *25*, 725–731. [CrossRef]

56. Sahu, A.; Kang, M.S.; Kompch, A.; Notthoff, C.; Wills, A.W.; Deng, N.; Winterer, M.; Frisbie, C.D.; Norris, D.J. Electronic Impurity Doping in CdSe Nanocrystals. *Nano Lett.* **2012**, *12*, 2587–2594. [CrossRef] [PubMed]

57. Liu, W.; Lin, Q.; Li, H.; Wu, K.; Robel, I.; Pietryga, J.; Klimov, V.I. Mn2+-Doped Lead Halide Perovskite Nanocrystals with Dual-Color Emission Controlled by Halide Content. *J. Am. Chem. Soc.* **2016**, *138*, 14954–14961. [CrossRef]

58. Galle, T.; Kazes, M.; Hübner, R.; Lox, J.; Khoshkhoo, M.S.; Sonntag, L.; Tietze, R.; Sayevich, V.; Oron, D.; Koitzsch, A.; et al. Colloidal Mercury-Doped CdSe Nanoplatelets with Dual Fluorescence. *Chem. Mater.* **2019**, *31*, 5065–5074. [CrossRef]

59. Sharma, M.; Olutas, M.; Yeltik, A.; Kelestemur, Y.; Sharma, A.; Delikanli, S.; Guzelturk, B.; Güngör, K.; McBride, J.R.; Demir, H.V. Understanding the Journey of Dopant Copper Ions in Atomically Flat Colloidal Nanocrystals of CdSe Nanoplatelets Using Partial Cation Exchange Reactions. *Chem. Mater.* **2018**, *30*, 3265–3275. [CrossRef]

60. Dufour, M.; Izquierdo, E.; Livache, C.; Martinez, B.; Silly, M.G.; Pons, T.; Lhuillier, E.; Delerue, C.; Ithurria, S. Doping as a Strategy to Tune Color of 2D Colloidal Nanoplatelets. *ACS Appl. Mater. Interfaces* **2019**, *11*, 10128–10134. [CrossRef]

61. Khan, A.H.; Pinchetti, V.; Tanghe, I.; Dang, Z.; Martín-García, B.; Hens, Z.; Van Thourhout, D.; Geiregat, P.; Brovelli, S.; Moreels, I. Tunable and Efficient Red to Near-Infrared Photoluminescence by Synergistic Exploitation of Core and Surface Silver Doping of CdSe Nanoplatelets. *Chem. Mater.* **2019**, *31*, 1450–1459. [CrossRef]

62. Fainblat, R.; Delikanli, S.; Spee, L.; Czerny, T.; Isik, F.; Sharma, V.K.; Demir, H.V.; Bacher, G. Impurity incorporation and exchange interactions in Co^{2+}-doped CdSe/CdS core/shell nanoplatelets. *J. Chem. Phys.* **2019**, *151*, 224708. [CrossRef] [PubMed]

63. Tan, Z.; Li, J.; Zhang, C.; Li, Z.; Hu, Q.; Xiao, Z.; Kamiya, T.; Hosono, H.; Niu, G.; Lifshitz, E.; et al. Highly Efficient Blue-Emitting Bi-Doped Cs_2SnCl_6 Perovskite Variant: Photoluminescence Induced by Impurity Doping. *Adv. Funct. Mater.* **2018**, *28*, 1801131. [CrossRef]

64. Sharma, M.; Güngör, K.; Yeltik, A.; Olutas, M.; Guzelturk, B.; Kelestemur, Y.; Erdem, T.; Delikanli, S.; McBride, J.R.; Demir, H.V. Near-Unity Emitting Copper-Doped Colloidal Semiconductor Quantum Wells for Luminescent Solar Concentrators. *Adv. Mater.* **2017**, *29*, 1700821. [CrossRef]

65. Hu, L.; Zhang, Z.; Patterson, R.J.; Hu, Y.; Chen, W.; Chen, C.; Li, D.; Hu, C.; Ge, C.; Chen, Z.; et al. Achieving high-performance PbS quantum dot solar cells by improving hole extraction through Ag doping. *Nano Energy* **2018**, *46*, 212–219. [CrossRef]

66. Kumawat, N.K.; Yuan, Z.; Bai, S.; Gao, F. Metal Doping/Alloying of Cesium Lead Halide Perovskite Nanocrystals and their Applications in Light-Emitting Diodes with Enhanced Efficiency and Stability. *Isr. J. Chem.* **2019**, *59*, 695–707. [CrossRef]

67. Zhang, X.; Li, L.; Sun, Z.; Luo, J. Rational chemical doping of metal halide perovskites. *Chem. Soc. Rev.* **2019**, *48*, 517–539. [CrossRef]

68. Lei, M.X.; Shi, C.Y.; Hai, B.Z.; Ji, Z.S. A comprehensive review of doping in perovskite nanocrystals/quantum dots: Evolution of structure, electronics, optics and light-emitting diodes. *Mater. Today Nano* **2019**, *6*, 100036.

69. Song, L.; Guo, X.; Hu, Y.; Lv, Y.; Lin, J.; Liu, Z.; Fan, Y.; Liu, X. Efficient Inorganic Perovskite Light-Emitting Diodes with Polyethylene Glycol Passivated Ultrathin $CsPbBr_3$ Films. *J. Phys. Chem. Lett.* **2017**, *8*, 4148–4154. [CrossRef]

70. Ke, Y.; Wang, N.; Kong, D.; Cao, Y.; He, Y.; Zhu, L.; Wang, Y.; Xue, C.; Peng, Q.; Gao, F.; et al. Defect Passivation for Red Perovskite Light-Emitting Diodes with Improved Brightness and Stability. *J. Phys. Chem. Lett.* **2019**, *10*, 380–385. [CrossRef]

71. Peng, X.-F.; Wu, X.-Y.; Ji, X.-X.; Ren, J.; Wang, Q.; Li, G.-Q.; Yang, X.-H. Modified Conducting Polymer Hole Injection Layer for High-Efficiency Perovskite Light-Emitting Devices: Enhanced Hole Injection and Reduced Luminescence Quenching. *J. Phys. Chem. Lett.* **2017**, *8*, 4691–4697. [CrossRef] [PubMed]

72. Liu, B.; Sharma, M.; Yu, J.; Shendre, S.; Hettiarachchi, C.; Sharma, A.; Yeltik, A.; Wang, L.; Sun, H.; Dang, C.; et al. Light-Emitting Diodes with Cu-Doped Colloidal Quantum Wells: From Ultrapure Green, Tunable Dual-Emission to White Light. *Small* **2019**, *15*, e1901983. [CrossRef] [PubMed]

73. Shi, Y.F.; Xi, J.; Lei, T.; Yuan, F.; Dai, J.F.; Ran, C.X.; Dong, H.; Jiao, B.; Hou, X.; Wu, Z.X. Rubidium doping for enhanced performance of highly efficient formamidinium-based perovskite light-emitting diodes. *ACS Appl. Mater. Inter.* **2018**, *10*, 9849–9857. [CrossRef] [PubMed]

74. Begum, R.; Chin, X.Y.; Li, M.; Damodaran, B.; Sum, T.C.; Mhaisalkar, S.G.; Mathews, N. Stable Sn^{2+} doped $FAPbI_3$ nanocrystals for near-infrared LEDs. *Chem. Commun.* **2019**, *55*, 5451–5454. [CrossRef]

75. Jiang, C.; Zhong, Z.; Liu, B.; He, Z.; Zou, J.; Wang, L.; Wang, J.; Peng, J.; Cao, Y. Coffee-Ring-Free Quantum Dot Thin Film Using Inkjet Printing from a Mixed-Solvent System on Modified ZnO Transport Layer for Light-Emitting Devices. *ACS Appl. Mater. Interfaces* **2016**, *8*, 26162–26168. [CrossRef]

76. Reiss, P.; Bleuse, J.; Pron, A. Highly Luminescent CdSe/ZnSe Core/Shell Nanocrystals of Low Size Dispersion. *Nano Lett.* **2002**, *2*, 781–784. [CrossRef]

77. He, Y.; Lu, H.-T.; Sai, L.-M.; Su, Y.-Y.; Hu, M.; Fan, C.; Huang, W.; Wang, L.-H. Microwave Synthesis of Water-Dispersed CdTe/CdS/ZnS Core-Shell-Shell Quantum Dots with Excellent Photostability and Biocompatibility. *Adv. Mater.* **2008**, *20*, 3416–3421. [CrossRef]

78. Murray, C.B.; Norris, D.J.; Bawendi, M.G. Synthesis and characterization of nearly monodisperse CdE (E=S, Se, Te) semiconductor nanocrystallites. *J. Am. Chem. Soc.* **1993**, *115*, 8706–8715. [CrossRef]

79. Talapin, D.V.; Mekis, I.; Götzinger, S.; Kornowski, A.; Benson, O.; Weller, H. CdSe/CdS/ZnS and CdSe/ZnSe/ZnS Core−Shell−Shell Nanocrystals. *J. Phys. Chem. B* **2004**, *108*, 18826–18831. [CrossRef]

80. Van Der Stam, W.; Grimaldi, G.; Geuchies, J.J.; Gudjonsdottir, S.; Van Uffelen, P.T.; Van Overeem, M.; Brynjarsson, B.; Kirkwood, N.; Houtepen, A.J. Electrochemical Modulation of the Photophysics of Surface-Localized Trap States in Core/Shell/(Shell) Quantum Dot Films. *Chem. Mater.* **2019**, *31*, 8484–8493. [CrossRef]

81. Liu, Y.; Dai, F.; Zhao, R.; Huai, X.; Han, J.; Wang, L. Aqueous synthesis of core/shell/shell CdSe/CdS/ZnS quantum dots for photocatalytic hydrogen generation. *J. Mater. Sci.* **2019**, *54*, 8571–8580. [CrossRef]

82. Jiang, C.; Liu, H.; Liu, B.; Zhong, Z.; Zou, J.; Wang, J.; Wang, L.; Peng, J.; Cao, Y. Improved performance of inverted quantum dots light emitting devices by introducing double hole transport layers. *Org. Electron.* **2016**, *31*, 82–89. [CrossRef]

83. Shi, L.; Yan, Z. Conversion efficiency of strained core/shell quantum dot solar cell: Converting from type-I to type-II structures. *J. Appl. Phys.* **2019**, *125*, 174302. [CrossRef]

84. Bekenstein, Y.; Dahl, J.C.; Huang, J.; Osowiecki, W.T.; Swabeck, J.; Chan, E.M.; Yang, P.; Alivisatos, A.P. The Making and Breaking of Lead-Free Double Perovskite Nanocrystals of Cesium Silver–Bismuth Halide Compositions. *Nano Lett.* **2018**, *18*, 3502–3508. [CrossRef] [PubMed]

85. Lu, D.; Zhang, Y.; Lai, M.; Lee, A.; Xie, C.; Lin, J.; Lei, T.; Lin, Z.; Kley, C.S.; Huang, J.; et al. Giant Light-Emission Enhancement in Lead Halide Perovskites by Surface Oxygen Passivation. *Nano Lett.* **2018**, *18*, 6967–6973. [CrossRef]

86. Folie, B.D.; Tan, J.A.; Huang, J.; Sercel, P.C.; Delor, M.; Lai, M.; Lyons, J.L.; Bernstein, N.; Efros, A.L.; Yang, P.; et al. Effect of Anisotropic Confinement on Electronic Structure and Dynamics of Band Edge Excitons in Inorganic Perovskite Nanowires. *J. Phys. Chem. A* **2020**, *124*, 1867–1876. [CrossRef]

87. Mai, R.; Wu, X.; Jiang, Y.; Meng, Y.; Liu, B.; Hu, X.; Roncali, J.; Zhou, G.; Liu, J.-M.; Kempa, K.; et al. An efficient multi-functional material based on polyether-substituted indolocarbazole for perovskite solar cells and solution-processed non-doped OLEDs. *J. Mater. Chem. A* **2019**, *7*, 1539–1547. [CrossRef]

88. Wang, L.; Liu, B.; Zhao, X.; Demir, H.V.; Gu, H.; Sun, H. Solvent-Assisted Surface Engineering for High-Performance All-Inorganic Perovskite Nanocrystal Light-Emitting Diodes. *ACS Appl. Mater. Interfaces* **2018**, *10*, 19828–19835. [CrossRef]

89. Chen, P.; Xiong, Z.; Wu, X.; Shao, M.; Ma, X.; Xiong, Z.; Gao, C.-H. Highly Efficient Perovskite Light-Emitting Diodes Incorporating Full Film Coverage and Bipolar Charge Injection. *J. Phys. Chem. Lett.* **2017**, *8*, 1810–1818. [CrossRef]

90. Wei, Y.; Li, X.; Chen, Y.; Cheng, Z.; Xiao, H.; Li, X.; Ding, J.; Lin, J. In Situ Light-Initiated Ligands Cross-Linking Enables Efficient All-Solution-Processed Perovskite Light-Emitting Diodes. *J. Phys. Chem. Lett.* **2020**, *11*, 1154–1161. [CrossRef]

91. Luo, D.; Chen, Q.; Qiu, Y.; Zhang, M.; Liu, B. Device Engineering for All-Inorganic Perovskite Light-Emitting Diodes. *Nano Mater.* **2019**, *9*, 1007. [CrossRef] [PubMed]

92. Huang, J.; Lai, M.; Lin, J.; Yang, P. Rich Chemistry in Inorganic Halide Perovskite Nanostructures. *Adv. Mater.* **2018**, *30*, 1802856. [CrossRef] [PubMed]

93. Prudnikau, A.V.; Chuvilin, A.; Artemyev, M. CdSe–CdS Nanoheteroplatelets with Efficient Photoexcitation of Central CdSe Region through Epitaxially Grown CdS Wings. *J. Am. Chem. Soc.* **2013**, *135*, 14476–14479. [CrossRef] [PubMed]

94. Tessier, M.D.; Spinicelli, P.; Dupont, D.; Patriarche, G.; Ithurria, S.; Dubertret, B. Efficient Exciton Concentrators Built from Colloidal Core/Crown CdSe/CdS Semiconductor Nanoplatelets. *Nano Lett.* **2014**, *14*, 207–213. [CrossRef]

95. Tessier, M.D.; Javaux, C.; Maksimovic, I.; Loriette, V.; Dubertret, B. Spectroscopy of Single CdSe Nanoplatelets. *ACS Nano* **2012**, *6*, 6751–6758. [CrossRef]

96. Wu, K.; Li, Q.; Jia, Y.; McBride, J.R.; Xie, Z.-X.; Lian, T. Efficient and Ultrafast Formation of Long-Lived Charge-Transfer Exciton State in Atomically Thin Cadmium Selenide/Cadmium Telluride Type-II Heteronanosheets. *ACS Nano* **2015**, *9*, 961–968. [CrossRef]

97. Kelestemur, Y.; Guzelturk, B.; Erdem, O.; Olutas, M.; Gungor, K.; Demir, H.V. Platelet-in-box colloidal quantum wells: CdSe/CdS@CdS core/crown@shell hetero-nanoplatelets. *Adv. Funct. Mater.* **2016**, *26*, 3570–3579. [CrossRef]

98. Joo, J.; Son, J.S.; Kwon, S.G.; Yu, J.H.; Hyeon, T. Low-Temperature Solution-Phase Synthesis of Quantum Well Structured CdSe Nanoribbons. *J. Am. Chem. Soc.* **2006**, *128*, 5632–5633. [CrossRef]

99. Ithurria, S.; Dubertret, B. Quasi 2D Colloidal CdSe Platelets with Thicknesses Controlled at the Atomic Level. *J. Am. Chem. Soc.* **2008**, *130*, 16504–16505. [CrossRef]

100. Xiao, P.; Huang, J.; Yan, D.; Luo, D.; Yuan, J.; Liu, B.; Liang, D. Emergence of Nanoplatelet Light-Emitting Diodes. *Materials* **2018**, *11*, 1376. [CrossRef]

101. Gao, Y.; Li, M.J.; Delikanli, S.; Zheng, H.Y.; Liu, B.Q.; Dang, C.; Sum, T.C.; Demir, H.V. Low-threshold lasing from colloidal CdSe/CdSeTe core/alloyed-crown type-II hetero-nanoplatelets. *Nanoscale* **2018**, *10*, 9466–9475. [CrossRef]

102. Sharma, M.; Delikanli, S.; Demir, H.V. Two-Dimensional CdSe-Based Nanoplatelets: Their Heterostructures, Doping, Photophysical Properties, and Applications. *Proc. IEEE* **2020**, *18*, 1–21. [CrossRef]

103. Altintas, Y.; Gungor, K.; Gao, Y.; Sak, M.; Quliyeva, U.; Bappi, G.; Mutlugun, E.; Sargent, E.H.; Demir, H.V.; Altıntas, Y. Giant Alloyed Hot Injection Shells Enable Ultralow Optical Gain Threshold in Colloidal Quantum Wells. *ACS Nano* **2019**, *13*, 10662–10670. [CrossRef]

104. Altintas, Y.; Quliyeva, U.; Güngör, K.; Erdem, O.; Kelestemur, Y.; Mutlugun, E.; Kovalenko, M.V.; Demir, H.V. Highly Stable, Near-Unity Efficiency Atomically Flat Semiconductor Nanocrystals of CdSe/ZnS Hetero-Nanoplatelets Enabled by ZnS-Shell Hot-Injection Growth. *Small* **2019**, *15*, 1804854. [CrossRef]

105. Rossinelli, A.A.; Rojo, H.; Mule, A.S.; Aellen, M.; Cocina, A.; De Leo, E.; Schäublin, R.; Norris, D.J.; Schaeublin, R. Compositional Grading for Efficient and Narrowband Emission in CdSe-Based Core/Shell Nanoplatelets. *Chem. Mater.* **2019**, *31*, 9567–9578. [CrossRef]

106. Nan, W.; Niu, Y.; Qin, H.; Cui, F.; Yang, Y.; Lai, R.; Lin, W.; Peng, X. Crystal Structure Control of Zinc-Blende CdSe/CdS Core/Shell Nanocrystals: Synthesis and Structure-Dependent Optical Properties. *J. Am. Chem. Soc.* **2012**, *134*, 19685–19693. [CrossRef] [PubMed]

107. Xia, X.; Liu, Z.; Du, G.; Li, Y.; Ma, M. Wurtzite and zinc-blende CdSe based core/shell semiconductor nanocrystals: Structure, morphology and photoluminescence. *J. Lumin.* **2010**, *130*, 1285–1291. [CrossRef]

108. Gao, Y.; Peng, X. Crystal Structure Control of CdSe Nanocrystals in Growth and Nucleation: Dominating Effects of Surface versus Interior Structure. *J. Am. Chem. Soc.* **2014**, *136*, 6724–6732. [CrossRef]

109. Bhargava, R.N.; Gallagher, D.; Hong, X.; Nurmikko, A. Optical properties of manganese-doped nanocrystals of ZnS. *Phys. Rev. Lett.* **1994**, *72*, 416–419. [CrossRef]

110. Kennedy, T.A.; Glaser, E.; Klein, P.B.; Bhargava, R.N. Symmetry and electronic structure of the Mn impurity in ZnS nanocrystals. *Phys. Rev. B* **1995**, *52*, R14356. [CrossRef]

111. Zhang, J.; Di, Q.; Liu, J.; Bai, B.; Xu, M.; Liu, J.; Liu, J. Heterovalent Doping in Colloidal Semiconductor Nanocrystals: Cation-Exchange-Enabled New Accesses to Tuning Dopant Luminescence and Electronic Impurities. *J. Phys. Chem. Lett.* **2017**, *8*, 4943–4953. [CrossRef] [PubMed]

112. Barrows, C.J.; Fainblat, R.; Gamelin, D.R. Excitonic Zeeman splittings in colloidal CdSe quantum dots doped with single magnetic impurities. *J. Mater. Chem. C* **2017**, *5*, 5232–5238. [CrossRef]

113. Delikanli, S.; Akgul, M.Z.; Murphy, J.; Barman, B.; Tsai, Y.; Scrace, T.; Zhang, P.; Bozok, B.; Hernández-Martínez, P.L.; Christodoulides, J.; et al. Mn^{2+}-Doped CdSe/CdS Core/Multishell Colloidal Quantum Wells Enabling Tunable Carrier–Dopant Exchange Interactions. *ACS Nano* **2015**, *9*, 12473–12479. [CrossRef] [PubMed]

114. Nasilowski, M.; Mahler, B.; Lhuillier, E.; Ithurria, S.; Dubertret, B. Two-Dimensional Colloidal Nanocrystals. *Chem. Rev.* **2016**, *116*, 10934–10982. [CrossRef] [PubMed]

115. Swarnkar, A.; Mir, W.J.; Nag, A. Can B-site doping or alloying improve thermal-and phase-stability of all-inorganic $CsPbX_3$ (X = Cl, Br, I) perovskites? *ACS Energy Lett.* **2018**, *3*, 286–289. [CrossRef]

116. Park, B.; Santra, S.; Holloway, P.H. Syntheses and applications of Mn-doped II-VI semiconductor nanocrystals. *J. Nanosci. Nanotechnol.* **2005**, *5*, 1364–1375.

117. Zhou, Y.; Zhao, Y. Chemical stability and instability of inorganic halide perovskites. *Energy Environ. Sci.* **2019**, *12*, 1495. [CrossRef]

118. Yu, J.H.; Kwon, S.-H.; Petrásek, Z.; Park, O.K.; Jun, S.W.; Shin, K.; Choi, M.; Park, Y.I.; Park, K.; Bin Na, H.; et al. High-resolution three-photon biomedical imaging using doped ZnS nanocrystals. *Nat. Mater.* **2013**, *12*, 359–366. [CrossRef]

119. Liu, B.; Gao, D.; Lan, L.; Wang, L.; Xu, M.; Zhu, X.; Zou, J.; Ning, H.; Peng, J.; Cao, Y. Harnessing charge and exciton distribution towards extremely high performance: The critical role of guests in single-emitting-layer white OLEDs. *Mater. Horiz.* **2015**, *2*, 536–544. [CrossRef]

120. Liu, B.; Xu, Z.; Zou, J.; Tao, H.; Xu, M.; Gao, D.; Lan, L.; Wang, L.; Ning, H.; Peng, J. High-performance hybrid white organic light-emitting diodes employing p-type interlayers. *J. Ind. Eng. Chem.* **2015**, *27*, 240–244. [CrossRef]

121. Liu, B.; Luo, D.; Zou, J.; Gao, D.; Ning, H.; Wang, L.; Peng, J.; Cao, Y. A host–guest system comprising high guest concentration to achieve simplified and high-performance hybrid white organic light-emitting diodes. *J. Mater. Chem. C* **2015**, *3*, 6359–6366. [CrossRef]

122. Luo, D.; Yang, Y.; Xiao, Y.; Zhao, Y.; Yang, Y.; Liu, B. Regulating Charge and Exciton Distribution in High-Performance Hybrid White Organic Light-Emitting Diodes with n-Type Interlayer Switch. *Nano-Micro Lett.* **2017**, *9*, 37. [CrossRef] [PubMed]

123. Luo, D.; Yang, Y.; Huang, L.; Liu, B.; Zhao, Y. High-performance hybrid white organic light-emitting diodes exploiting blue thermally activated delayed fluorescent dyes. *Dye. Pigment.* **2017**, *147*, 83–89. [CrossRef]

124. Zhang, X.; Lin, H.; Huang, H.; Reckmeier, C.; Zhang, Y.; Choy, W.C.H.; Rogach, A. Enhancing the Brightness of Cesium Lead Halide Perovskite Nanocrystal Based Green Light-Emitting Devices through the Interface Engineering with Perfluorinated Ionomer. *Nano Lett.* **2016**, *16*, 1415–1420. [CrossRef] [PubMed]

125. Liu, B.; Delikanli, S.; Gao, Y.; DeDe, D.; Güngör, K.; Demir, H.V. Nanocrystal light-emitting diodes based on type II nanoplatelets. *Nano Energy* **2018**, *47*, 115–122. [CrossRef]

126. Xiang, C.; Koo, W.; So, F.; Sasabe, H.; Kido, J. A systematic study on efficiency enhancements in phosphorescent green, red and blue microcavity organic light emitting devices. *Light. Sci. Appl.* **2013**, *2*, e74. [CrossRef]

127. Xiao, P.; Dong, T.; Xie, J.; Luo, D.; Yuan, J.; Liu, B. Emergence of White Organic Light-Emitting Diodes Based on Thermally Activated Delayed Fluorescence. *Appl. Sci.* **2018**, *8*, 299. [CrossRef]

128. Bai-Quan, L.; Dong-Yu, G.; Jian-Bin, W.; Xi, W.; Lei, W.; Jian-Hua, Z.; Hong-Long, N.; Jun-Biao, P. Progress of White Organic Light-Emitting Diodes. *Acta Physico-Chimica Sin.* **2015**, *31*, 1823–1852. [CrossRef]

129. Zhang, L.; Li, X.-L.; Luo, D.; Xiao, P.; Xiao, W.; Song, Y.; Ang, Q.; Liu, B. Strategies to Achieve High-Performance White Organic Light-Emitting Diodes. *Materials* **2017**, *10*, 1378. [CrossRef]

130. Pu, Y.-J.; Chiba, T.; Ideta, K.; Takahashi, S.; Aizawa, N.; Hikichi, T.; Kido, J. Light-Emitting Devices: Fabrication of Organic Light-Emitting Devices Comprising Stacked Light-Emitting Units by Solution-Based Processes. *Adv. Mater.* **2015**, *27*, 1327–1332. [CrossRef]

131. Shi, Y.; Wu, W.; Dong, H.; Li, G.; Xi, K.; Divitini, G.; Ran, C.; Yuan, F.; Zhang, M.; Jiao, B.; et al. A Strategy for Architecture Design of Crystalline Perovskite Light-Emitting Diodes with High Performance. *Adv. Mater.* **2018**, *30*, 1800251. [CrossRef] [PubMed]

132. Shi, Z.; Li, S.; Li, Y.; Ji, H.; Li, X.; Wu, D.; Xu, T.; Chen, Y.; Tian, Y.; Zhang, Y.; et al. Strategy of Solution-Processed All-Inorganic Heterostructure for Humidity/Temperature-Stable Perovskite Quantum Dot Light-Emitting Diodes. *ACS Nano* **2018**, *12*, 1462–1472. [CrossRef]

133. Luo, D.; Xiao, Y.; Hao, M.; Zhao, Y.; Yang, Y.; Gao, Y.; Liu, B. Doping-free white organic light-emitting diodes without blue molecular emitter: An unexplored approach to achieve high performance via exciplex emission. *Appl. Phys. Lett.* **2017**, *110*, 061105. [CrossRef]

134. Ying, L.; Ho, C.-L.; Wu, H.; Cao, Y.; Wong, W.-Y. White Polymer Light-Emitting Devices for Solid-State Lighting: Materials, Devices, and Recent Progress. *Adv. Mater.* **2014**, *26*, 2459–2473. [CrossRef] [PubMed]

135. Chen, B.; Liu, B.; Zeng, J.; Nie, H.; Xiong, Y.; Zou, J.; Ning, H.; Wang, Z.; Zhao, Z.; Tang, B.Z. Efficient Bipolar Blue AIEgens for High-Performance Nondoped Blue OLEDs and Hybrid White OLEDs. *Adv. Funct. Mater.* **2018**, *28*, 1803369. [CrossRef]

136. Chen, Y.-H.; Ma, D.-G.; Sun, H.-D.; Chen, J.-S.; Guo, Q.-X.; Wang, Q.; Zhao, Y. Organic semiconductor heterojunctions: Electrode-independent charge injectors for high-performance organic light-emitting diodes. *Light. Sci. Appl.* **2016**, *5*, e16042. [CrossRef]

137. Luo, D.; Li, X.-L.; Zhao, Y.; Gao, Y.; Liu, B. High-Performance Blue Molecular Emitter-Free and Doping-Free Hybrid White Organic Light-Emitting Diodes: An Alternative Concept To Manipulate Charges and Excitons Based on Exciplex and Electroplex Emission. *ACS Photonics* **2017**, *4*, 1566–1575. [CrossRef]

138. Du, X.; Tao, S.; Huang, Y.; Yang, X.; Ding, X.; Zhang, X. Efficient fluorescence/phosphorescence white organic light-emitting diodes with ultra high color stability and mild efficiency roll-off. *Appl. Phys. Lett.* **2015**, *107*, 183304. [CrossRef]

139. Liu, B.; Xu, M.; Tao, H.; Ying, L.; Zou, J.; Wu, H.; Peng, J. Highly efficient red phosphorescent organic light-emitting diodes based on solution processed emissive layer. *J. Lumin.* **2013**, *142*, 35–39. [CrossRef]

140. Sun, N.; Zhao, Y.; Zhao, F.; Chen, Y.; Yang, D.; Chen, J.; Ma, D. A white organic light-emitting diode with ultra-high color rendering index, high efficiency, and extremely low efficiency roll-off. *Appl. Phys. Lett.* **2014**, *105*, 013303. [CrossRef]

141. Luo, D.; Chen, Q.; Gao, Y.; Zhang, M.; Liu, B. Extremely Simplified, High-Performance, and Doping-Free White Organic Light-Emitting Diodes Based on a Single Thermally Activated Delayed Fluorescent Emitter. *ACS Energy Lett.* **2018**, *3*, 1531–1538. [CrossRef]

142. Liu, B.; Xu, M.; Wang, L.; Tao, H.; Su, Y.; Gao, D.; Zou, J.; Lan, L.; Peng, J. Comprehensive Study on the Electron Transport Layer in Blue Flourescent Organic Light-Emitting Diodes. *ECS J. Solid State Sci. Technol.* **2015**, *2*, R258–R261. [CrossRef]

143. Krotkus, S.; Kasemann, D.; Lenk, S.; Leo, K.; Reineke, S. Adjustable white-light emission from a photo-structured micro-OLED array. *Light. Sci. Appl.* **2016**, *5*, e16121. [CrossRef]

144. Guo, J.J.; Li, X.L.; Nie, H.; Luo, W.W.; Gan, S.F.; Hu, S.M.; Hu, R.R.; Qin, A.J.; Zhao, Z.J.; Su, S.J.; et al. Achieving high-performance nondoped OLEDs with extremely small efficiency roll-off by combining aggregation-induced emission and thermally activated delayed fluorescence. *Adv. Funct. Mater.* **2017**, *27*, 1606458. [CrossRef]

145. Liu, B.; Zou, J.; Zhou, Z.; Wang, L.; Xu, M.; Tao, H.; Gao, D.; Lan, L.; Ning, H.; Peng, J. Efficient single-emitting layer hybrid white organic light-emitting diodes with low efficiency roll-off, stable color and extremely high luminance. *J. Ind. Eng. Chem.* **2015**, *30*, 85–91. [CrossRef]

146. Shi, Z.; Li, Y.; Zhang, Y.; Chen, Y.; Li, X.; Wu, D.; Xu, T.; Shan, C.; Du, G. High-Efficiency and Air-Stable Perovskite Quantum Dots Light-Emitting Diodes with an All-Inorganic Heterostructure. *Nano Lett.* **2017**, *17*, 313–321. [CrossRef] [PubMed]

147. Shi, Z.; Li, Y.; Li, S.; Li, X.; Wu, D.; Xu, T.; Tian, Y.; Chen, Y.; Zhang, Y.; Zhang, B.; et al. Localized Surface Plasmon Enhanced All-Inorganic Perovskite Quantum Dot Light-Emitting Diodes Based on Coaxial Core/Shell Heterojunction Architecture. *Adv. Funct. Mater.* **2018**, *28*, 1707031. [CrossRef]

148. Zhang, F.; Song, J.; Han, B.; Fang, T.; Li, J.; Zeng, H. High-effciency pure-color inorganic halide perovskite emitters for ultrahigh-defnition displays: Progressfor backlighting displays and electrically driven devices. *Small Methods* **2018**, *2*, 1700382. [CrossRef]

149. Ji, W.; Shen, H.; Zhang, H.; Kang, Z.; Zhang, H. Over 800% efficiency enhancement of all-inorganic quantum-dot light emitting diodes with an ultrathin alumina passivating layer. *Nanoscale* **2018**, *10*, 11103–11109. [CrossRef]

150. Lin, Q.; Wang, L.; Li, Z.; Shen, H.; Guo, L.; Kuang, Y.; Wang, H.; Li, L.S. Nonblinking Quantum-Dot-Based Blue Light-Emitting Diodes with High Efficiency and a Balanced Charge-Injection Process. *ACS Photonics* **2018**, *5*, 939–946. [CrossRef]

151. Ji, W.; Liu, S.; Zhang, H.; Wang, R.; Xie, W.; Zhang, H. Ultrasonic Spray Processed, Highly Efficient All-Inorganic Quantum-Dot Light-Emitting Diodes. *ACS Photonics* **2017**, *4*, 1271–1278. [CrossRef]

152. Sun, Y.; Jiang, Y.; Sun, X.W.; Zhang, S.; Chen, S. Beyond OLED: Efficient Quantum Dot Light-Emitting Diodes for Display and Lighting Application. *Chem. Rec.* **2019**, *19*, 1729–1752. [CrossRef] [PubMed]

153. Yao, E.-P.; Yang, Z.; Meng, L.; Sun, P.; Dong, S.; Yang, Y.; Yang, Y. High-Brightness Blue and White LEDs based on Inorganic Perovskite Nanocrystals and their Composites. *Adv. Mater.* **2017**, *29*, 1606859. [CrossRef] [PubMed]

154. Li, G.; Rivarola, F.W.R.; Davis, N.J.L.K.; Bai, S.; Jellicoe, T.; De La Peña, F.; Hou, S.; Ducati, C.; Gao, F.; Friend, R.H.; et al. Highly Efficient Perovskite Nanocrystal Light-Emitting Diodes Enabled by a Universal Crosslinking Method. *Adv. Mater.* **2016**, *28*, 3528–3534. [CrossRef] [PubMed]

155. Li, X.; Wu, Y.; Zhang, S.; Cai, B.; Gu, Y.; Song, J.; Zeng, H. CsPbX$_3$ Quantum Dots for Lighting and Displays: Room-Temperature Synthesis, Photoluminescence Superiorities, Underlying Origins and White Light-Emitting Diodes. *Adv. Funct. Mater.* **2016**, *26*, 2435–2445. [CrossRef]

156. Coe-Sullivan, S.; Woo, W.-K.; Steckel, J.S.; Bawendi, M.; Bulović, V. Tuning the performance of hybrid organic/inorganic quantum dot light-emitting devices. *Org. Electron.* **2003**, *4*, 123–130. [CrossRef]

157. Chaudhuri, R.G.; Paria, S. Core/Shell Nanoparticles: Classes, Properties, Synthesis Mechanisms, Characterization, and Applications. *Chem. Rev.* **2012**, *112*, 2373–2433. [CrossRef]

158. Fang, T.; Zhang, F.; Yuan, S.; Zeng, H.; Song, J. Recent advances and prospects toward blue perovskite materials and light-emitting diodes. *InfoMat* **2019**, *1*, 211–233. [CrossRef]

159. Khan, Q.; Subramanian, A.; Yu, G.; Maaz, K.; Li, D.; Sagar, R.U.R.; Chen, K.; Lei, W.; Shabbir, B.; Zhangb, Y. Structure optimization of perovskite quantum dot light-emitting diodes. *Nanoscale* **2019**, *11*, 5021–5029. [CrossRef]

160. Wang, K.-H.; Zhu, B.-S.; Yao, J.-S.; Yao, H.-B. Chemical regulation of metal halide perovskite nanomaterials for efficient light-emitting diodes. *Sci. China Ser. B Chem.* **2018**, *61*, 1047–1061. [CrossRef]

161. Liu, B.; Xu, M.; Wang, L.; Tao, H.; Su, Y.; Gao, D.; Lan, L.; Zou, J.; Peng, J. Very-High Color Rendering Index Hybrid White Organic Light-Emitting Diodes with Double Emitting Nanolayers. *Nano-Micro Lett.* **2014**, *6*, 335–339. [CrossRef]

162. Liu, B.; Luo, D.; Gao, D.; Wang, X.; Xu, M.; Zou, J.; Ning, H.; Wang, L.; Peng, J.; Cao, Y. An ideal host-guest system to accomplish high-performance greenish yellow and hybrid white organic light-emitting diodes. *Org. Electron.* **2015**, *27*, 29–34. [CrossRef]

163. Liu, B.-Q.; Wang, L.; Gao, D.-Y.; Zou, J.; Ning, H.-L.; Peng, J.-B.; Cao, Y. Extremely high-efficiency and ultrasimplified hybrid white organic light-emitting diodes exploiting double multifunctional blue emitting layers. *Light. Sci. Appl.* **2016**, *5*, e16137. [CrossRef] [PubMed]

164. Reineke, S.; Lindner, F.; Schwartz, G.; Seidler, N.; Walzer, K.; Lüssem, B.; Leo, K. White organic light-emitting diodes with fluorescent tube efficiency. *Nature* **2009**, *459*, 234. [CrossRef] [PubMed]

165. Schwartz, G.; Pfeiffer, M.; Reineke, S.; Walzer, K.; Leo, K. Harvesting Triplet Excitons from Fluorescent Blue Emitters in White Organic Light-Emitting Diodes. *Adv. Mater.* **2007**, *19*, 3672–3676. [CrossRef]

166. Ye, J.; Zheng, C.-J.; Ou, X.-M.; Zhang, X.; Fung, M.-K.; Lee, C. Management of Singlet and Triplet Excitons in a Single Emission Layer: A Simple Approach for a High-Efficiency Fluorescence/Phosphorescence Hybrid White Organic Light-Emitting Device. *Adv. Mater.* **2012**, *24*, 3410–3414. [CrossRef]

167. Kumar, S.; Jagielski, J.; Kallikounis, N.; Kim, Y.-H.; Wolf, C.; Jenny, F.; Tian, T.; Hofer, C.J.; Chiu, Y.-C.; Stark, W.J.; et al. Ultrapure Green Light-Emitting Diodes Using Two-Dimensional Formamidinium Perovskites: Achieving Recommendation 2020 Color Coordinates. *Nano Lett.* **2017**, *17*, 5277–5284. [CrossRef]

168. Polovitsyn, A.; Dang, Z.; Movilla, J.L.; Martín-García, B.; Khan, A.H.; Bertrand, G.H.V.; Brescia, R.; Moreels, I. Synthesis of Air-Stable CdSe/ZnS Core–Shell Nanoplatelets with Tunable Emission Wavelength. *Chem. Mater.* **2017**, *29*, 5671–5680. [CrossRef]

169. Davis, A.H.; Hofman, E.; Chen, K.; Li, Z.; Khammang, A.; Zamani, H.; Franck, J.M.; Maye, M.M.; Meulenberg, R.W.; Zheng, W. Exciton Energy Shifts and Tunable Dopant Emission in Manganese-Doped Two-Dimensional CdS/ZnS Core/Shell Nanoplatelets. *Chem. Mater.* **2019**, *31*, 2516–2523. [CrossRef]

170. Liu, B.-Q.; Tao, H.; Su, Y.-J.; Gao, D.-Y.; Lan, L.; Zou, J.; Peng, J.-B.; Bai-Quan, L.; Hong, T.; Yue-Ju, S.; et al. Color-stable, reduced efficiency roll-off hybrid white organic light emitting diodes with ultra high brightness. *Chin. Phys. B* **2013**, *22*, 077303. [CrossRef]

171. Liu, B.; Tao, H.; Wang, L.; Gao, D.; Liu, W.; Zou, J.; Xu, M.; Ning, H.; Peng, J.; Cao, Y. High-performance doping-free hybrid white organic light-emitting diodes: The exploitation of ultrathin emitting nanolayers (<1 nm). *Nano Energy* **2016**, *26*, 26–36.

172. Schwartz, G.; Ke, T.-H.; Wu, C.-C.; Walzer, K.; Leo, K. Balanced ambipolar charge carrier mobility in mixed layers for application in hybrid white organic light-emitting diodes. *Appl. Phys. Lett.* **2008**, *93*, 73304. [CrossRef]

173. Wu, H.; Zhang, Y.; Lu, M.; Zhang, X.; Sun, C.; Zhang, T.; Colvin, V.L.; Yu, W.W. Surface ligand modification of cesium lead bromide nanocrystals for improved light-emitting performance. *Nanoscale* **2018**, *10*, 4173–4178. [CrossRef]

174. Wang, H.; Zhang, X.; Wu, Q.; Cao, F.; Yang, D.; Shang, Y.; Ning, Z.; Zhang, W.; Zheng, W.; Yan, Y.; et al. Trifluoroacetate induced small-grained $CsPbBr_3$ perovskite films result in efficient and stable light-emitting devices. *Nat. Commun.* **2019**, *10*, 665. [CrossRef] [PubMed]

175. Kim, D.-H.; D'Aléo, A.; Chen, X.-K.; Sandanayaka, A.D.S.; Yao, D.; Zhao, L.; Komino, T.; Zaborova, E.; Canard, G.; Tsuchiya, Y.; et al. High-efficiency electroluminescence and amplified spontaneous emission from a thermally activated delayed fluorescent near-infrared emitter. *Nat. Photonics* **2018**, *12*, 98. [CrossRef]

176. Galland, C.; Ghosh, Y.; Steinbrück, A.; Hollingsworth, J.A.; Htoon, H.; Klimov, V.I. Lifetime blinking in nonblinking nanocrystal quantum dots. *Nat. Commun.* **2012**, *3*, 908. [CrossRef] [PubMed]

177. Kumawat, N.K.; Swarnkar, A.; Nag, A.; Kabra, D. Ligand Engineering to Improve the Luminance Efficiency of CsPbBr$_3$ Nanocrystal Based Light-Emitting Diodes. *J. Phys. Chem. C* **2018**, *122*, 13767–13772. [CrossRef]

178. Jin, F.; Zhao, B.; Chu, B.; Zhao, H.; Su, Z.; Li, W.; Zhu, F. Morphology control towards bright and stable inorganic halide perovskite light-emitting diodes. *J. Mater. Chem. C* **2018**, *6*, 1573–1578. [CrossRef]

179. Suyver, J.F.; Wuister, S.F.; Kelly, J.J.; Meijerink, A. Synthesis and Photoluminescence of Nanocrystalline ZnS:Mn^{2+}. *Nano Lett.* **2001**, *1*, 429–433. [CrossRef]

180. Pradhan, N.; Goorskey, D.; Thessing, J.; Peng, X. An Alternative of CdSe Nanocrystal Emitters: Pure and Tunable Impurity Emissions in ZnSe Nanocrystals. *J. Am. Chem. Soc.* **2005**, *127*, 17586–17587. [CrossRef]

181. Yang, Y.; Chen, O.; Angerhofer, A.; Cao, Y.C. Radial-Position-Controlled Doping in CdS/ZnS Core/Shell Nanocrystals. *J. Am. Chem. Soc.* **2006**, *128*, 12428–12429. [CrossRef]

182. Yang, Y.; Chen, O.; Angerhofer, A.; Cao, Y.C. On Doping CdS/ZnS Core/Shell Nanocrystals with Mn. *J. Am. Chem. Soc.* **2008**, *130*, 15649–15661. [CrossRef]

183. Karan, N.S.; Sarma, D.D.; Kadam, R.M.; Pradhan, N. Doping Transition Metal (Mn or Cu) Ions in Semiconductor Nanocrystals. *J. Phys. Chem. Lett.* **2010**, *1*, 2863–2866. [CrossRef]

184. Shen, H.; Wang, H.; Li, X.; Niu, J.Z.; Wang, H.; Chen, X.; Li, L.S. Phosphine-free synthesis of high quality ZnSe, ZnSe/ZnS, and Cu-, Mn-doped ZnSe nanocrystals. *Dalton Trans.* **2009**, *47*, 10534–10540. [CrossRef] [PubMed]

185. Jana, S.; Srivastava, B.B.; Pradhan, N. Correlation of Dopant States and Host Bandgap in Dual-Doped Semiconductor Nanocrystals. *J. Phys. Chem. Lett.* **2011**, *2*, 1747–1752. [CrossRef]

186. Xie, R.; Peng, X. Synthesis of Cu-Doped InP Nanocrystals (d-dots) with ZnSe Diffusion Barrier as Efficient and Color-Tunable NIR Emitters. *J. Am. Chem. Soc.* **2009**, *131*, 10645–10651. [CrossRef] [PubMed]

187. Sethi, R.; Kumar, L.; Sharma, P.K.; Pandey, A. Tunable Visible Emission of Ag-Doped CdZnS Alloy Quantum Dots. *Nanoscale Res. Lett.* **2010**, *5*, 96. [CrossRef]

188. Zhao, F.A.; Xiao, H.; Bai, X.-M.; Zu, X.T. Effects of Ag doping on the electronic and optical properties of CdSe quantum dots. *Phys. Chem. Chem. Phys.* **2019**, *21*, 16108–16119. [CrossRef]

189. Kroupa, D.M.; Hughes, B.K.; Miller, E.M.; Moore, D.T.; Anderson, N.; Chernomordik, B.D.; Nozik, A.J.; Beard, M. Synthesis and Spectroscopy of Silver-Doped PbSe Quantum Dots. *J. Am. Chem. Soc.* **2017**, *139*, 10382–10394. [CrossRef]

190. Nelson, H.D.; Hinterding, S.O.M.; Fainblat, R.; Creutz, S.E.; Li, X.; Gamelin, D.R. Mid-Gap States and Normal vs Inverted Bonding in Luminescent Cu$^+$- and Ag$^+$- Doped CdSe Nanocrystals. *J. Am. Chem. Soc.* **2017**, *139*, 6411–6421. [CrossRef]

191. Luo, J.; Wang, X.; Li, S.; Liu, J.; Guo, Y.; Niu, G.; Yao, L.; Fu, Y.; Gao, L.; Dong, Q.; et al. Efficient and stable emission of warm-white light from lead-free halide double perovskites. *Nature* **2018**, *563*, 541. [CrossRef]

192. Tong, Y.; Yao, E.-P.; Manzi, A.; Bladt, E.; Wang, K.; Döblinger, M.; Bals, S.; Müller-Buschbaum, P.; Urban, A.S.; Polavarapu, L.; et al. Spontaneous Self-Assembly of Perovskite Nanocrystals into Electronically Coupled Supercrystals: Toward Filling the Green Gap. *Adv. Mater.* **2018**, *30*, 1801117. [CrossRef] [PubMed]

193. Yue, Y.; Zhu, D.; Zhang, N.; Zhu, G.; Su, Z.-M. Ligand-Induced Tunable Dual-Color Emission Based on Lead Halide Perovskites for White Light-Emitting Diodes. *ACS Appl. Mater. Interfaces* **2019**, *11*, 15898–15904. [CrossRef] [PubMed]

194. Brovelli, S.; Galland, C.; Viswanatha, R.; Klimov, V.I. Tuning Radiative Recombination in Cu-Doped Nanocrystals via Electrochemical Control of Surface Trapping. *Nano Lett.* **2012**, *12*, 4372–4379. [CrossRef] [PubMed]

195. Lozhkina, O.A.; Murashkina, A.A.; Shilovskikh, V.V.; Kapitonov, Y.V.; Ryabchuk, V.K.; Emeline, A.V.; Miyasaka, T. Invalidity of Band-Gap Engineering Concept for Bi^{3+} Heterovalent Doping in CsPbBr$_3$ Halide Perovskite. *J. Phys. Chem. Lett.* **2018**, *9*, 5408–5411. [CrossRef]

196. Hoshi, K.; Chiba, T.; Sato, J.; Hayashi, Y.; Takahashi, Y.; Ebe, H.; Ohisa, S.; Kido, J. Purification of Perovskite Quantum Dots Using Low-Dielectric-Constant Washing Solvent "Diglyme" for Highly Efficient Light-Emitting Devices. *ACS Appl. Mater. Interfaces* **2018**, *10*, 24607–24612. [CrossRef]

197. Zhou, C.; Tian, Y.; Khabou, O.; Worku, M.; Zhou, Y.; Hurley, J.; Lin, H.; Ma, B. Manganese-Doped One-Dimensional Organic Lead Bromide Perovskites with Bright White Emissions. *ACS Appl. Mater. Interfaces* **2017**, *9*, 40446–40451. [CrossRef]

198. Thapa, S.; Adhikari, G.C.; Zhu, H.; Grigoriev, A.; Zhu, P. Zn-Alloyed All-Inorganic Halide Perovskite-Based White Light-Emitting Diodes with Superior Color Quality. *Sci. Rep.* **2019**, *9*, 18636. [CrossRef]

199. Mocatta, D.; Cohen, G.; Schattner, J.; Millo, O.; Rabani, E.; Banin, U. Heavily Doped Semiconductor Nanocrystal Quantum Dots. *Science* **2011**, *332*, 77–81. [CrossRef] [PubMed]

200. Aqili, A.K.; Saleh, A.J.; Ali, Z.; Al-Omari, S. Ag doped ZnTe films prepared by closed space sublimation and an ion exchange process. *J. Alloy. Compd.* **2012**, *520*, 83–88. [CrossRef]

201. Cho, H.; Wolf, C.; Kim, J.S.; Yun, H.J.; Bae, S.S.; Kim, H.; Heo, J.-M.; Ahn, S.; Lee, T.-W. High-Efficiency Solution-Processed Inorganic Metal Halide Perovskite Light-Emitting Diodes. *Adv. Mater.* **2017**, *29*, 1700579. [CrossRef] [PubMed]

202. Lupanab, O.; Pauporté, T.; Le Bahers, T.; Viana, B.; Ciofini, I. Wavelength-Emission Tuning of ZnO Nanowire-Based Light-Emitting Diodes by Cu Doping: Experimental and Computational Insights. *Adv. Funct. Mater.* **2011**, *21*, 3564–3572. [CrossRef]

203. Liu, B.; Wang, L.; Gu, H.; Sun, H.; Demir, H.V. Highly Efficient Green Light-Emitting Diodes from All-Inorganic Perovskite Nanocrystals Enabled by a New Electron Transport Layer. *Adv. Opt. Mater.* **2018**, *5*, 1800220. [CrossRef]

204. Supran, G.J.; Shirasaki, Y.; Song, K.W.; Caruge, J.-M.; Kazlas, P.T.; Coe-Sullivan, S.; Andrew, T.L.; Bawendi, M.G.; Bulović, V. QLEDs for displays and solid-state lighting. *MRS Bull.* **2013**, *38*, 703–711. [CrossRef]

205. Ye, F.; Zhang, H.; Wang, P.; Li, W.; Li, D.; Du, B.; Liu, D.; Wang, T. Methylammonium-Mediated Crystallization of Cesium-Based 2D/3D Perovskites toward High-Efficiency Light-Emitting Diodes. *ACS Appl. Mater. Interfaces* **2019**, *11*, 43452–43459. [CrossRef]

206. Schwartz, G.; Reineke, S.; Rosenow, T.C.; Walzer, K.; Leo, K. Triplet Harvesting in Hybrid White Organic Light-Emitting Diodes. *Adv. Funct. Mater.* **2009**, *19*, 1319–1333. [CrossRef]

207. Liu, B.; Nie, H.; Zhou, X.; Hu, S.; Luo, D.; Gao, D.; Zou, J.; Xu, M.; Wang, L.; Zhao, Z.; et al. Manipulation of Charge and Exciton Distribution Based on Blue Aggregation-Induced Emission Fluorophors: A Novel Concept to Achieve High-Performance Hybrid White Organic Light-Emitting Diodes. *Adv. Funct. Mater.* **2016**, *26*, 776–783. [CrossRef]

208. Adachi, C.; Baldo, M.A.; Thompson, M.E.; Forrest, S.R. Nearly 100% internal phosphorescence efficiency in an organic light-emitting device. *J. Appl. Phys.* **2001**, *90*, 5048–5051. [CrossRef]

209. Liu, B.; Xu, M.; Tao, H.; Su, Y.; Gao, D.; Zou, J.; Lan, L.; Peng, J. The effect of spacer in hybrid white organic light emitting diodes. *Chin. Sci. Bull.* **2014**, *59*, 3090–3097. [CrossRef]

210. Chen, Y.; Chen, J.; Ma, D.; Yan, D.; Wang, L.; Zhu, F. High power efficiency tandem organic light-emitting diodes based on bulk heterojunction organic bipolar charge generation layer. *Appl. Phys. Lett.* **2011**, *98*, 243309. [CrossRef]

211. Zhou, J.; Zou, J.; Dai, C.; Zhang, Y.; Luo, X.; Liu, B. High-Efficiency and High-Luminance Three-Color White Organic Light-Emitting Diodes with Low Efficiency Roll-Off. *ECS J. Solid State Sci. Technol.* **2018**, *7*, R99–R103. [CrossRef]

212. Xiao, P.; Huang, J.; Yu, Y.; Yuan, J.; Luo, D.; Liu, B.; Liang, D. Recent Advances of Exciplex-Based White Organic Light-Emitting Diodes. *Appl. Sci.* **2018**, *8*, 1449. [CrossRef]

213. Liu, B.; Wang, L.; Xu, M.; Tao, H.; Xia, X.; Zou, J.; Su, Y.; Gao, D.; Lan, L.; Peng, J. Simultaneous achievement of low efficiency roll-off and stable color in highly efficient single-emitting-layer phosphorescent white organic light-emitting diodes. *J. Mater. Chem. C* **2014**, *2*, 5870–5877. [CrossRef]

214. Liu, B.; Xu, M.; Wang, L.; Yan, X.; Tao, H.; Su, Y.; Gao, D.; Lan, L.; Zou, J.; Peng, J. Investigation and optimization of each organic layer: A simple but effective approach towards achieving high-efficiency hybrid white organic light-emitting diodes. *Org. Electron.* **2014**, *15*, 926–936. [CrossRef]

215. Liu, B.; Zou, J.; Su, Y.; Gao, D.; Lan, L.; Tao, H.; Peng, J. Hybrid white organic light emitting diodes with low efficiency roll-off, stable color and extreme brightness. *J. Lumin.* **2014**, *151*, 161–164. [CrossRef]

216. Schwartz, G.; Fehse, K.; Pfeiffer, M.; Walzer, K.; Leo, K. Highly efficient white organic light emitting diodes comprising an interlayer to separate fluorescent and phosphorescent regions. *Appl. Phys. Lett.* **2006**, *89*, 083509. [CrossRef]

217. Boroumand, F.; Hammiche, A.; Hill, G.; Lidzey, D.G. Characterizing Joule Heating in Polymer Light-Emitting Diodes Using a Scanning Thermal Microscope. *Adv. Mater.* **2004**, *16*, 252. [CrossRef]

218. Liu, B.; Xu, M.; Wang, L.; Su, Y.; Gao, D.; Tao, H.; Lan, L.; Zou, J.; Peng, J. High-Performance Hybrid White Organic Light-Emitting Diodes Comprising Ultrathin Blue and Orange Emissive Layers. *Appl. Phys. Express* **2013**, *6*, 122101. [CrossRef]

219. Byeon, S.Y.; Kim, J.; Lee, D.R.; Han, S.H.; Forrest, S.R.; Lee, J.Y. Nearly 100% Horizontal Dipole Orientation and Upconversion Efficiency in Blue Thermally Activated Delayed Fluorescent Emitters. *Adv. Opt. Mater.* **2018**, *6*, 1701340. [CrossRef]

220. Huang, J.; Yang, Y.; Xue, S.; Yang, B.; Liu, S.; Shen, J. Photoluminescence and electroluminescence of ZnS:Cu nanocrystals in polymeric networks. *Appl. Phys. Lett.* **1997**, *70*, 2335–2337. [CrossRef]

221. Que, W.; Zhou, Y.; Lam, Y.L.; Chan, Y.C.; Kam, C.H.; Liu, B.; Gan, L.M.; Chew, C.H.; Xu, G.Q.; Chua, S.J.; et al. Photoluminescence and electroluminescence from copper doped zinc sulphide nanocrystals/polymer composite. *Appl. Phys. Lett.* **1998**, *73*, 2727–2729. [CrossRef]

222. Park, B.; Holloway, P.H. Enhanced photoluminescence from CdS:Mn/ZnS core/shell quantum dots. *Appl. Phys. Lett.* **2003**, *82*, 1965–1967.

223. Yang, H.; Holloway, P.H. Electroluminescence from Hybrid Conjugated Polymer–CdS:Mn/ZnS Core/Shell Nanocrystals Devices. *J. Phys. Chem. B* **2003**, *107*, 9705–9710. [CrossRef]

224. De La Torre, J.; Souifi, A.; Poncet, A.; Busseret, C.; Lemiti, M.; Bremond, G.; Guillot, G.; González, O.; Garrido, B.; Morante, J.R.; et al. Optical properties of silicon nanocrystal LEDs. *Phys. E Low-Dimens. Syst. Nanostruct.* **2003**, *16*, 326–330. [CrossRef]

225. Park, B.; Holloway, P.H.; Ratna, B.B. Photoluminescent and electroluminescent properties of Mn-doped ZnS nanocrystals. *J. Appl. Phys.* **2003**, *93*, 586–592.

226. Knowles, K.E.; Hartstein, K.H.; Kilburn, T.B.; Marchioro, A.; Nelson, H.D.; Whitham, P.J.; Gamelin, D.R. Luminescent Colloidal Semiconductor Nanocrystals Containing Copper: Synthesis, Photophysics, and Applications. *Chem. Rev.* **2016**, *116*, 10820–10851. [CrossRef]

227. Stouwdam, J.W.; Janssen, R. Electroluminescent Cu-doped CdS Quantum Dots. *Adv. Mater.* **2009**, *21*, 2916–2920. [CrossRef]

228. Ling, Y.; Yuan, Z.; Tian, Y.; Wang, X.; Wang, J.; Xin, Y.; Hanson, K.; Ma, B.; Gao, H. Bright Light-Emitting Diodes Based on Organometal Halide Perovskite Nanoplatelets. *Adv. Mater.* **2016**, *28*, 305–311. [CrossRef]

229. Ji, H.; Shi, Z.; Sun, X.; Li, Y.; Li, S.; Lei, L.; Wu, D.; Xu, T.; Li, X.; Du, G. Vapor-Assisted Solution Approach for High-Quality Perovskite CH$_3$NH$_3$PbBr$_3$ Thin Films for High-Performance Green Light-Emitting Diode Applications. *ACS Appl. Mater. Interfaces* **2017**, *9*, 42893–42904. [CrossRef]

230. Rastogi, P.; Palazon, F.; Prato, M.; Di Stasio, F.; Krahne, R. Enhancing the Performance of CdSe/CdS Dot-in-Rod Light-Emitting Diodes via Surface Ligand Modification. *ACS Appl. Mater. Interfaces* **2018**, *10*, 5665–5672. [CrossRef]

231. Yang, D.; Zou, Y.; Li, P.; Liu, Q.; Wu, L.; Hu, H.; Xu, Y.; Sun, B.; Zhang, Q.; Lee, S.-T.; et al. Large-scale synthesis of ultrathin cesium lead bromide perovskite nanoplates with precisely tunable dimensions and their application in blue light-emitting diodes. *Nano Energy* **2018**, *47*, 235–242. [CrossRef]

232. Gangishetty, M.K.; Hou, S.; Quan, Q.; Congreve, D.N. Blue Perovskite LEDs: Reducing Architecture Limitations for Efficient Blue Perovskite Light-Emitting Diodes. *Adv. Mater.* **2018**, *30*, 1706226. [CrossRef]

233. Ling, Y.; Tian, Y.; Wang, X.; Wang, J.C.; Knox, J.M.; Perez-Orive, F.; Du, Y.; Tan, L.; Hanson, K.; Ma, B.; et al. Enhanced optical and electrical properties of polymer-assisted all-inorganic perovskites for light-emitting diodes. *Adv. Mater.* **2016**, *28*, 8983–8989. [CrossRef] [PubMed]

234. Khan, A.H.; Dalui, A.; Mukherjee, S.; Segre, C.U.; Sarma, D.D.; Acharya, S. Efficient Solid-State Light-Emitting CuCdS Nanocrystals Synthesized in Air. *Angew. Chem. Int. Ed.* **2015**, *54*, 2643–2648. [CrossRef] [PubMed]

235. Bae, W.K.; Kwak, J.; Lim, J.; Lee, N.; Nam, M.K.; Char, K.; Lee, C.; Lee, S. Multicolored Light-Emitting Diodes Based on All-Quantum-Dot Multilayer Films Using Layer-by-Layer Assembly Method. *Nano Lett.* **2010**, *10*, 2368–2373. [CrossRef]

236. Lee, K.-H.; Lee, J.H.; Kang, H.-D.; Park, B.; Kwon, Y.; Ko, H.; Lee, C.; Lee, J.; Park, B. Over 40 cd/A Efficient Green Quantum Dot Electroluminescent Device Comprising Uniquely Large-Sized Quantum Dots. *ACS Nano* **2014**, *8*, 4893–4901. [CrossRef]

237. Pauporté, T.; Lupanab, O.; Zhang, J.; Tugsuz, T.; Ciofini, I.; Labat, F.; Viana, B. Low-Temperature Preparation of Ag-Doped ZnO Nanowire Arrays, DFT Study, and Application to Light-Emitting Diode. *ACS Appl. Mater. Interfaces* **2015**, *7*, 11871–11880. [CrossRef]

238. Yoon, C.; Yang, K.P.; Kim, J.; Shin, K.; Lee, K. Fabrication of highly transparent and luminescent quantum dot/polymer nanocomposite for light emitting diode using amphiphilic polymer-modified quantum dots. *Chem. Eng. J.* **2020**, *382*, 122792. [CrossRef]

239. Xuan, T.; Xie, R.-J. Recent processes on light-emitting lead-free metal halide perovskites. *Chem. Eng. J.* **2020**, *393*, 124757. [CrossRef]

240. Zhong, H.; Wang, Z.; Bovero, E.; Lu, Z.; Van Veggel, F.C.J.M.; Scholes, G.D. Colloidal $CuInSe_2$ Nanocrystals in the Quantum Confinement Regime: Synthesis, Optical Properties, and Electroluminescence. *J. Phys. Chem. C* **2011**, *115*, 12396–12402. [CrossRef]

241. Srivastava, B.B.; Jana, S.; Pradhan, N. Doping Cu in Semiconductor Nanocrystals: Some Old and Some New Physical Insights. *J. Am. Chem. Soc.* **2011**, *133*, 1007–1015. [CrossRef] [PubMed]

242. Zhang, W.; Zhou, X.; Zhong, X. One-Pot Noninjection Synthesis of Cu-Doped $Zn_xCd_{1-x}S$ Nanocrystals with Emission Color Tunable over Entire Visible Spectrum. *Inorg. Chem.* **2012**, *51*, 3579–3587. [CrossRef] [PubMed]

243. Chen, Y.; Huang, L.; Li, S.; Pan, D. Aqueous synthesis of glutathione-capped Cu^+ and Ag^+-doped $Zn_xCd_{1−x}S$ quantum dots with full color emission. *J. Mater. Chem. C* **2013**, *1*, 751–756. [CrossRef]

244. Sarkar, S.; Karan, N.S.; Pradhan, N. Ultrasmall Color-Tunable Copper-Doped Ternary Semiconductor Nanocrystal Emitters. *Angew. Chem. Int. Ed.* **2011**, *50*, 6065–6069. [CrossRef]

245. Zhang, W.; Lou, Q.; Ji, W.; Zhao, J.; Zhong, X. Color-Tunable Highly Bright Photoluminescence of Cadmium-Free Cu-Doped Zn–In–S Nanocrystals and Electroluminescence. *Chem. Mater.* **2014**, *26*, 1204–1212. [CrossRef]

246. Tan, Z.; Zhang, Y.; Xie, C.; Su, H.; Liu, J.; Zhang, C.; Dellas, N.; Mohney, S.E.; Wang, Y.; Wang, J.; et al. Near-Band-Edge Electroluminescence from Heavy-Metal-Free Colloidal Quantum Dots. *Adv. Mater.* **2011**, *23*, 3553–3558. [CrossRef]

247. Chen, B.; Zhong, H.; Zhang, W.; Tan, Z.; Li, Y.; Yu, C.; Zhai, T.; Bando, Y.; Yang, S.; Zou, B. Highly Emissive and Color-Tunable $CuInS_2$-Based Colloidal Semiconductor Nanocrystals: Off-Stoichiometry Effects and Improved Electroluminescence Performance. *Adv. Funct. Mater.* **2012**, *22*, 2081–2088. [CrossRef]

248. de Trizio, L.; Prato, M.; Genovese, A.; Casu, A.; Povia, M.; Simonutti, R.; Alcocer, M.J.P.; D'Andrea, C.; Tassone, F.; Manna, L. Strongly fluorescent quaternary Cu-In-Zn-S nanocrystals prepared from $Cu_{1-x}InS_2$ nanocrystals by partial cation exchange. *Chem. Mater.* **2012**, *24*, 2400–2406. [CrossRef]

249. Wu, T.; Zhang, Q.; Hou, Y.; Wang, L.; Mao, C.; Zheng, S.-T.; Bu, X.; Feng, P. Monocopper Doping in Cd-In-S Supertetrahedral Nanocluster via Two-Step Strategy and Enhanced Photoelectric Response. *J. Am. Chem. Soc.* **2013**, *135*, 10250–10253. [CrossRef]

250. Zhang, J.; Xie, R.; Yang, W. A Simple Route for Highly Luminescent Quaternary Cu-Zn-In-S Nanocrystal Emitters. *Chem. Mater.* **2011**, *23*, 3357–3361. [CrossRef]

251. Xiang, W.; Yang, H.-L.; Liang, X.; Zhong, J.; Wang, J.; Luo, L.; Xie, C.-P. Direct synthesis of highly luminescent Cu–Zn–In–S quaternary nanocrystals with tunable photoluminescence spectra and decay times. *J. Mater. Chem. C* **2013**, *1*, 2014–2020. [CrossRef]

252. Yuan, X.; Ma, R.; Zhang, W.; Hua, J.; Meng, X.; Zhong, X.; Zhang, J.; Zhao, J.; Li, H. Dual Emissive Manganese and Copper Co-Doped Zn–In–S Quantum Dots as a Single Color-Converter for High Color Rendering White-Light-Emitting Diodes. *ACS Appl. Mater. Interfaces* **2015**, *7*, 8659–8666. [CrossRef] [PubMed]

253. Zhang, Q.-H.; Tian, Y.; Wang, C.-F.; Chen, S. Construction of Ag-doped Zn–In–S quantum dots toward white LEDs and 3D luminescent patterning. *RSC Adv.* **2016**, *6*, 47616–47622. [CrossRef]

254. Perumal, A.; Shendre, S.; Li, M.; Tay, Y.K.E.; Sharma, V.K.; Chen, S.; Wei, Z.; Liu, Q.; Gao, Y.; Buenconsejo, P.J.S.; et al. High brightness formamidinium lead bromide perovskite nanocrystal light emitting devices. *Sci. Rep.* **2016**, *6*, 36733. [CrossRef] [PubMed]

255. Fang, Z.; Chen, W.; Shi, Y.; Zhao, J.; Chu, S.; Zhang, J.; Xiao, Z. Dual Passivation of Perovskite Defects for Light-Emitting Diodes with External Quantum Efficiency Exceeding 20%. *Adv. Funct. Mater.* **2020**, *30*, 1909754. [CrossRef]

256. Zhang, C.; Kuang, D.-B.; Wu, W. A Review of Diverse Halide Perovskite Morphologies for Efficient Optoelectronic Applications. *Small Methods* **2020**, *4*, 1900662. [CrossRef]

257. Hu, Y.; Wang, Q.; Shi, Y.-L.; Li, M.; Zhang, L.; Wang, Z.-K.; Liao, L.-S. Vacuum-evaporated all-inorganic cesium lead bromine perovskites for high-performance light-emitting diodes. *J. Mater. Chem. C* **2017**, *5*, 8144–8149. [CrossRef]

258. Li, Z.; Dong, J.; Liu, C.; Guo, J.; Shen, L.; Guo, W. Surface Passivation of Perovskite Solar Cells Toward Improved Efficiency and Stability. *Nano-Micro Lett.* **2019**, *11*, 50. [CrossRef]

259. Kim, M.; Jeon, S.K.; Yu, E.; Hwang, S.-H.; Lee, J.Y. Highly efficient and color tunable thermally activated delayed fluorescent emitters using a "twin emitter" molecular design. *Chem. Commun.* **2016**, *52*, 339–342. [CrossRef]

260. Song, Y.H.; Park, S.-Y.; Yoo, J.S.; Park, W.K.; Kim, H.S.; Choi, S.H.; Bin Kwon, S.; Kang, B.K.; Kim, J.P.; Jung, H.; et al. Efficient and stable green-emitting $CsPbBr_3$ perovskite nanocrystals in a microcapsule for light emitting diodes. *Chem. Eng. J.* **2018**, *352*, 957–963. [CrossRef]

261. Butkus, J.; Vashishtha, P.; Chen, K.; Gallaher, J.K.; Prasad, S.K.K.; Metin, D.Z.; Laufersky, G.; Gaston, N.; Halpert, J.E.; Hodgkiss, J.M. The Evolution of Quantum Confinement in $CsPbBr_3$ Perovskite Nanocrystals. *Chem. Mater.* **2017**, *29*, 3644–3652. [CrossRef]

262. Lau, C.F.J.; Zhang, M.; Deng, X.; Zheng, J.; Bing, J.; Ma, Q.; Kim, J.; Hu, L.; Green, M.A.; Huang, S.; et al. Strontium-Doped Low-Temperature-Processed $CsPbI_2Br$ Perovskite Solar Cells. *ACS Energy Lett.* **2017**, *2*, 2319–2325. [CrossRef]

263. Liang, J.; Zhao, P.; Wang, C.; Wang, Y.; Hu, Y.; Zhu, G.; Ma, L.; Liu, J.; Jin, Z. $CsPb_{0.9}Sn_{0.1}IBr_2$ Based All-Inorganic Perovskite Solar Cells with Exceptional Efficiency and Stability. *J. Am. Chem. Soc.* **2017**, *139*, 14009–14012. [CrossRef] [PubMed]

264. Liu, F.; Ding, C.; Zhang, Y.; Ripolles, T.S.; Kamisaka, T.; Toyoda, T.; Hayase, S.; Minemoto, T.; Yoshino, K.; Dai, S.; et al. Colloidal Synthesis of Air-Stable Alloyed $CsSn_{1-x}Pb_xI_3$ Perovskite Nanocrystals for Use in Solar Cells. *J. Am. Chem. Soc.* **2017**, *139*, 16708–16719. [CrossRef]

265. Kulkarni, S.A.; Mhaisalkar, S.G.; Mathews, N.; Boix, P.P. Perovskite Nanoparticles: Synthesis, Properties, and Novel Applications in Photovoltaics and LEDs. *Small Methods* **2019**, *3*, 1800231. [CrossRef]

266. Van Der Stam, W.; Geuchies, J.J.; Altantzis, T.; Bos, K.H.W.V.D.; Meeldijk, J.D.; Van Aert, S.; Bals, S.; Vanmaekelbergh, D.; Donega, C.D.M. Highly Emissive Divalent-Ion-Doped Colloidal $CsPb_{1-x}M_xBr_3$ Perovskite Nanocrystals through Cation Exchange. *J. Am. Chem. Soc.* **2017**, *139*, 4087–4097. [CrossRef]

267. Majher, J.D.; Gray, M.B.; Strom, T.A.; Woodward, P.M. $Cs_2NaBiCl_6$:Mn^{2+}—A New Orange-Red Halide Double Perovskite Phosphor. *Chem. Mater.* **2019**, *31*, 1738–1744. [CrossRef]

268. Akkerman, Q.A.; Meggiolaro, D.; Dang, Z.; De Angelis, F.; Manna, L. Fluorescent Alloy $CsPb_xMn_{1-x}I_3$ Perovskite Nanocrystals with High Structural and Optical Stability. *ACS Energy Lett.* **2017**, *2*, 2183–2186. [CrossRef]

269. Jena, A.K.; Kulkarni, A.; Sanehira, Y.; Ikegami, M.; Miyasaka, T. Stabilization of α-$CsPbI_3$ in Ambient Room Temperature Conditions by Incorporating Eu into $CsPbI_3$. *Chem. Mater.* **2018**, *30*, 6668–6674. [CrossRef]

270. Lu, M.; Zhang, X.; Bai, X.; Wu, H.; Shen, X.; Zhang, Y.; Zhang, W.; Zheng, W.; Song, H.; Yu, W.W.; et al. Spontaneous Silver Doping and Surface Passivation of $CsPbI_3$ Perovskite Active Layer Enable Light-Emitting Devices with an External Quantum Efficiency of 11.2%. *ACS Energy Lett.* **2018**, *3*, 1571–1577. [CrossRef]

271. Lin, K.-M.; Lin, R.-L.; Hsiao, W.-T.; Kang, Y.-C.; Chou, C.-Y.; Wang, Y.-Z. Effects of the structural properties of metal oxide/Ag/metal oxide multilayer transparent electrodes on their optoelectronic performances. *J. Mater. Sci. Mater. Electron.* **2017**, *25*, 12363–12371. [CrossRef]

272. Yambem, S.D.; Ullah, M.; Tandy, K.; Burn, P.L.; Namdas, E.B. ITO-free top emitting organic light emitting diodes with enhanced light out-coupling. *Laser Photonics Rev.* **2014**, *8*, 165–171. [CrossRef]

273. Jeong, D.; Lim, C.; Kim, M.; Jeong, K.; Kim, J.H.; Kim, J.; Park, J.G.; Min, K.S.; Lee, J. Self-assembled monolayer modified MoO_3/Au/MoO_3 multilayer anodes for high performance OLEDs. *Electron. Mater. Lett.* **2017**, *13*, 16–24. [CrossRef]

274. Lu, M.; Zhang, X.; Zhang, Y.; Guo, J.; Shen, X.; Yu, W.W.; Rogach, A. Simultaneous Strontium Doping and Chlorine Surface Passivation Improve Luminescence Intensity and Stability of $CsPbI_3$ Nanocrystals Enabling Efficient Light-Emitting Devices. *Adv. Mater.* **2018**, *30*, 1804691. [CrossRef] [PubMed]

275. Yao, J.-S.; Ge, J.; Wang, K.-H.; Zhang, G.; Zhu, B.-S.; Chen, C.; Zhang, Q.; Luo, Y.; Yu, S.-H.; Yao, H.-B. Few-Nanometer-Sized α-$CsPbI_3$ Quantum Dots Enabled by Strontium Substitution and Iodide Passivation for Efficient Red-Light Emitting Diodes. *J. Am. Chem. Soc.* **2019**, *141*, 2069–2079. [CrossRef]

276. Shen, X.; Zhang, Y.; Kershaw, S.V.; Li, T.; Wang, C.; Zhang, X.; Wang, W.; Li, D.; Wang, Y.; Lu, M.; et al. Zn-Alloyed $CsPbI_3$ Nanocrystals for Highly Efficient Perovskite Light-Emitting Devices. *Nano Lett.* **2019**, *19*, 1552–1559. [CrossRef]

277. Lu, M.; Guo, J.; Lu, P.; Zhang, L.; Zhang, Y.; Dai, Q.; Hu, Y.; Colvin, V.L.; Yu, W.W. Ammonium Thiocyanate-Passivated $CsPbI_3$ Perovskite Nanocrystals for Efficient Red Light-Emitting Diodes. *J. Phys. Chem. C* **2019**, *123*, 22787–22792. [CrossRef]

278. Zhang, J.; Zhang, L.; Cai, P.; Xue, X.; Wang, M.; Zhang, J.; Tu, G. Enhancing stability of red perovskite nanocrystals through copper substitution for efficient light-emitting diodes. *Nano Energy* **2019**, *62*, 434–441. [CrossRef]

279. Li, J.; Chen, J.; Xu, L.; Liu, S.; Lan, S.; Li, X.; Song, J. A zinc non-halide dopant strategy enables efficient perovskite CsPbI$_3$ quantum dot-based light-emitting diodes. *Mater. Chem. Front.* **2020**, *4*, 1444–1453. [CrossRef]

280. Wei, Y.; Cheng, Z.; Lin, J. An overview on enhancing the stability of lead halide perovskite quantum dots and their applications in phosphor-converted LEDs. *Chem. Soc. Rev.* **2019**, *48*, 310–350. [CrossRef]

281. Guvenc, C.M.; Yalcinkaya, Y.; Ozen, S.; Sahin, H.; Demir, M.M. Gd^{3+}-Doped α-CsPbI^3 Nanocrystals with Better Phase Stability and Optical Properties. *J. Phys. Chem. C* **2019**, *123*, 24865–24872. [CrossRef]

282. Lee, J.-W.; Kim, D.-H.; Kim, H.-S.; Seo, S.-W.; Cho, S.M.; Park, N.-G. Formamidinium and Cesium Hybridization for Photo- and Moisture-Stable Perovskite Solar Cell. *Adv. Energy Mater.* **2015**, *5*, 1501310. [CrossRef]

283. Hu, Y.; Bai, F.; Liu, X.; Ji, Q.; Miao, X.; Qiu, T.; Zhang, S. Bismuth Incorporation Stabilized α-CsPbI$_3$ for Fully Inorganic Perovskite Solar Cells. *ACS Energy Lett.* **2017**, *2*, 2219–2227. [CrossRef]

284. Sun, J.; Yang, J.H.; Lee, J.I.; Cho, J.H.; Kang, M.S. Lead-Free Perovskite Nanocrystals for Light-Emitting Devices. *J. Phys. Chem. Lett.* **2018**, *9*, 1573–1583. [CrossRef] [PubMed]

285. Huang, H.; Lin, H.; Kershaw, S.V.; Susha, A.S.; Choy, W.C.H.; Rogach, A. Polyhedral Oligomeric Silsesquioxane Enhances the Brightness of Perovskite Nanocrystal-Based Green Light-Emitting Devices. *J. Phys. Chem. Lett.* **2016**, *7*, 4398–4404. [CrossRef]

286. Zhang, X.; Xu, B.; Zhang, J.; Gao, Y.; Zheng, Y.; Wang, K.; Sun, X.W. All-Inorganic Perovskite Nanocrystals for High-Efficiency Light Emitting Diodes: Dual-Phase CsPbBr$_3$-CsPb$_2$Br$_5$ Composites. *Adv. Funct. Mater.* **2016**, *26*, 4595–4600. [CrossRef]

287. Yi, C.; Meloni, S.; Boziki, A.; Astani, N.A.; Grätzel, C.; Luo, J.; Zakeeruddin, S.M.; Rothlisberger, U. Entropic stabilization of mixed A-cation ABX$_3$ metal halide perovskites for high performance perovskite solar cells. *Energy Environ. Sci.* **2016**, *9*, 656–662. [CrossRef]

288. Kulbak, M.; Cahen, D.; Hodes, G. How Important Is the Organic Part of Lead Halide Perovskite Photovoltaic Cells? Efficient CsPbBr$_3$ Cells. *J. Phys. Chem. Lett.* **2015**, *6*, 2452–2456. [CrossRef]

289. Protesescu, L.; Yakunin, S.; Bodnarchuk, M.I.; Krieg, F.; Caputo, R.; Hendon, C.H.; Yang, R.X.; Walsh, A.; Kovalenko, M.V. Nanocrystals of Cesium Lead Halide Perovskites (CsPbX$_3$, X = Cl, Br, and I): Novel Optoelectronic Materials Showing Bright Emission with Wide Color Gamut. *Nano Lett.* **2015**, *15*, 3692. [CrossRef]

290. Stoumpos, C.C.; Malliakas, C.D.; Peters, J.; Liu, Z.; Sebastian, M.; Im, J.; Chasapis, T.C.; Wibowo, A.C.; Chung, D.Y.; Freeman, A.J.; et al. Crystal Growth of the Perovskite Semiconductor CsPbBr$_3$: A New Material for High-Energy Radiation Detection. *Cryst. Growth Des.* **2013**, *13*, 2722–2727. [CrossRef]

291. Boopathi, K.M.; Huang, T.-Y.; Budiawan, W.; Mohan, R.; Lin, M.-Y.; Lee, C.-H.; Ho, K.-C.; Chu, C.W. Synergistic improvements in stability and performance of lead iodide perovskite solar cells incorporating salt additives. *J. Mater. Chem. A* **2016**, *4*, 1591–1597. [CrossRef]

292. Hao, F.; Stoumpos, C.C.; Cao, D.H.; Chang, R.P.H.; Kanatzidis, M.G. Lead-free solid-state organic–inorganic halide perovskite solar cells. *Nat. Photonics* **2014**, *8*, 489–494. [CrossRef]

293. Zhang, X.L.; Liu, H.; Wang, W.G.; Zhang, J.B.; Xu, B.; Karen, K.L.; Zheng, Y.J.; Liu, S.; Chen, S.M.; Wang, K.; et al. Hybrid perovskite light-emitting diodes based on perovskite nanocrystals with organic-inorganic mixed cations. *Adv. Mater.* **2017**, *29*, 1606405. [CrossRef] [PubMed]

294. Xu, B.; Wang, W.; Zhang, X.; Cao, W.; Wu, D.; Liu, S.; Dai, H.; Chen, S.; Wang, K.; Sun, X.W. Bright and efficient light-emitting diodes based on MA/Cs double cation perovskite nanocrystals. *J. Mater. Chem. C* **2017**, *5*, 6123–6128. [CrossRef]

295. Mei, G.; Zhang, Y.; Xu, B.; Liu, H.; Zhong, J.; Shi, K.; Sun, X.W.; Wang, K. Bright and efficient light-emitting diodes based on perovskite quantum dots with formamidine-methylamine hybrid cations. *J. Phys. D Appl. Phys.* **2018**, *51*, 454003. [CrossRef]

296. Song, J.; Li, J.; Xu, L.; Li, J.; Zhang, F.; Han, B.; Shan, Q.; Zeng, H. Room-Temperature Triple-Ligand Surface Engineering Synergistically Boosts Ink Stability, Recombination Dynamics, and Charge Injection toward EQE-11.6% Perovskite QLEDs. *Adv. Mater.* **2018**, *30*, 180076. [CrossRef]

297. Zou, S.; Liu, Y.; Li, J.; Liu, C.; Feng, R.; Jiang, F.; Li, Y.; Song, J.; Zeng, H.; Hong, M.; et al. Stabilizing Cesium Lead Halide Perovskite Lattice through Mn(II) Substitution for Air-Stable Light-Emitting Diodes. *J. Am. Chem. Soc.* **2017**, *139*, 11443–11450. [CrossRef]

298. Yao, J.-S.; Ge, J.; Han, B.-N.; Wang, K.-H.; Yao, H.-B.; Yu, H.-L.; Li, J.-H.; Zhu, B.-S.; Song, J.; Chen, C.; et al. Ce^{3+}-Doping to Modulate Photoluminescence Kinetics for Efficient $CsPbBr_3$ Nanocrystals Based Light-Emitting Diodes. *J. Am. Chem. Soc.* **2018**, *140*, 3626–3634. [CrossRef]

299. Wang, H.-C.; Wang, W.; Tang, A.; Tsai, H.-Y.; Bao, Z.; Ihara, T.; Yarita, N.; Tahara, H.; Kanemitsu, Y.; Chen, S.; et al. High-Performance $CsPb_{1-x}Sn_xBr_3$ Perovskite Quantum Dots for Light-Emitting Diodes. *Angew. Chem. Int. Ed.* **2017**, *56*, 13650–13654. [CrossRef]

300. Huang, Q.; Zou, Y.; Bourelle, S.A.; Zhai, T.; Wu, T.; Tan, Y.; Li, Y.; Li, J.; Duhm, S.; Song, T.; et al. Suppressing defect states in $CsPbBr_3$ perovskite via magnesium substitution for efficient all-inorganic light-emitting diodes. *Nanoscale Horiz.* **2019**, *4*, 924–932. [CrossRef]

301. Wu, B.; Zhou, Y.; Xing, G.; Xu, Q.; Garces, H.F.; Solanki, A.; Goh, T.W.; Padture, N.P.; Sum, T.C. Long Minority-Carrier Diffusion Length and Low Surface-Recombination Velocity in Inorganic Lead-Free $CsSnI_3$ Perovskite Crystal for Solar Cells. *Adv. Funct. Mater.* **2017**, *27*, 1604818. [CrossRef]

302. Xing, G.; Kumar, M.H.; Chong, W.K.; Liu, X.; Cai, Y.; Ding, H.; Asta, M.; Grätzel, M.; Mhaisalkar, S.G.; Mathews, N.; et al. Solution-Processed Tin-Based Perovskite for Near-Infrared Lasing. *Adv. Mater.* **2016**, *28*, 8191–8196. [CrossRef] [PubMed]

303. Jellicoe, T.C.; Richter, J.M.; Glass, H.F.J.; Tabachnyk, M.; Brady, R.; Dutton, S.E.; Rao, A.; Friend, R.H.; Credgington, D.; Greenham, N.C.; et al. Synthesis and Optical Properties of Lead-Free Cesium Tin Halide Perovskite Nanocrystals. *J. Am. Chem. Soc.* **2016**, *138*, 2941–2944. [CrossRef] [PubMed]

304. Saparov, B.; Sun, J.-P.; Meng, W.; Xiao, Z.; Duan, H.-S.; Gunawan, O.; Shin, D.; Hill, I.G.; Yan, Y.; Mitzi, D.B. Thin-Film Deposition and Characterization of a Sn-Deficient Perovskite Derivative Cs_2SnI_6. *Chem. Mater.* **2016**, *28*, 2315–2322. [CrossRef]

305. Baek, S.; Kang, S.; Son, C.; Shin, S.J.; Kim, J.H.; Park, J.; Kim, S.-W. Highly Stable All-Inorganic Perovskite Quantum Dots Using a ZnX_2-Trioctylphosphine-Oxide: Application for High-Performance Full-Color Light-Emitting Diode. *Adv. Opt. Mater.* **2020**, *8*. [CrossRef]

306. Wang, Y.; Teng, Y.; Lu, P.; Shen, X.; Jia, P.; Lu, M.; Shi, Z.; Dong, B.; Yu, W.W.; Zhang, Y. Low Roll-Off Perovskite Quantum Dot Light-Emitting Diodes Achieved by Augmenting Hole Mobility. *Adv. Funct. Mater.* **2020**, *30*. [CrossRef]

307. Zhang, X.; Zeng, Q.; Xiong, Y.; Ji, T.; Wang, C.; Shen, X.; Lu, M.; Wang, H.; Wen, S.; Zhang, Y.; et al. Energy Level Modification with Carbon Dot Interlayers Enables Efficient Perovskite Solar Cells and Quantum Dot Based Light-Emitting Diodes. *Adv. Funct. Mater.* **2020**, *30*, 1910530. [CrossRef]

308. Zhang, B.-B.; Yuan, S.; Ma, J.-P.; Zhou, Y.; Hou, J.; Chen, X.; Zheng, W.; Shen, H.; Wang, X.-C.; Sun, B.; et al. General Mild Reaction Creates Highly Luminescent Organic-Ligand-Lacking Halide Perovskite Nanocrystals for Efficient Light-Emitting Diodes. *J. Am. Chem. Soc.* **2019**, *141*, 15423–15432. [CrossRef]

309. Bi, C.; Wang, S.; Li, Q.; Kershaw, S.V.; Tian, J.; Rogach, A. Thermally Stable Copper(II)-Doped Cesium Lead Halide Perovskite Quantum Dots with Strong Blue Emission. *J. Phys. Chem. Lett.* **2019**, *10*, 943–952. [CrossRef]

310. Wang, Y.; Cao, S.; Li, J.; Li, H.; Yuan, X.; Zhao, J. Improved ultraviolet radiation stability of Mn^{2+}-doped $CsPbCl_3$ nanocrystals via B-site Sn doping. *CrystEngComm* **2019**, *21*, 6238–6245. [CrossRef]

311. Liu, H.; Wu, Z.; Shao, J.; Yao, D.; Gao, H.; Liu, Y.; Yu, W.; Zhang, H.; Yang, B. $CsPbxMn_{1-x}Cl_3$ Perovskite Quantum Dots with High Mn Substitution Ratio. *ACS Nano* **2017**, *11*, 2239–2247. [CrossRef] [PubMed]

312. Lin, C.C.; Xu, K.Y.; Wang, D.; Meijerink, A. Luminescent manganese-doped $CsPbCl_3$ perovskite quantum dots. *Sci. Rep.* **2017**, *7*, 45906. [CrossRef] [PubMed]

313. Das Adhikari, S.; Dutta, S.K.; Dutta, A.; Guria, A.K.; Pradhan, N. Chemically Tailoring the Dopant Emission in Manganese-Doped $CsPbCl_3$ Perovskite Nanocrystals. *Angew. Chem. Int. Ed.* **2017**, *56*, 8746–8750. [CrossRef] [PubMed]

314. Parobek, D.; Roman, B.J.; Dong, Y.; Jin, H.; Lee, E.; Sheldon, M.; Son, D.H. Exciton-to-Dopant Energy Transfer in Mn-Doped Cesium Lead Halide Perovskite Nanocrystals. *Nano Lett.* **2016**, *16*, 7376–7380. [CrossRef]

315. Hou, S.; Gangishetty, M.K.; Quan, Q.; Congreve, D.N. Efficient Blue and White Perovskite Light-Emitting Diodes via Manganese Doping. *Joule* **2018**, *2*, 2421–2433. [CrossRef]

316. Gangishetty, M.K.; Sanders, S.N.; Congreve, D.N. Mn^{2+} Doping Enhances the Brightness, Efficiency, and Stability of Bulk Perovskite Light-Emitting Diodes. *ACS Photonics* **2019**, *6*, 1111–1117. [CrossRef]

317. Pan, G.C.; Bai, X.; Xu, W.; Chen, X.; Zhai, Y.; Zhu, J.; Shao, H.; Ding, N.; Xu, L.; Dong, B.; et al. Bright Blue Light Emission of Ni^{2+} Ion-Doped CsPbCl$_x$Br$_{3-x}$ Perovskite Quantum Dots Enabling Efficient Light-Emitting Devices. *ACS Appl. Mater. Interfaces* **2020**, *12*, 14195–14202. [CrossRef]

318. Fan, F.; Kanjanaboos, P.; Saravanapavanantham, M.; Beauregard, E.; Ingram, G.; Yassitepe, E.; Adachi, M.M.; Voznyy, O.; Johnston, A.K.; Walters, G. Colloidal CdSe$_{1-X}$S$_X$ nanoplatelets with narrow and continuously-tunable electroluminescence. *Nano Lett.* **2015**, *15*, 4611–4615. [CrossRef]

319. Giovanella, U.; Pasini, M.; Lorenzon, M.; Galeotti, F.; Lucchi, C.; Meinardi, F.; Luzzati, S.; Dubertret, B.; Brovelli, S. Efficient Solution-Processed Nanoplatelet-Based Light-Emitting Diodes with High Operational Stability in Air. *Nano Lett.* **2018**, *18*, 3441–3448. [CrossRef]

320. Dufour, M.; Qu, J.; Greboval, C.; Méthivier, C.; Lhuillier, E.; Ithurria, S. Halide Ligands To Release Strain in Cadmium Chalcogenide Nanoplatelets and Achieve High Brightness. *ACS Nano* **2019**, *13*, 5326–5334. [CrossRef]

321. Kelestemur, Y.; Shynkarenko, Y.; Anni, M.; Yakunin, S.; De Giorgi, M.L.; Kovalenko, M.V. Colloidal CdSe Quantum Wells with Graded Shell Composition for Low-Threshold Amplified Spontaneous Emission and Highly Efficient Electroluminescence. *ACS Nano* **2019**, *13*, 13899–13909. [CrossRef] [PubMed]

322. Kim, W.D.; Kim, D.; Yoon, D.-E.; Lee, H.; Lim, J.; Bae, W.K.; Lee, D.C. Pushing the Efficiency Envelope for Semiconductor Nanocrystal-Based Electroluminescence Devices Using Anisotropic Nanocrystals. *Chem. Mater.* **2019**, *31*, 3066–3082. [CrossRef]

323. Liu, B.; Wang, L.; Xu, M.; Tao, H.; Gao, D.; Zou, J.; Lan, L.; Ning, H.; Peng, J.; Cao, Y. Extremely stable-color flexible white organic light-emitting diodes with efficiency exceeding 100 lm W^{-1}. *J. Mater. Chem. C* **2014**, *2*, 9836–9841. [CrossRef]

324. Ou, Q.; Zhou, L.; Li, Y.; Shen, S.; Chen, J.-D.; Li, C.; Wang, Q.-K.; Lee, S.-T.; Tang, J.-X. Light-Emitting Diodes: Extremely Efficient White Organic Light-Emitting Diodes for General Lighting. *Adv. Funct. Mater.* **2014**, *24*, 7249. [CrossRef]

325. Xu, L.-H.; Ou, Q.; Li, Y.; Zhang, Y.-B.; Zhao, X.-D.; Xiang, H.-Y.; Chen, J.-D.; Zhou, L.; Lee, S.-T.; Tang, J.-X. Microcavity-Free Broadband Light Outcoupling Enhancement in Flexible Organic Light-Emitting Diodes with Nanostructured Transparent Metal–Dielectric Composite Electrodes. *ACS Nano* **2016**, *10*, 1625–1632. [CrossRef] [PubMed]

326. Christodoulou, S.; Climente, J.I.; Planelles, J.; Brescia, R.; Prato, M.; Martín-García, B.; Khan, A.H.; Moreels, I. Chloride-Induced Thickness Control in CdSe Nanoplatelets. *Nano Lett.* **2018**, *18*, 6248–6254. [CrossRef] [PubMed]

327. Guzelturk, B.; Erdem, O.; Olutas, M.; Kelestemur, Y.; Demir, H.V. Stacking in Colloidal Nanoplatelets: Tuning Excitonic Properties. *ACS Nano* **2014**, *8*, 12524–12538. [CrossRef]

328. Erdem, O.; Güngör, K.; Guzelturk, B.; Tanriover, I.; Sak, M.; Olutas, M.; DeDe, D.; Kelestemur, Y.; Demir, H.V. Orientation-Controlled Nonradiative Energy Transfer to Colloidal Nanoplatelets: Engineering Dipole Orientation Factor. *Nano Lett.* **2019**, *19*, 4297–4305. [CrossRef]

329. Mir, W.J.; Jagadeeswararao, M.; Das, S.; Nag, A. Colloidal Mn-Doped Cesium Lead Halide Perovskite Nanoplatelets. *ACS Energy Lett.* **2017**, *2*, 537–543. [CrossRef]

330. Gao, Z.; Sun, C.; Liu, H.; Shi, S.; Geng, C.; Wang, L.; Su, S.; Tian, K.; Zhang, Z.H.; Bi, W. White light-emitting diodes based on carbon dots and Mn-doped CsPbMnCl$_3$ nanocrystals. *Nanotechnology* **2019**, *30*, 245201. [CrossRef]

331. Pan, G.; Bai, X.; Xu, W.; Chen, X.; Zhou, D.; Zhu, J.; Shao, H.; Zhai, Y.; Dong, B.; Xu, L.; et al. Impurity Ions Codoped Cesium Lead Halide Perovskite Nanocrystals with Bright White Light Emission toward Ultraviolet–White Light-Emitting Diode. *ACS Appl. Mater. Interfaces* **2018**, *10*, 39040–39048. [CrossRef] [PubMed]

332. Lu, M.; Wu, H.; Zhang, X.; Wang, H.; Hu, Y.; Colvin, V.L.; Zhang, Y.; Yu, W.W. Highly Flexible CsPbI$_3$ Perovskite Nanocrystal Light-Emitting Diodes. *ChemNanoMat* **2019**, *5*, 313–317. [CrossRef]

333. Luo, D.; Chen, Q.; Liu, B.; Qiu, Y. Emergence of Flexible White Organic Light-Emitting Diodes. *Polymers* **2019**, *11*, 384. [CrossRef] [PubMed]

334. Zhang, L.; Xiao, W.; Wu, W.; Liu, B. Research Progress on Flexible Oxide-Based Thin Film Transistors. *Appl. Sci.* **2019**, *9*, 773. [CrossRef]

335. Jou, J.-H.; Kumar, S.; Agrawal, A.; Li, T.-H.; Sahoo, S. Approaches for fabricating high efficiency organic light emitting diodes. *J. Mater. Chem. C* **2015**, *3*, 2974–3002. [CrossRef]

336. Xiao, P.; Huang, J.; Yu, Y.; Liu, B. Recent Developments in Tandem White Organic Light-Emitting Diodes. *Molecules* **2019**, *24*, 151. [CrossRef]

337. Liu, B.; Wang, L.; Tao, H.; Xu, M.; Zou, J.; Ning, H.; Peng, J.; Cao, Y. Doping-free tandem white organic light-emitting diodes. *Sci. Bull.* **2017**, *62*, 1193–1200. [CrossRef]

338. Hong, T.; Gao, D.; Liu, B.; Wang, L.; Zou, J.; Xu, M.; Peng, J. Enhancement of tandem organic light-emitting diode performance by inserting an ultra-thin Ag layer in charge generation layer. *Acta Phys. Sin.* **2017**, *1*, 017302.

339. Wood, V.; Halpert, J.E.; Panzer, M.J.; Bawendi, M.G.; Bulović, V. Alternating Current Driven Electroluminescence from ZnSe/ZnS:Mn/ZnS Nanocrystals. *Nano Lett.* **2009**, *9*, 2367–2371. [CrossRef]

340. Zaumseil, J.; Donley, C.L.; Kim, J.-S.; Friend, R.H.; Sirringhaus, H. Efficient Top-Gate, Ambipolar, Light-Emitting Field-Effect Transistors Based on a Green-Light-Emitting Polyfluorene. *Adv. Mater.* **2006**, *18*, 2708. [CrossRef]

341. Hurni, C.A.; David, A.; Cich, M.J.; Aldaz, R.I.; Ellis, B.; Huang, K.; Tyagi, A.; Delille, R.A.; Craven, M.D.; Steranka, F.M.; et al. Bulk GaN flip-chip violet light-emitting diodes with optimized efficiency for high-power operation. *Appl. Phys. Lett.* **2015**, *106*, 031101. [CrossRef]

342. Bhardwaj, J.; Cesaratto, J.M.; Wildeson, I.H.; Choy, H.; Tandon, A.; Soer, W.A.; Schmidt, P.J.; Spinger, B.; Deb, P.; Shchekin, O.B.; et al. Progress in high-luminance LED technology for solid-state lighting. *Phys. Status Solidi A* **2017**, *214*, 1600826. [CrossRef]

343. Wierer, J.J.; David, A.; Megens, M.M. III-nitride photonic-crystal light-emitting diodes with high extraction efficiency. *Nat. Photonics* **2009**, *3*, 163–169. [CrossRef]

344. Pust, P.; Schmidt, P.J.; Schnick, W. A revolution in lighting. *Nat. Mater.* **2015**, *14*, 454–458. [CrossRef]

345. Zhu, P.; Tansu, N. Effect of packing density and packing geometry on light extraction of III-nitride light-emitting diodes with microsphere arrays. *Photonics Res.* **2015**, *3*, 184–191. [CrossRef]

346. Zhu, P.; Tansu, N. Resonant cavity effect optimization of III-nitride thin-film flip-chip light-emitting diodes with microsphere arrays. *Appl. Opt.* **2015**, *54*, 6305–6312. [CrossRef]

347. Kumawat, N.K.; Liu, X.-K.; Kabra, D.; Gao, F. Blue perovskite light-emitting diodes: Progress, challenges and future directions. *Nanoscale* **2019**, *11*, 2109–2120. [CrossRef]

348. Sun, Y.; Giebink, N.C.; Kanno, H.; Ma, B.; Thompson, M.E.; Forrest, S.R. Management of singlet and triplet excitons for efficient white organic light-emitting devices. *Natrre* **2006**, *440*, 908–912. [CrossRef]

349. Liu, B.; Xu, M.; Wang, L.; Zou, J.; Tao, H.; Su, Y.; Gao, D.; Ning, H.; Lan, L.; Peng, J. Regulating charges and excitons in simplified hybrid white organic light-emitting diodes: The key role of concentration in single dopant host–guest systems. *Org. Electron.* **2014**, *15*, 2616–2623. [CrossRef]

350. Liu, B.; Wang, L.; Zou, J.; Tao, H.; Su, Y.; Gao, D.; Xu, M.; Lan, L.; Peng, J. Investigation on spacers and structures: A simple but effective approach toward high-performance hybrid white organic light emitting diodes. *Synth. Met.* **2013**, *184*, 5–9. [CrossRef]

351. Liu, B.; Lan, L.; Zou, J.; Peng, J. A novel organic light-emitting diode by utilizing double hole injection layer. *Acta Phys. Sin.* **2013**, *62*, 087302.

352. Jou, J.-H.; Hsieh, C.-Y.; Tseng, J.-R.; Peng, S.-H.; Jou, Y.-C.; Hong, J.H.; Shen, S.-M.; Tang, M.-C.; Chen, P.-C.; Lin, C.-H. Candle Light-Style Organic Light-Emitting Diodes. *Adv. Funct. Mater.* **2013**, *23*, 2750–2757. [CrossRef]

353. Yang, B.; Chen, J.S.; Yang, S.Q.; Hong, F.; Sun, L.; Han, P.G.; Pullerits, T.; Deng, W.Q.; Han, K.L. Lead-free sliver-bismuch halide double perovskite nanocrystals. *Angew. Chem. Int. Ed.* **2018**, *57*, 5359–5363. [CrossRef]

354. Stranks, S.D.; Snaith, H.J. Metal-halide perovskites for photovoltaic and light-emitting devices. *Nat. Nanotechnol.* **2015**, *10*, 391–402. [CrossRef] [PubMed]

355. Adhikari, G.C.; Thapa, S.; Zhu, H.; Zhu, P. Mg^{2+}-Alloyed All-Inorganic Halide Perovskites for White Light-Emitting Diodes by 3D-Printing Method. *Adv. Opt. Mater.* **2019**, *7*, 1900916. [CrossRef]

356. Liu, Y.; Jing, Y.; Zhao, J.; Liu, Q.; Xia, Z. Design Optimization of Lead-Free Perovskite $Cs_2AgInCl_6$:Bi Nanocrystals with 11.4% Photoluminescence Quantum Yield. *Chem. Mater.* **2019**, *31*, 3333–3339. [CrossRef]

357. Sasabe, H.; Kido, J. Development of high performance OLEDs for general lighting. *J. Mater. Chem. C* **2013**, *1*, 1699–1707. [CrossRef]

358. Liu, B.; Wang, L.; Xu, M.; Tao, H.; Zou, J.; Gao, D.; Lan, L.; Ning, H.; Peng, J.; Cao, Y. Efficient hybrid white organic light-emitting diodes with extremely long lifetime: The effect of n-type interlayer. *Sci. Rep.* **2014**, *4*, 7198. [CrossRef]

359. Zhang, D.; Cai, M.; Zhang, Y.; Zhang, D.; Duan, L. Sterically shielded blue thermally activated delayed fluorescence emitters with improved efficiency and stability. *Mater. Horiz.* **2016**, *3*, 145–151. [CrossRef]

360. Bao, J.; Hadjiev, V.G. Origin of Luminescent Centers and Edge States in Low-Dimensional Lead Halide Perovskites: Controversies, Challenges and Instructive Approaches. *Nano-Micro Lett.* **2019**, *11*, 26. [CrossRef]

361. Lee, I.; Lee, J.Y. Molecular design of deep blue fluorescent emitters with 20% external quantum efficiency and narrow emission spectrum. *Org. Electron.* **2016**, *29*, 160–164. [CrossRef]

362. Liu, B.; Xu, M.; Wang, L.; Tao, H.; Su, Y.; Gao, D.; Lan, L.; Zou, J.; Peng, J. Simplified hybrid white organic light-emitting diodes with efficiency/efficiency roll-off/color rendering index/color-stability trade-off. *Phys. Status solidi (RRL)-Rapid Res. Lett.* **2014**, *8*, 719–723. [CrossRef]

363. Liu, B.; Nie, H.; Lin, G.; Hu, S.; Gao, D.; Zou, J.; Xu, M.; Wang, L.; Zhao, Z.; Ning, H.; et al. High-Performance Doping-Free Hybrid White OLEDs Based on Blue Aggregation-Induced Emission Luminogens. *ACS Appl. Mater. Interfaces* **2017**, *9*, 34162–34171. [CrossRef] [PubMed]

364. Dameron, A.A.; Davidson, S.D.; Burton, B.B.; Carcia, P.F.; McLean, R.S.; George, S.M. Gas Diffusion Barriers on Polymers Using Multilayers Fabricated by Al_2O_3 and Rapid SiO_2 Atomic Layer Deposition. *J. Phys. Chem. C* **2008**, *112*, 4573–4580. [CrossRef]

365. Seo, S.-W.; Jung, E.; Seo, S.J.; Chae, H.; Chung, H.K.; Cho, S.M. Toward fully flexible multilayer moisture-barriers for organic light-emitting diodes. *J. Appl. Phys.* **2013**, *114*, 143505. [CrossRef]

366. Park, J.-S.; Chae, H.; Chung, H.K.; Lee, S.I. Thin film encapsulation for flexible AM-OLED: A review. *Semicond. Sci. Technol.* **2011**, *26*, 34001. [CrossRef]

367. Fakharuddin, A.; Shabbir, U.; Qiu, W.; Iqbal, T.; Sultan, M.; Heremans, P.; Schmidt-Mende, L. Inorganic and Layered Perovskites for Optoelectronic Devices. *Adv. Mater.* **2019**, *31*, 1807095. [CrossRef]

368. Wang, L.; Fu, K.; Sun, R.; Lian, H.; Hu, X.; Zhang, Y. Ultra-stable $CsPbBr_3$ Perovskite Nanosheets for X-Ray Imaging Screen. *Nano-Micro Lett.* **2019**, *11*, 52. [CrossRef]

369. Ren, J.; Zhou, X.; Wang, Y. Dual-emitting $CsPbX_3$@ZJU-28 (X = Cl, Br, I) composites with enhanced stability and unique optical properties for multifunctional applications. *Chem. Eng. J.* **2020**. [CrossRef]

370. Konopsky, V.N.; Prokhorov, V.; Lypenko, D.; Dmitriev, A.; Alieva, E.; Dietler, G.; Sekatskii, S. Electrical Excitation of Long-Range Surface Plasmons in PC/OLED Structure with Two Metal Nanolayers. *Nano-Micro Lett.* **2020**, *12*, 35. [CrossRef]

371. Kim, J.H.; Han, S.H.; Lee, J.Y. Concentration quenching resistant donor-acceptor molecular structure for high efciency and long lifetime thermally activated delayed fluorescent organic light-emitting diodes via suppressed non-radiative channel. *Chem. Eng. J.* **2020**, *395*, 125159. [CrossRef]

372. Xiao, P.; Huang, J.; Dong, T.; Xie, J.; Yuan, J.; Luo, D.; Liu, B. Room-Temperature Fabricated Thin-Film Transistors Based on Compounds with Lanthanum and Main Family Element Boron. *Molecules* **2018**, *23*, 1373. [CrossRef] [PubMed]